


POLITECNICO DI MILANO

Dipartimento di Scienze e Tecnologie Aerospaziali

Master Thesis in Aeronautical Engineering

Academic Year 2015/2016

Comparison of GCH4/GOX Rocket Combustion Chambers

Author:
Valeria SCAGLIONE
836760

Advisor:
Luciano GALFETTI

Co-Advisor TUM:
Maria Palma CELANO
Oskar J. HAIDN

21 December 2016

The Earth is the cradle of humanity,
but man kind cannot stay in the cradle forever.

K. E. Tsiolkovski

Acknowledgements

Questo progetto di tesi rappresenta solo il culmine di anni di studio, sacrifici, durante i quali ho avuto la fortuna di avere accanto parenti e amici.

Vorrei ringraziare i miei genitori, sempre pronti a sostenermi, a incoraggiarmi, a darmi la forza per superare ogni delusione, a gioire per ogni mio successo. Grazie per avermi dato la possibilità di studiare, grazie per avermi sempre lasciato libera di scegliere la mia strada, ma essermi stati vicini in ogni decisione.

Ringrazio il Prof. Galfetti per la sua disponibilità e i preziosi insegnamenti umani e professionali.

Ringrazio il Prof. Haidn, Mariella Celano e Simona Silvestri, senza i quali questa tesi non esisterebbe, per avermi dato la possibilità di fare unesperienza unica.

Grazie Andrea per avermi fatto ridere tra una lezione e laltra.

Grazie Simone per avermi sempre incoraggiata ad ogni esame.

Grazie Carmelo per essermi stato vicino in questi anni.

Grazie per la nostra amicizia diventata un punto cardine della mia vita.

Grazie Fabiola per le nostre tisane notturne.

Grazie Geny, Roberta, Monica ed Elena, perché le vere amicizie durano per sempre.

Grazie Francesca per le nostre giornate di studio estive e le nostre serate alcoliche.

Grazie Maria Teresa per aver condiviso con me una delle esperienze più belle della mia vita. Grazie per avermi fatto ridere quando niente andava per il meglio.

Grazie zia Dadà, per essere sempre presente nei traguardi più importanti della mia vita.

Abstract

This thesis aims to compare two different subscale combustion chambers, operating with a propellant combination of gaseous methane (GCH4) and gaseous oxygen (GOx). In the current study, results from an experimental investigation on a single-element and a multi-element shear coaxial injector, having a square and a rectangular cross section, are presented. The similarities and the differences between the two combustion chambers in terms of geometries and operating conditions are analysed in detail. Developing new combustors, comparisons between two different combustion chambers, as geometric and thermodynamic characteristics, are often made in order to predict performances. In this work, detailed informations about pressure and temperature distribution along the chamber axis are reported for the two combustion chambers. In addition, it is considered the temperature profile versus time for the two hardware. All results are examined at different operating conditions, particularly, varying the chamber pressure and the mixture ratio. As a result, through this thesis the higher combustion efficiency of the multi-element respect to the single-element combustion chamber is demonstrated.

Estratto in lingua italiana

Questo lavoro di tesi ha l'obiettivo di fornire un confronto tra due camere di combustione in sottoscala per endoreattori a liquido. Le camere di combustione sono caratterizzate da due diverse geometrie e differiscono nel numero di iniettori. Infatti la camera a singolo elemento è a sezione quadrata e presenta un solo iniettore disposto in posizione centrale. La camera a multi elemento ha sezione rettangolare e presenta cinque iniettori disposti lungo lasse trasversale.
Entrambe le camere utilizzano, come propellente, la coppia metano/ossigeno, essendo una delle soluzioni più promettenti per il futuro nel campo della propulsione spaziale. Infatti, la coppia metano/ossigeno risulta essere un propellente a minor impatto ambientare se paragonato ai propellenti a base di idrazina, e minori costi di gestione rispetto alla coppia idrogeno/ossigeno.
Il lavoro è stato svolto presso il Lehrstuhl für Flugantriebe (LFT) della Technische Universität München (TUM), dove diverse campagne di test sono state eseguite sulle due camere al fine di misurare la pressione e la temperatura. Durante questo lavoro, è stato studiato l'andamento della pressione e della temperatura sia nel tempo sia lungo l'asse delle camere di combustione, evideniando similitudini e differenze, dovute alla diversa geometria e al diverso numero di iniettori. Tutti i risultati sono stati ottenuti variando il rapporto di miscela da 2.6 a 3.4 e la pressione nominale da 10 a 20 bar.
Il confronto tra le due camere di combustione mira allo studio del processo di combustione. Tramite l'analisi della pressione in funzione dell'asse della camera è possibile osservare che nella camera multi-elemento, le fine della combustione è più evidente rispetto alla camera singolo-elemento. Nella camera singolo elemento si evince che la variazione del gradiente di temperatura dT/dt è maggiore a causa della maggior influenza delle pareti sull'unico iniettore presente, confermata dal maggior valore del rapporto tra il volume della camera e la superficie delle pareti della camera. Dal confronto tra le due camere di combustione per endoreattori a liquido, è stato ricavato che la camera a multi-elemento ha un'efficienza di combustione

maggiore rispetto a quella della camera a singolo elemento, grazie a un miglior miscelamento e a una minor influenza delle pareti della camera, per tutte le condizioni operative considerate in questo lavoro.

Indice

Elenco delle figure

Elenco delle tabelle

Nomenclature

α	Heat transfer coefficient
Δt_r	Residence stay time
$\dot{m}$	Mass flow rate
$\dot{q}$	Heat flux
ϵ	Expansion ratio
ϵ_c	Contraction ratio
η	Efficiency
γ	Specific heat ratio
ρ	Density
a	Sonic velocity
A_c	Combustion chamber area
A_t	Throat area
c^*	Characteristic velocity
c_p	Specific heat at constant pressure
c_v	Specific heat at constant volume
F	Thrust
g_0	Gravity acceleration

J Momentum flux ratio

L Combustion chamber length

l^* Characteristic length

M Mach number

M_m Molar mass

O/F Mixture ratio

p Pressure

R Gas constant

T Temperature

V Volume

v Velocity

VR Velocity ratio

List of abbreviations

GCH4	Gaseous methane
GOx	Gaseous oxidizer
AW	Adiabatic wall
TCXXXX	Thermocouple Chamber for the single-element combustion chamber

Each 'X' corresponds to the following item in this sequence:

- X : L (Long segment) - S (Short segment)
- X : U (Up) - D (Down)
- X : Axial position
- X : 1mm - 2mm - 3mm (Distance from the hot wall)

TCXXXXXXXX Thermocouple Chamber for the multi-element combustion chamber

Each 'X' corresponds to the following item in this sequence:

- X : A (A segment) - B (B segment)
- X : U (Up) - D (Down)
- XX : Axial position
- X : Y-position
- X : L (Left) - C (Center) - R (Right)
- XX : 1mm - 2mm - 3mm (Distance from the hot wall)

Capitolo 1

Introduction

Nowadays, liquid rocket engines used for space exploration and transfer into an orbit are mostly based on cryogenic propellants, as liquid oxygen/liquid hydrogen (LOx/LH2), due to high specific impulse (about 450 s) and low pollution.
Thanks to lower operational and handling cost, increased the attention for alternative propellants, as hydrocarbon, for future launch vehicle. One of the most promising propellant combinations is oxygen/methane (GOx/GCH4). This is a consequence of its high thermal conductivity, specific heat and low viscosity, respect to other hydrocarbons. In addition, methane shows, compared to other potential candidates, better overall performances, higher specific impulse, no risks for human health, simple extractability from natural gases and a density six-times higher than hydrogen, when stored in liquid state at typical tank pressures, [4]. This propellant combination is used for the subscale rocket combustion chambers at Institute for Flight Propulsion of the Technische Universität München.
The main focus of this thesis is to characterize the chamber wall heat transfer and reconstruct the temperature and pressure profiles along chamber axis for two different rocket combustion chambers. Experiments are conducted for a gas-gas shear coaxial injector element over a wide range of pressure and mixture ratio.
The two rectangular combustion chambers, considered in this thesis, are characterized by a different numbers of injectors: a single-element combustion chamber, which has only one injector, and a multi-element combustion chamber, characterized by five injectors. The decrease of injection element numbers results in more simplicity, lower fabrication cost and higher reliability of the engine. For these reasons, the aims pursued by injector designers is based on reducing the number of elements, in order to test a smaller combustion chamber and, than, extracting the results for a combustion chamber with higher elements number.

Capitolo 2

Theoretical Basics

Liquid propellant rocket engines use liquid propellants that are fed under pressure from tanks into a thrust chamber. The mostly used is liquid bi-propellant, which consists of a liquid oxidizer and a liquid fuel. The propellants react in a thrust chamber, in order to generate hot gases. Through a converging-diverging nozzle, the hot gases are accelerated and ejected at a high velocity, imparting momentum to the vehicle.

2.1 Definition of of basic parameters

2.1.1 Specific Impulse

The specific impulse I_s is an indication of engine efficiency and it is defined as the ratio between the thrust and the the weight flow of the propellants. The specif impulse is measured at sea level with a $g_0 = 9.81 m/s$

$$I_s = \frac{F}{\dot{m} g_0} \tag{2.1}$$

An engine with a high specific impulse is more efficient because it produces more thrust, considering the same amount of propellant.
It is possible to define the specific impulse as a function of the thrust coefficient 2.3 and the characteristic velocity 2.4, as shown in the following relation 2.2.

$$I_s = \frac{c_F c^*}{g_0} \tag{2.2}$$

2.1.2 Thrust Coefficient

By definition, the thrust coefficient c_F quantifies how much increases the thrust with respect to the static value exerted on the nozzle throat area, thanks to the presence of the supersonic divergent.

$$c_F = \frac{F}{p_c A_{th}} \tag{2.3}$$

Typical values of c_F for current thermal engines are in the interval from 1 to 2. The quantity c_F is considered a parameter of merit for the gasdynamic nozzle of thermal engines.

2.1.3 Ideal Thermodynamic Rocket Condition

In this section, the ideal thermodynamic rocket condition is introduced, in order to obtain simple mathematical relationships for relevant basic thermodynamic principles. The assumptions for an ideal rocket are the following:

- The fluid is homogeneous and gaseous and obeys the perfect gas law
- There are not shock waves, discontinuities, friction and boundary layer effects
- The propellant flow is steady, constant and adiabatic
- Chemical equilibrium is established within the rocket chamber and the gas composition does not change in the nozzle (frozen flow)
- The exhaust gas has an axially directed velocity
- The gas velocity, pressure, temperature, and density are all uniform across any section normal to the nozzle axis

Thanks to these assumptions, for chemical rocket propulsion the measured actual performance is usually between 1 and 6 % below the calculated ideal value [1].

2.1.4 Characteristic Velocity

Another important parameter is the characteristic velocity c^*, used to compare propellant combinations and combustion chamber designs and it is defined in the following Equation 2.4.

$$c^* = \frac{p_c A_{th}}{\dot{m}} \tag{2.4}$$

It is basically a function of the propellant characteristics and combustion chamber design and it is independent of nozzle characteristics. Typical values of c^* for thermal engines in general fall in the interval 1500 to 3000 m/s [1]. In particular, for gaseous methane and oxygen, as considered in this project, a typical value of characteristic veloctiy is of about 1800 m/s.
Considering an ideal condition, the characteristic velocity c^*_{theo} is a function of the chamber temperature T_c and the propellant properties (γ, M_m). In fact, it is possible to define the ideal characteristic velocity as following.

$$c^*_{theo} = \sqrt{\frac{RT_c}{M_m \gamma} \left(\frac{\gamma+1}{2}\right)^{\frac{\gamma+1}{\gamma-1}}} \tag{2.5}$$

2.1.5 Combustion Efficiency

In order to judge the performance of an injection system, an important parameter is the combustion efficiency. It is defined as the ratio between the experimental and the theoretical characteristic velocity.

$$\eta^* = \frac{c^*_{exp}}{c^*_{theo}} \tag{2.6}$$

The combustion efficiency is a measure of the effectiveness of a combustion chamber to convert the chemical energy contained in the propellant into thermal energy used by the process. Possible heat, mixing and evaporation losses have to be considered.
The ideal characteristic velocity is calculated according with CEA2, under the hypothesis of infinite injection area (see figure 2.1, [11]), complete and adiabatic combustion, ideal gas, one dimensional form for continuity, momentum and energy law and chemical equilibrium of combustion.

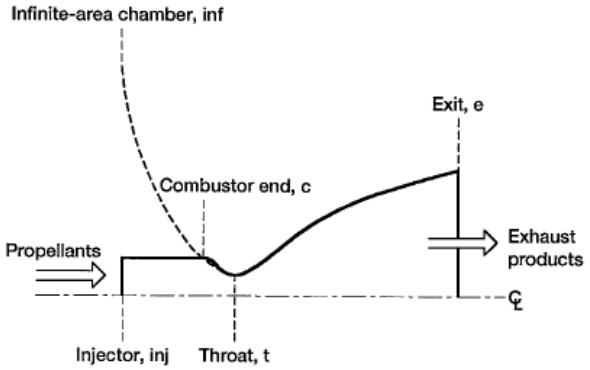

Figura 2.1: Schematics of a rocket combustion chamber with finite-area and infinite-area

The inputs for the calculation are:

- the thermal properties and the enthalpy of the propellants

- the propellant mixture ratio
- the total combustion chamber pressure
- the chamber contraction ratio

2.1.6 Characteristic Length

The characteristic length l^* is an useful parameter to characterize the rocket combustion chambers. It permits to define the scale of a physical system and to characterize the residence time in the combustion chamber.

$$l^* = \frac{V_c}{A_{th}} \tag{2.7}$$

Larger characteristic length means a bigger combustion chamber volume, so an increase of the weight and of the frictional losses. An higher value of the characteristic length also leads to a higher surface area, which has to be cooled, so heat transfer is incremented and improved cooling is requested. As a consequence, thermal losses are incremented. The characteristic length is defined by the selection of oxidizer and fuel fair, pressure, injector design, chamber geometry and mixture ratio.

2.1.7 Combustion Residence Time

The combustion residence time of the propellant gases is the average value of the time spent by each molecule or atom within the chamber volume, t_r.

$$t_r = \frac{\rho_c V_c}{\dot{m}} \tag{2.8}$$

The minimum residence time at which a good performance is attained defines the chamber volume that gives essentially complete combustion and it includes the time necessary for vaporization rate for liquid propellants, activation, and complete burning of the propellant.
Using the definition of the characteristic length l^* (See Equation (2.7)) and of the characteristic velocity c^* (See Equation (2.4)), the residence time equation become:

$$t_r = \frac{\rho_c l^* A_{th}}{\dot{m}} = \frac{\rho_c l^* c^*}{p_c} \tag{2.9}$$

Under the hypothesis of ideal gas, the ideal residence time is a function of the characteristic length, the combustion temperature and the propellant properties.

$$\Delta t_r = l^* \frac{1}{\Gamma} \sqrt{\frac{M_m}{R T_c}} \tag{2.10}$$

The value of the residence time varies according to the propellants and has to be experimentally determined. Typical values are of 0.001 to 0.040 s depending on propellants and combustion chamber, as known in [1].

2.1.8 Contraction Area Ratio

For a nozzle under the hypothesis of isentropic flow, the contraction area ratio ϵ is defined as the ratio between the cross-sectional area for gas flow at the nozzle inlet A_c and the one at the throat A_{th}. Thanks to Equation 2.11, the contraction area ratio is a function of Mach number and specific heat ratio.

$$\epsilon = \frac{A_c}{A_{th}} = \frac{1}{M}\sqrt{\left(\frac{1+\frac{\gamma+1}{2}M^2}{1+\frac{\gamma+1}{2}}\right)^{\frac{\gamma+1}{\gamma-1}}} \tag{2.11}$$

2.1.9 Hydraulic Diameter

The hydraulic diameter is defined as four times the ratio between the the cross-sectional area A and the wetted perimeter P of the cross-section. It can be used to calculate the dimensionless Reynolds Number. For a rectangular chamber, where the height and width are respectively a and b, the hydraulic diameter is defined as in following Equation 2.12.

$$d_H = \frac{4A}{P} = \frac{2ab}{a+b} \tag{2.12}$$

2.1.10 Thermal Conductivity

The thermal conductivity is defined as the capacity of a material to conduct heat. According to Fourier's law 2.13, the thermal conductivity is the ratio between the heat flux across a material and the temperature gradient.

$$\vec{q} = \lambda\nabla(T) \tag{2.13}$$

It is a property of the material and it is independent from the body dimensions. A material with an higher thermal conductivity is used in heat sink applications because it is less insulating.

2.2 Heat transfer

Usually, in a rocket combustion chamber, the temperature achieved during the combustion is in the range of 2500K-3500K. In spite, in this subscale chamber lower temperature are reached,

it is important to know how cool down the system, in order to avoid the high thermal loads and stresses.
There are several types of cooling techniques in rocket engines, usually the most used are:

- Steady-State Techniques: the heat transfer rate and the temperature on the wall reach thermal equilibrium. In this category, the most utilized are regenerative cooling and radiative cooling.
  The convective heat transfer $\dot{q}$ from the flow to the chamber walls is given by the following Equation 2.14.
  $$\dot{q} = h(T_{aw} - T_w) \tag{2.14}$$
  where h is the convective heat transfer coefficient. In order to know the heat transfer coefficient, the correlation of Cinjarew is used.
  $$Nu = 0.0162(RePr)^{0.82} \left(\frac{T_{aw}}{T_w}\right)^{0.35} \tag{2.15}$$

- Transient Techniques (Heat Sink): the wall temperature increases continuously, and consequently the time of operation is limited. In this category, capacitive cooling and ablative cooling are found.

2.2.1 Heat Sink Method

The technique used in this thesis is the capacitive one, in which a material absorbs the most amount of heat. In the "heat-sink" method, the combustion chamber and the nozzle are made from a high-conductivity material. During combustion, the high thermal conductivity of the copper keeps the inside wall from melting as the heat rapidly flows into the interior of the mass. After the run, the temperature of the copper mass comes to equilibrium and by measuring this temperature, the total amount of heat absorbed can be calculated from the known mass and specific heat of the copper.
The cumulative heat method is adopted by the observation of the time evolution of the temperature signal during the hot run. At the time interval t_{eval}, the temperature distribution is fully established and quasi-steady-state conditions can be assumed.
Assuming a constant heat flux, the temperature may be considered to equally change at any point of the control volume. The accumulated heat can be calculated by an energy balance for a control volume, where the difference between the incoming and outcoming energy is equal to the stored one.
$$\dot{E}_{in} - \dot{E}_{out} = \dot{E}_{st} \tag{2.16}$$

Thanks to the overall energy balance, the transient temperature response is given by the following Equation 2.17, expressed in terms of heat flux.

$$\dot{q}_{in} - \dot{q}_{out} = \frac{\rho c V}{A_{hw}} \frac{dT}{dt} \tag{2.17}$$

Thanks to the measurement of the temperature during the hot run, the temperature gradient over time is calculated. Then, the equation 2.17 is applied to all thermocouples mounted in the two rocket combustion chambers.
The properties of the copper, as density, heat capacity and conductivity are assumed constant and the heat flux dispersed outside the chamber, due to natural convection, can be considered negligible. This means that $\dot{q}_{out}$ is equal to zero.

2.3 Scaling Methods of Combustion Process

Developing new combustor, a comparison between measured performance in a combustor and predicted performance in another one is made. Usually , the two combustors have a different geometry. Scaling is defined as "the ability to design new combustion devices with predictable performance on the basis of test experience with old devices" [5]. As a consequence, it is possible to use a smaller combustor, in order to reduce costs for manufacturing development hardware and for testing.

2.3.1 Set of Similarity Parameters

It is possible to obtain a set of similarity parameters, writing the conservation equation for mass, momentum and energy in non dimensional form, as Penner done in [5]. This groups of parameters for steady aerothermochemistry, in liquid propellant rocket combustion chambers, are valid for reacting gas mixture, neglecting radiant heat transfer and thermal diffusion effects.

$$\text{Reynolds number: } Re = \frac{\rho v L}{\mu}$$

$$\text{Schmidt number: } Sc = \frac{\mu}{\rho D}$$

$$\text{Prandtl number: } Pr = \frac{c_p \mu}{\gamma}$$

$$\text{Mach number: } M = \frac{v}{a}$$

$$\text{Froude number: } Fr = \frac{v^2}{gL}$$

$$\Phi = \frac{v^2}{2c_v T}$$

$$\text{Specific heat ratio: } \gamma = \frac{c_p}{c_v}$$

$$\text{First Damköhler number: } Da_i = \frac{L}{\nu \Delta t}$$

$$\text{Third Damköhler number: } Da_{iii} = \frac{\Delta q L}{\nu c_p T \Delta t}$$

The Reynold number is defined as the ratio between the inertial to viscous force; the Schmidt number is the ratio of kinetic viscosity to molecular diffusivity; the Prandtl number is the ratio of momentum diffusivity to thermal diffusivity; the Mach number is the ratio of velocity to sonic velocity; the Froude number is the ratio of inertial forces to gravitational forces.
The two Damköhler numbers introduce possible chemical changes in the flow. In particular, Da_i is defined as the ratio of the rate of convection time L/ν to chemical time Δt and Da_{iii} is the ratio of the rate of heat addition per unit volume by chemical reaction, $\Delta q/\Delta t$, and the rate of removal of heat by convection of enthalpy, $\nu c_p T/L$.
The heat capacity ratio is defined as is the ratio of the heat capacity at constant pressure to heat capacity at constant volume. Assuming a perfect gas, the specific heat ratio will be constant for each temperature and mixture ratio. It's possible to observe that the non dimensional parameter Φ, introduced by Penner, is a function of specific heat ratio and Mach number.
Under the hypothesis of homogeneous, low velocity flow systems without significant external force, the set of nine similarity parameters can be reduced to five groups.

2.3.2 Pennier-Tsien Scaling Rule

This is the first approach. Penner assumed the chamber pressure as a constant. As a consequence, the density is constant for the same injection temperature. Assuming that the two combustors use the same propellant, the same mixture ratio and the same propellant inlet temperature, Sc and Pr numbers are constant. Being Da_{iii} constant only if Da_i is constant, the set of parameters is reduced into Re and Da_i numbers.
In order to have a constant Re number, the following relationship has to be verified.

$$v_1 L_1 = v_2 L_2 \tag{2.18}$$

Combining Re and Da_i number:

$$\frac{\Delta t_{c,1}}{\Delta t_{c,2}} = \frac{L_1 v_2}{L_2 v_1} = \left(\frac{L_1}{L_2}\right)^2 \tag{2.19}$$

The equation 2.19 described that, having a constant chamber pressure, temperature and chemical properties, the ratio of chemical reaction times for two combustion chambers 1 and 2 is proportional to the square of the ratio of its length scales.

2.3.3 Crocco Scaling Rule

This is a different approach, where the chemical conversion time is inversely proportional to the chamber pressure, generating a scaling rule that preserves combustion similarity and Re, but not M, causing dimensions and thrust to scale with chamber pressure as a function of that power.

$$\Delta t_c \propto \frac{1}{p_c^m} \tag{2.20}$$

The main different from the Penner-Tsien is that the pressure is not constant. As a consequence of these considerations, we can obtain the following relationships.

$$\frac{\Delta t_{c,1}}{\Delta t_{c,2}} = \left(\frac{L_1}{L_2}\right)^{\left(\frac{2m}{m+1}\right)} \tag{2.21}$$

$$\frac{\nu_1}{\nu_2} = \left(\frac{L_1}{L_2}\right)^{\left(\frac{1-m}{m+1}\right)} \tag{2.22}$$

$$\frac{d_1}{d_2} = \left(\frac{L_1}{L_2}\right)^{\left(\frac{m}{m+1}\right)} \tag{2.23}$$

$$\frac{p_1}{p_2} = \left(\frac{L_2}{L_1}\right)^{\left(\frac{2}{m+1}\right)} \tag{2.24}$$

Finally, for a constant chamber temperature and propellant properties, the chemical conversion times must be reduced as the length scales are reduced, while the velocities are equals and the pressures are increased.

2.4 Scaling Methods of Performance

Combustion stability, heat transfer and injection are mostly influenced by the injection elements. It is possible to find a relationship between full-size and subscale characteristic exhaust

velocity performance, which is given by the following relation, [5].

$$\eta_{c,f} = X_{ia,ss}\eta_{c,s} \tag{2.25}$$

Comparison between single-element performance and multi-element performance consists on the determination of $X_{ia,ss}$.
Exist two different methods of scaling full-size combustors with small-sized hardware: in the first one is based on using identical injector elements while the second one is based on using photo-scaled injector elements. In this work, only the first one is considered because the injector element geometry is the same in the small-size and full-scale combustors.

2.4.1 Identical Injector Elements

The Identical Injector Elements method consider the same injector element geometry; for this reason, the Re of the injector features has to be the same in the small-size and in the full-size chamber. Otherwise the Re of the combustion in the small-size chamber may or may not be similar to the Re of the combustion in the full-size chamber, depending upon chamber geometry similarity. Having a different length of combustion chamber determines different vaporization and mixing efficiencies, while keeping the contraction ratio constant retains at least the M at the head end of the chamber.

2.4.2 Photo Scaled Injector Elements

The Photo Scaled Injector Elements method is different from the previous, thanks to a variation of injector dimensions. It is characterized by a not constant Re number, in the injection elements and in the combustion chamber, between the two scaled combustion chambers. For combustion stability, suggests that changing the d/V characteristic in relation to the combustion chamber diameter maintains a constant combustion stability margin. An example of a photo-scaled combustor can be a reduction in element dimensions proportional with the chamber diameter reduction, while maintaining constant injection velocity and constant chamber pressure. Keeping the chamber pressure constant, the contraction ratios will be the same. Both injection and chamber characteristic Re will be different from the two chambers. As a consequence, atomization, vaporization, mixing will be different.

Capitolo 3

Hardware and Experimental Set-Up

In this chapter, it is possible to find a brief description of the tools and the set-up, used by the 'Institute of Flight Propulsion', in order to achieve the results and the operating conditions used during the test.

3.1 Test Facility

The "Lehrstuhl für Turbomaschinen und Flugantriebe" (LTF) has designed a test facility, in order to test small rocket chamber. For the single-element combustion chamber the test facility is called MoRaP (Mobiler Raketen Prüfstand) and it is shown in the Figure 3.1. The rocket combustion chambers are in a subscale condition and can accomplish a maximum thrust of 500 N. A subscale rocket combustion chamber is a small scale combustion chamber, used to evaluate the performances. With a subscale combustion chamber is simpler and more capable of meeting a wide range of testing conditions respect to a full scale one, but the results obtained in a subscale are close to a real rocket combustion chamber.

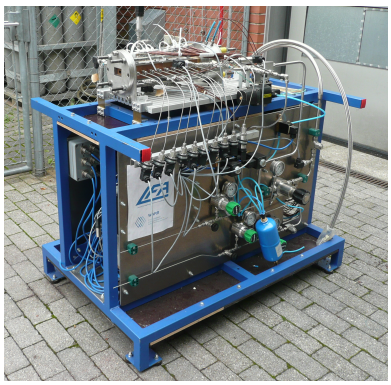

Figura 3.1: Test Facility for the Single-Element Combustion Chamber

The green propellant used is the combination gaseous oxygen (GOx) and gaseous methane (GCH4). The test facility provides nitrogen systems for the control of dome-loaded pressure regulators as well as for purging feed lines prior to and after test. The movable test bench allows experiments with gaseous methane and gaseous oxygen for designed interface pressures up to 50 bar. The present test campaign is performed using two modular combustion chambers, one with a square cross section and the other one with a rectangular cross section. Both combustion chambers are designed for a testing time of up to 4 s, considering a chamber pressure varying from 10 to 20 bar and mixture ratio from 2.6 to 3.4.
The single-element rocket combustion chamber is shown in Figure 3.2a, while the multi-element rocket combustion chamber in Figure 3.2b.

Figura 3.2: Combustion Chamber

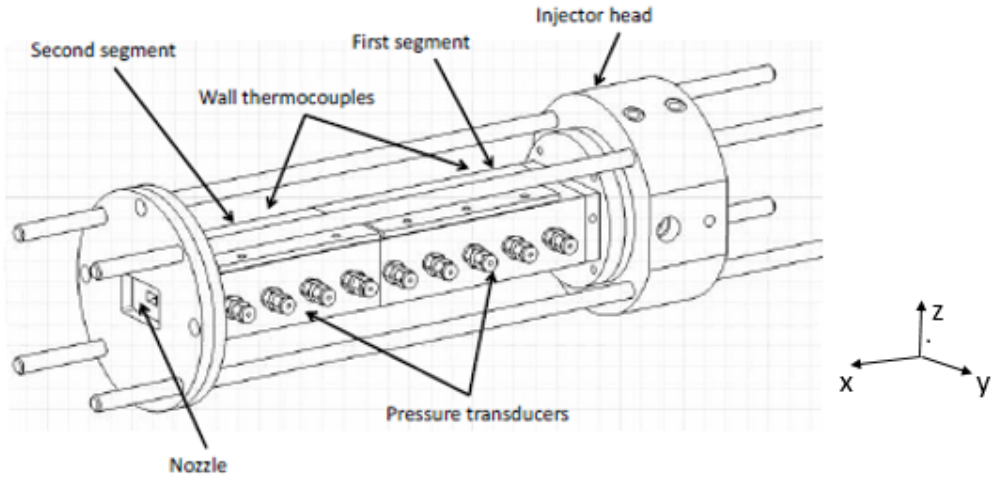

(a) Single-Element Combustion Chamber

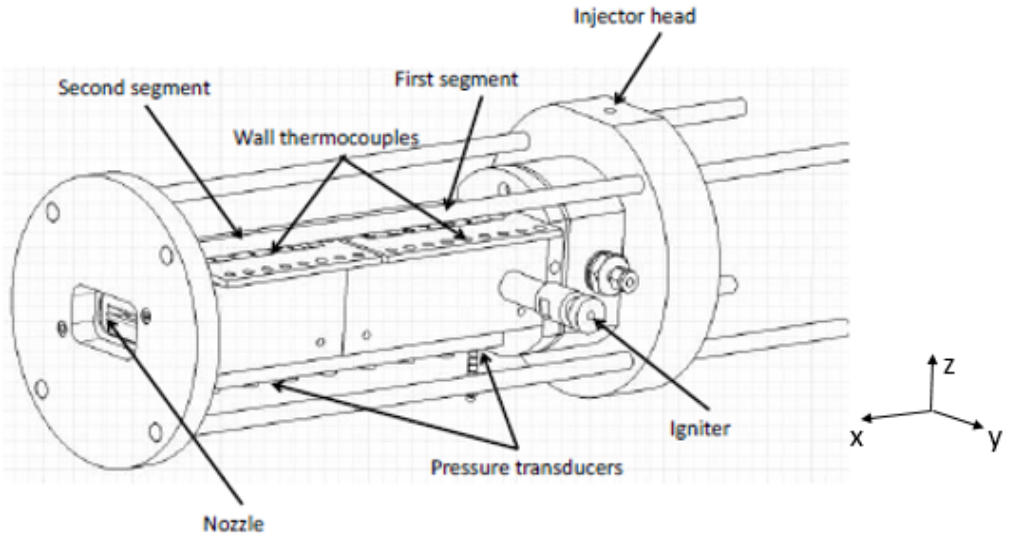

(b) Multi-Element Combustion Chamber

In each chamber, it is possible to distinguish an injector head and a three-piece chamber: a long segment, a short segment and a nozzle segment, which is convergent. Both segments have a constant cross section: a rectangular one for the multi-element combustion chamber and a square cross section for the single-element one.
For both combustion chambers, the material used for the chamber segments and the nozzle segment is the oxygen-free copper (Cu-HCP). The oxygen-free copper is a group of high conductivity copper alloys, which is electrolytically refined, in order to reduce the quantity of oxygen. For the oxygen-free copper, the thermal conductivity, defined in 2.13, is equal to 386 $W/(mK)$. This is the main reason to use it in a capacitive combustion chamber.
In addition to a higher thermal conductivity, the oxygen-free copper has an excellent corrosion resistance and a good electrical conductivity, which permits an higher transfer energy. Other important characteristics of this material are: the resistance to hydrogen embrittlement, an excellent formability, a good weldability..

3.2 Injector design

In a Liquid Propellant Rocket Engine (LPRE), the pressurized propellant, is injected into the combustion chamber, where it burns. After burning, the propellant is expanded through the nozzle. The role of the injector is to mix the propellant as fast and uniformly as possible, avoiding high thermal loads at the combustion chamber walls. Fast mixing implies a shorter combustion chamber. Minimizing the chamber length is a key goal for liquid rocket engine, in order to reduce weight. The decrease of the chamber length is limited by the increase of the local heat transfer to the chamber wall, resulting in possible material burn-out and crack.
The injection geometry is kept constant for single and multi-element rocket combustion chambers. In order to permit a comparison between the two combustion chambers, also the distance between the injector and the wall is considered constant in both configurations. In both configurations, a shear coaxial injector element is used, as shown in 3.3.

In order to have homogeneous conditions, in terms of temperature and pressure, and to reduce the influence of upstream feed lines, two porous plates are placed in the oxidizer and fuel manifolds respectively. Four equally spaced fins at an angle of 45 degrees to the chamber central plane are implemented to center the injector in the faceplate. The chamber sections of the single-element combustion chamber are held together by four tie rods having spiral springs to assure constant clamping force during thermal expansion of the chamber. The entire assembly is capacitive cooled in order to keep the design flexible and more accessible for temperature measurements.

The most important parameters of the two combustion chambers, referred to the injection geometry, are shown in the following table 3.1.

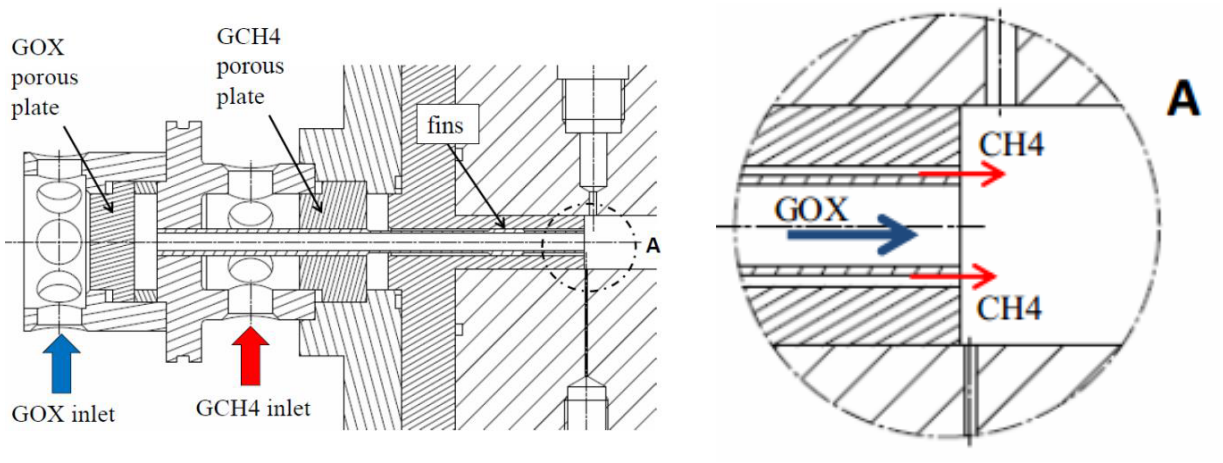

Figura 3.3: Single shear coaxial injector design

Injector configurations	***Value***	***Unit***
GOx Diameter	4	[mm]
GCH4 Outer Diameter	6	[mm]
GCH4 Inner Diameter	5	[mm]
GCH4 Hydraulic Diameter	1	[mm]
GOX post recess	0	[mm]
Injector Area Ratio AGCH4/AGOX	0.69	[-]

Tabella 3.1: Dimensions of the single-element injector

For a shear coaxial injector the mixing efficiency is mainly driven by the shear forces between the propellants. In order to characterize injector conditions, non dimensional numbers, as the discharge coefficient c_d, the velocity ratio VR and the momentum flux ratio J are used. The discharge coefficient is defined as the ratio between the real mass flow rate to the ideal one.

$$c_d = \frac{\dot{m}_r}{\dot{m}_{id}} \tag{3.1}$$

The velocity and the momentum flux ratio represent, respectively, the velocity and the momentum ratio between the methane and the oxygen orifices.

$$VR = \frac{v_{GCH4}}{v_{GOx}} \tag{3.2}$$

$$J = \frac{(\rho v^2)_{GCH4}}{(\rho v^2)_{GOx}} \tag{3.3}$$

Using the same injection geometry for both combustion chambers, these non-dimensional parameters are considered identical in both hardware. Changing the mixture ratio and the propellant mass flow rate, the velocity ratio will change. Typical values of the velocity ratio are

from 0.89 to 1.1. Varying the injection pressure, typical values of the momentum flux ratio are from 0.38 to 0.62.

3.3 Instrumentation

In order to analyse the parameters of both combustion chambers, a large number of sensors with a good space resolution is required. For a better understanding the complex combustion processes, equally spaced pressure transducers are found in both hardware. The pressure sensors provide the measurement of the wall pressure distribution p(z) along the chamber axis. The type of pressure transducers is WIKA A10 and they are connected through metal pipes filled with anti-icing liquid to the chamber protecting the pressure sensors from hot gas contact and icing. The pressure sensors are individually calibrated and operated at a data acquisition rate of 100 Hz.
Another interesting parameters is the chamber temperature along chamber axis, measured thanks to thermocouples, distributed along axial direction. Differently from the single-element combustion chamber, where the thermocouples are situated only in the middle plane, in the multi-element combustion chamber, it is possible to find a distribution of thermocouples also in a transversal axis (along y-axis). Two different thermocouples are situated in both combustion chambers: type T and type K, both have diameters of 0.5 mm. The type K are used to characterize the injector conditions, instead the type T to characterize the combustion chamber. The type T thermocouples are mounted with a regular path of 17 mm in the upper surface of the first and second segment, with a distance of 1 mm (d1) to the hot wall along the central plane of the combustion chamber. Only in the first segment, the type T thermocouples are also situated at 2 mm (d2) and 3 mm (d3) from the hot wall. In the multi-element combustion chamber, the type T thermocouples are also situated in the down surface of the first and second segment.

In order to ensure a continuous contact between the tip of the thermocouples and the base of the hole, a spring loaded system provide a constant force of about 2 N. Furthermore, in the single-element combustion chamber, two coaxial type T thermocouples (Medtherm) are mounted with the hot wall. These Medtherm thermocouples are press-fitted into the chamber wall, in corresponding axial positions in the lower surface of the first segment. In order to ensure a better contact, the tip has been polished to match the flat surface of the combustion chamber. For both combustion chambers, along the chamber axis, it is used the same number of thermocouples, which are seventeen in the upper side with a distance of 1 mm from the hot chamber wall. The nozzle segment has any sensors.
In order to calculate the most important parameters and observe the combustion process, the pressure and temperature sensors are attached at various locations. Thank to connections

Figura 3.4: Position of the thermocouples along chamber axis

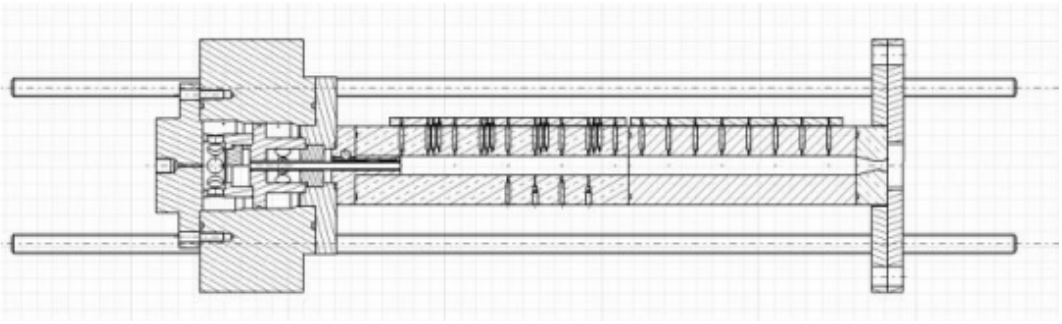

(a) Single-Element Combustion Chamber

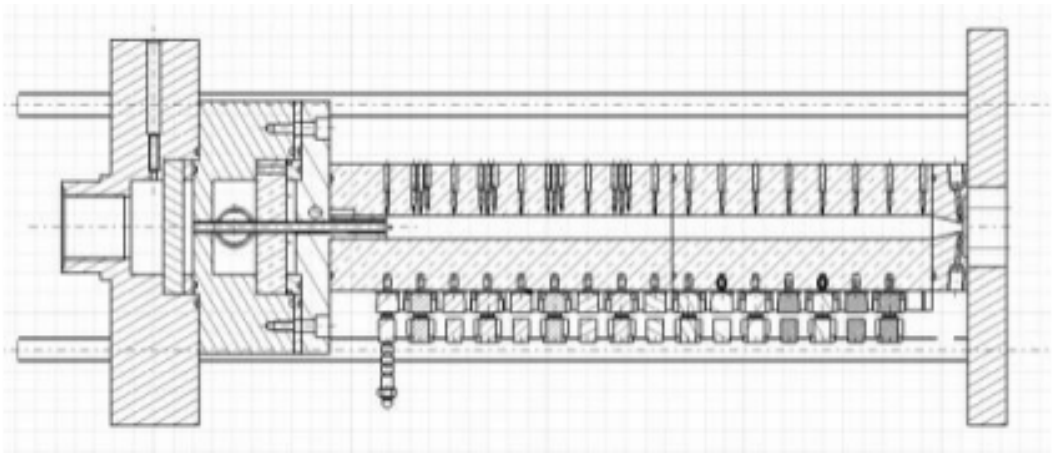

(b) Multi-Element Combustion Chamber

through digital and analog channels, the signal is transmitted to a data acquisition system. A data acquisition system permits to convert the resulting samples into digital numeric values. For this reason, the test apparatus is controlled by LabVIEW software, in order to monitor and record the pressure in the combustion chambers, oxidizer line, and fuel line and to control the ignition system.

3.4 Operating Conditions

Thanks to a torch igniter, it is possible to have the ignition of the two combustion chamber. In the single-element combustion chamber, the igniter is situated in a central axial position at the end of the first segment. In the multi-element combustion chamber, instead the igniter is mounted close to the faceplate. The mass flow rates in the single combustion chamber (GCH4, GOX, GN2 for purge) are determined by sonic orifices in the propellant feed lines. It is necessary to choose the diameters of the feed line, in order to set the propellant mass flow rate. In the multi-element combustion chamber, it is important to calibrate the feed line, prior to the test campaign, with gaseous nitrogen thanks to a Coriolis flow meter. Since the pressure values

upstream the orifice are influenced by the mass flow rates, flow checks are required in order to accurately set the pressure regulators.
The burning time is kept constant for all the tests to 3 s and the similar hot run sequence between the test campaigns has been used, in order to prevent any damage. In fact, for a heat-sink hardware, we have to fix a maximum operating duration, which is determined by the capacity of the materials to absorb heat.
To ensure reliability and repeatability, for each load point, the test will be done at least twice. Different test are performed for both combustion chamber at different values of pressure and mixture ratio but only five load points can be compared. The approach used to test the two combustion chambers is the same: the reference chamber pressure is kept constant and the mixture ratio is changing between 2.6, 3.0 and 3.4. The test is done for two different value of the nominal chamber pressure: 10 and 20 bar. Due to transient nature of the rocket combustion

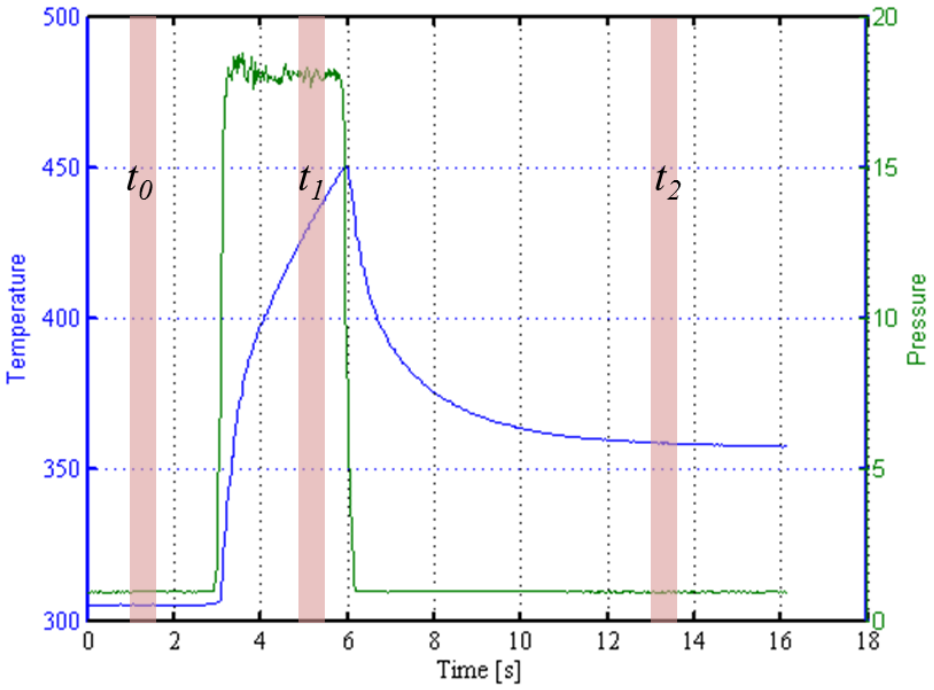

Figura 3.5: Evaluation time

chambers, three time intervals are chosen for the evaluation of the test data. As shown in figure 3.5, during the hot run, three different time are selected: t_0, t_1 and t_2. Characterizing starting conditions, the first time interval t_0 is located prior to ignition of the chamber. The second and main evaluation interval t_1 is located at 2/3 of the hot run, and its duration is 0.5 s. The last evaluation point t_2 is located at the end of the test sequence, in order to have some informations about shut down conditions.

Capitolo 4

Geometry of the two Combustion Chamber

This chapter provides an overview of the investigated subscale rocket combustion chambers, highlight the similarities and the differences, in terms of geometry and non-dimensional parameters.

4.1 Literature Review of Injector Design

For over 50 years, the injector research has been ongoing. The importance of the injector inlet flow is due to a significant influence on combustion performance. For this reason, it is important to understand the injector characteristics in order to determine the nature of the flow in the combustion chamber. In particular, the injector geometry has large influences on flow in the combustion chamber.
Historically, injectors have been designed using experimental techniques and empirical calculations, starting with a design, which is built and tested. Then, some improvements were made based on the results.
One of the most important studies was by Calhoon, who analyses the cold-fire and hot-fire testing to study the injector characteristics. The results of these tests were used along with a number of additional multi-element, in order to design the injector. At the end, also the injector was fabricated and tested for performance and to know heat flux characteristics and combustion stability.
Hutt and Cramer found that the measure of energy release from a single elements flow field is a good approximation of the efficiency of the entire core, if it is assumed that all of the injectors in the core are identical. In particular, the mixing characteristics of a single injector can be used to determine the element pattern and spacing needed for good mixing efficiency.

Calhoon tested also a multiple element injector chamber such that the radial spacing of the elements could be varied. During the cold flow test, it was found that the propellant mixing increased when multiple elements were used.
An other discover was based on the distance between the injector element, element spacing only had a slight influence on the mixing efficiency. In partcular, as the distance between the elements increased, the mixing efficiency increased. This was due to large recirculation regions that brought flow from the well-mixed far region to the near field. When recirculation effects are compensated, Calhoon found that there is no significant difference between the single-element and the multi-element combustion chamber mixing. This, in theory, indicates that a satisfactory combustion analysis can be done using only a single injector.

4.2 Single-Element Rocket Combustion Chamber

A significant portion of injector research has been conducted using experiments consisting of a single-element injector. The single-element analysis is often used as a starting point in modelling full combustor flow. For this reason, single-element injectors are often used in injector experimentation to approximate the mixing effects of the injector.
The single-element rocket combustion chamber, examined in this work, consists of an injector head, two chamber segments and a nozzle segment. The long segment has a length of 174 mm, the short one has a length of 145 mm and it is followed by a nozzle which is 20 mm length. All segments have an outer rectangular cross-section of 85mm x 50mm. The chamber itself has an inner square cross-section of 12 mm x 12 mm with a rectangular throat cross section of 12 mm x 4.8 mm resulting in a contraction ratio of 2.5.

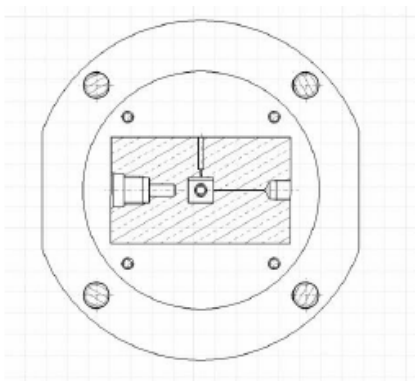

Figura 4.1: Single Element Combustion Chamber

For the single-element rocket combustion chamber nine equally pressure transducers (from PC0 to PC8) are used to measure the static pressure along the chamber axis. Pressure sensors are located with an axial spacing of 34mm, starting from the injector faceplate. In order to measure the temperature in the combustion chamber, seventeen thermocouples are located on

the upper side, along the chamber axis, at 1 mm far from the wall chamber. In addition, other thermocouples are situated at 2 and 3 mm from the hot wall.

4.3 Multi-Element Rocket Combustion Chamber

A multi-element combustion chamber is formed by an array of injector elements, and can be contain hundreds of injector elements. Small changes in the design of the injector and the pattern of elements on the injector face can significantly alter the performance of the combustor. In fact, mixing increases dramatically when a higher number of elements is used. For this reason, the injector elements have to be arranged to maximize the propellant mixing and to lead to overall better performance.

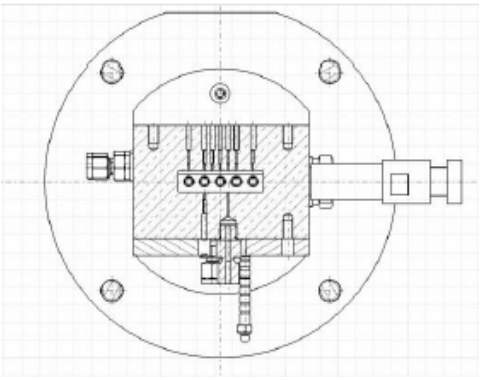

Figura 4.2: Multi Element Combustion Chamber

As the single-element, also the multi-element rocket combustion chamber considered in this thesis, is composed by three different parts: the first segment, the second one and the nozzle. The chamber has an inner cross sectional area of 12 mm x 48 mm, instead the throat cross section has a dimension of 48 mm x 4.8 mm, in order to ensure the same contraction ratio of the single-element combustion chamber of 2.5. Differently from the single-element combustion chamber, the multi-element one has five injectors. The interaction between individual elements plays an important role in fuel/oxidizer mixing characteristics and combustion chamber thermal environment.
In the multi-element rocket combustion chamber, along chamber axis, sixteen pressure transducers and seventeen thermocouples at 1 mm from the hot wall are mounted. All sensors are equidistantly located along the chamber axis starting from the injector faceplate.

Geometric Characteristics	Single-Element	Multi-Element	Unity
Chamber Length	290	277	$[mm]$
Chamber Width	12	12	$[mm]$
Chamber Height	12	48	$[mm]$
Chamber Area	144	576	$[mm^2]$
Chamber Volume	41760	159552	$[mm^3]$
Chamber Wall Area	13920	33240	$[mm^2]$
Throat Width	12	48	$[mm]$
Throat Height	4,8	4,8	$[mm]$
Throat Area	57,6	230,4	$[mm^2]$
Chambera Contraction Area Ratio	2,5	2,5	[-]
Chamber Volume to Wall Area Ratio	3	4,8	[-]
Characteristic Length	749	717	$[mm]$
Chamber Hydraulic Diameter	12	19,2	$[mm]$

Tabella 4.1: Geometric comparison between the two rocket combustion chamber

4.4 Similarities and Differences

One of the most important parameter, which influences the efficiency of a combustion chamber, is the geometry. For this reason, it is necessary to consider the two most important features of the combustion chamber: its length and its shape. The length of the combustion chamber influences the overall vaporization and mixing efficiency. In particular, increasing the chamber length can increase the overall performance but often at a much slower rate, depending on the injector element design.

The two rocket combustion chambers have different geometric parameters as length, height and width, but keeping the same contraction area ratio. Thanks to the same contraction ratio and the same injector design, the mixing process in the developing combustion flow field is kept similar. As a consequence, thanks to the relation between the Mach number and the contraction area ratio, as shown in Equation 2.11, also the Mach number is the same for the two combustion chambers and it is equal to 0.24 . For a Mach number below a value of 0.3, the flow is quasi-steady and isothermal. As a consequence, compressibility effects will be small and it is possible to consider the flow as incompressible.

A consequence of different geometric dimensions is the characteristic length which is higher for the single-element combustion chamber; this confirms higher frictional and thermal losses in the single-element one. Related to characteristic length, also the residence time is different between the two combustion chambers, according with Equation 2.10.

Another consequence of the two different geometries is the amount of heat absorbed by the chamber walls. In fact, the ratio between the chamber volume V_c and the surface area A_w is higher for the multi-element combustion chamber. This parameter has an important effect

on the heat transfer, as shown in equation 2.17, because it means that the multi-element combustion chamber has a lower temperature gradient in the time (dT/dt), due to less present surface. In fact, in the single-element combustion chamber we have just an injector which is surrounded by four wall. On the contrary, in the multi-element one, five injectors are presented, so each injector is surrounded, at least, by two walls and one flow, coming from the close injector.

Another similarity is based on the propellant used, which is the same for both combustion chambers: GCH4/GOx. For this reason, all propellant properties are the same. All fluid properties are the same between the two combustion chambers. As a consequence, Prandtl and Schmidth numbers which are functions of the fluid properties have to be equal for the two combustion chamber. This means that the momentum and thermal effects have to be similar between the two combustion chambers.

Due to the different geometries, also the hydraulic diameter,as confirmed by Equation 2.12, is higher for the multi-element rocket combustion chamber. This means a different Reynolds number between the two combustion chambers, therefore also the Nusselt number is different, as shown by the correlation of Cinjarew in Equation 2.15.

Capitolo 5

Elaboration and results

In this chapter, the result of the experimental work are presented, showing the pressure and the temperature trend along time and chamber axis. The main focus is to find similarities and differences between the two combustion chambers. Due to the transient behaviour of the rocket combustion chambers, mean values are calculated for evaluating performance parameters, temperature and heat flux distributions.

5.1 Pressure Trend along Chamber Axis

In this section the pressure behaviour for the two different combustion chambers along the chamber axis is reported. The pressure is measured through some pressure transducers, which are different as numbers for the two combustion chambers. In particular, the single-element combustion chamber uses nine pressure sensors and in the multi-element one, sixteen transducers are mounted. For this reason, the resolution of the pressure trend shown by the multi-element combustion chamber is more accurate respect to the single-element one.

Starting the test, the propellant is injected into the combustion chamber through the injector. Due to the abrupt variation of the cross section, the flow decelerates and the pressure increases, so the flow change its direction, creating a re-circulation zone. The re-circulation zone acts to improve the mixing of the propellant in order to reduce the instabilities in a combustion process. Then, the combustion process starts and lasts three seconds. Due to combustion process, the propellant injected accelerates, from the injection velocity to the hot gas velocity. According to Bernoulli's equation, the static pressure will decrease until the end of combustion. The end of combustion is confirmed by a flattening of the pressure trend over chamber axis. It is not possible to determine exactly the stagnation point, because the pressure transducers are located in different axial positions between the two combustion chambers.

Figura 5.1: Pressure trend along z axis at 10 bar

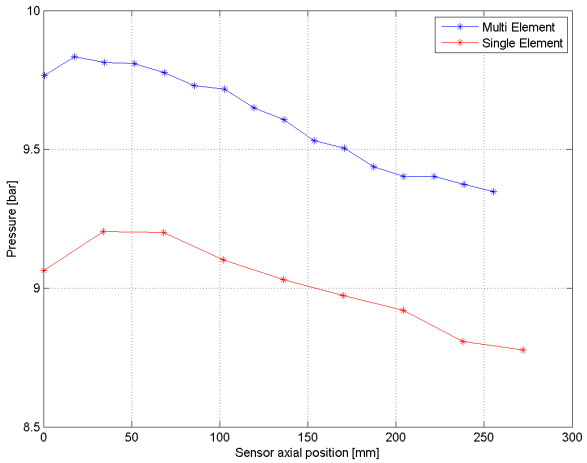

(a) 10 bar and O/F=2.6

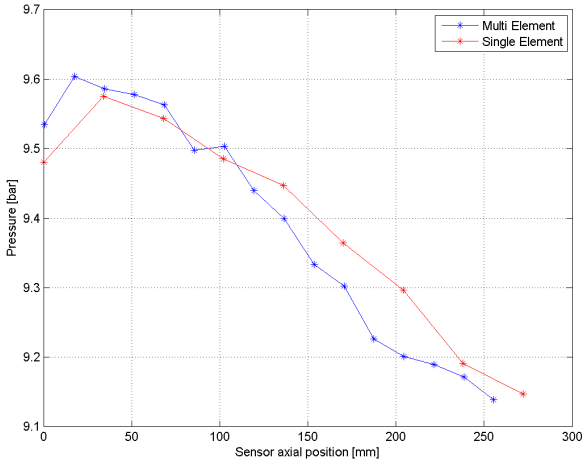

(b) 10 bar and O/F=3.0

The first difference between the two combustion chambers is given by the number of sensors used. In the previous figures 5.1a, 5.1b, 5.2a, 5.2b, 5.2c, the pressure trend over chamber axis is reported, for five load points: pressure at 10 and 20 bar and mixture ratio equal to 2.6 and 3.0 and the last one has a pressure of 20 bar and a mixture ratio of 3.4.
For the two combustion chambers, different values of pressure are reached and, in any case, the nominal pressure is not achieved. For the nominal 20 bar tests, 5.2a, 5.2b, a larger gap in pressure (about 1 bar) is observed and the single-element combustion chamber reaches higher values of pressure respect the multi-element one. On the other hand, for the nominal 10 bar tests and at $O/F = 2.6$, the multi-element combustion chamber approaches the nominal value more than the single element one. This pressure difference is also presented in the last load point, in Figure 5.2c. Differently from the other load points, with a mixture ratio of 3.4, the multi-element combustion chamber achieves higher value of pressure.

Figura 5.2: Pressure trend along z axis at 20 bar

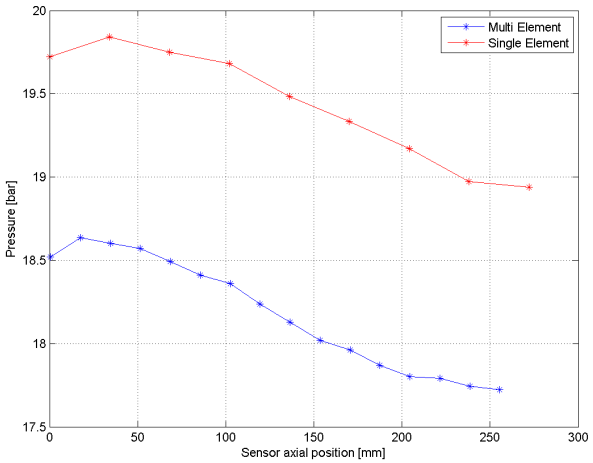

(a) 20 bar and O/F=2.6

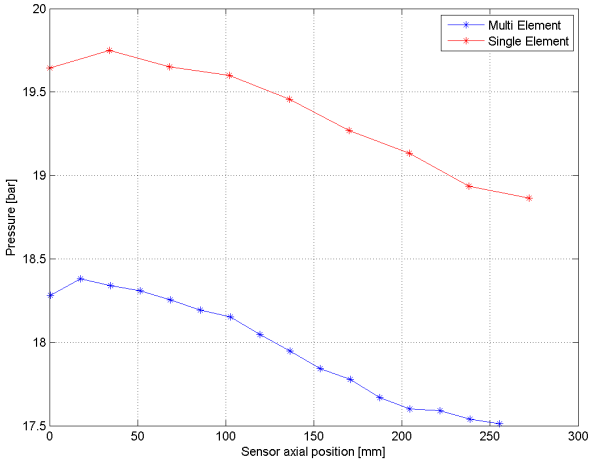

(b) 20 bar and O/F=3.0

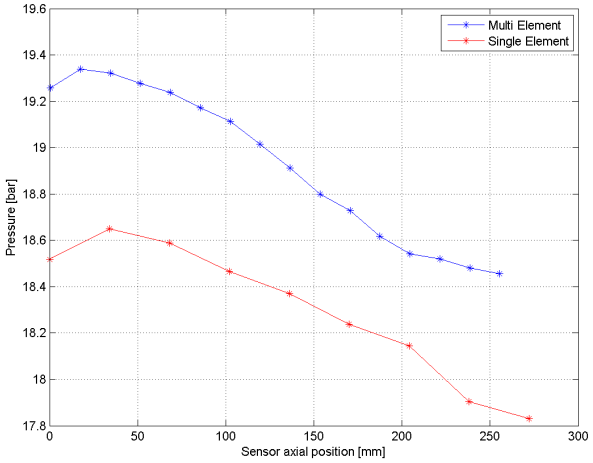

(c) 20 bar and O/F=3.4

Figura 5.3: Normalized pressure at 10 bar and O/F=2.6

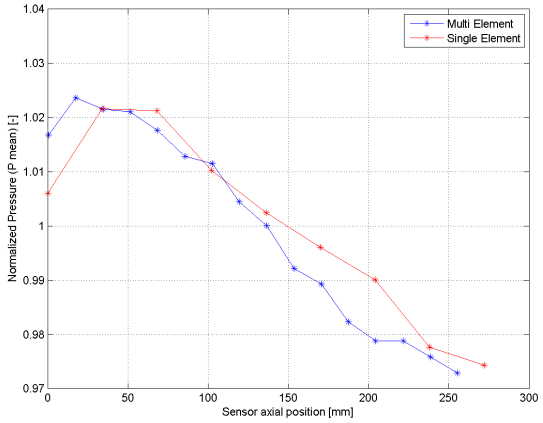

(a) Normalization respect p_{mean}

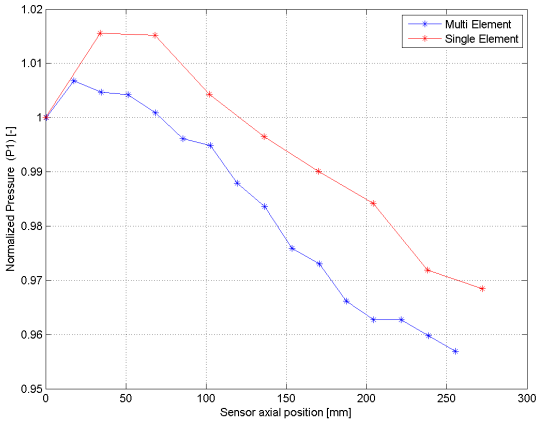

(b) Normalization respect p_1

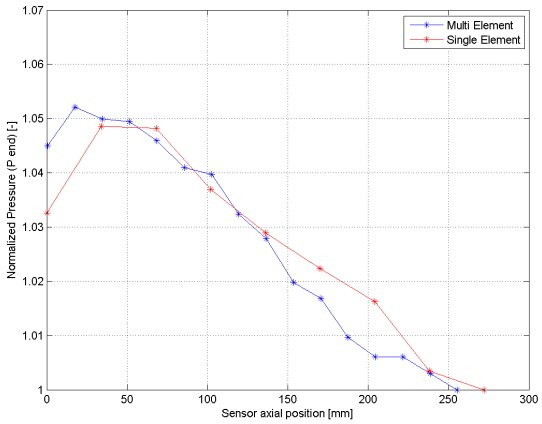

(c) Normalization respect p_{end}

In order to better understanding the behaviour of the two combustion chambers, it is necessary to normalize the chamber pressure. Three different normalizations are chosen with respect to the mean pressure, the pressure measured by the first transducer and the pressure measured by the last transducers.

The first normalization is obtained dividing every value of pressure, given by each sensor, to the mean value of pressure. In this way, it is possible to have a trend of the chamber pressure, as a function of the deviation of the pressure from the mean value. For this reason, this normalization represents the best solution. Dividing each pressure value by the value measured by the first pressure transducer (PC0), the second normalization is given. This normalization is useful to highlight the end of pressure trend, in order to analyse the end of the combustion process. With the second normalization, the error committed is due to make equal the injector velocities of the two hardware, which are different in a real case. The third normalization is based on the ratio between each pressure value and the pressure measured by the last transducer (PC8 for the single-element combustion chamber and PC15 for the multi-element one). In this

way, it is possible to investigate the re-circulation zone, due to the inlet propellant. The third normalization generates the same end pressure, producing an error on the combustion efficiency value.
The Figures 5.3, 5.4, 5.5, 5.6 and 5.7 show the normalized pressure distribution along the chamber axis for different mean chamber pressures and mixture ratios.
Analysing the pressure trend along chamber axis, it is possible to observe that at 10 bar and $O/F = 2.6$, reported in Figure 5.3, the recirculation zone is larger in the single-element combustion chamber, respect to the multi-element one. Thanks to the higher injector velocities for methane and oxygen, the flow decelerates rapidly resulting in a higher pressure according to Bernoulli's equation. For the single-element combustion chamber, the pressure drop is bigger than for the multi-element one, as showing in Figure 5.3b.
The stagnation point, shown by the pressure peak, corresponds to the axial position of the re-circulation zone. Moreover, the recirculation zone of the single-element combustion chamber seems to be larger determining a longer residence time, which indicates a better mixing of the propellant, but it is not possible to take an exact conclusion, due to a different number of pressure sensors in the two different hardware.

Refer to Figure 5.4b, the recirculation zone is more significant in the single-element combustion chamber. This means that a difference exist between the two combustion chambers, not only as pressure drop, as shown in Table 5.1, defined as the different between the pressure peak and the pressure of the first sensor (PC0), but also as length. For this reason, the recirculation zone in a single-element combustion chamber lasts further along the chamber axis for a combustion with a nominal pressure at 10 bar. The mixture ratio influences the recirculation zone; in fact increasing the amount of oxygen, respect to the methane, the pressure peak and the length of the recirculation zone decrease, as shown in Figures 5.3b and 5.4b. Thanks to Figures 5.3c and 5.4c, at a pressure of 10 bar, the multi-element combustion chamber has a pressure decay, as difference between the pressure measured by the first sensor and the pressure measured by the last sensor, higher than the one of the single-element chamber. Increasing the mixture ratio, the difference of the pressure decay, between the two combustion chambers, decreases (See Table 5.1).

Investigating the normalized pressure behaviour at 20 bar, the recirculation zone is decreasing respect to the previous conditions. In particular, the pressure peak, due to the presence of the recirculation zone, is decreasing and it is almost similar between the two combustion chambers. In addition, it is possible to evaluate a longer recirculation zone for the single-element combustion chamber respect to the multi-element one, as shown in Figures 5.5b and 5.6b.
Increasing the mixture ratio, from 2.6 to 3.0, keeping a constant pressure of 20 bar, the re-circulation zone ends for a lower value of the chamber axis for the single-element combustion chamber.

Figura 5.4: Normalized pressure at 10 bar and O/F=3.0

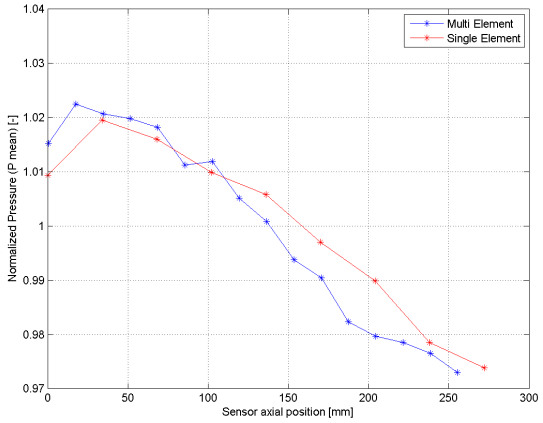

(a) Normalization respect p_{mean}

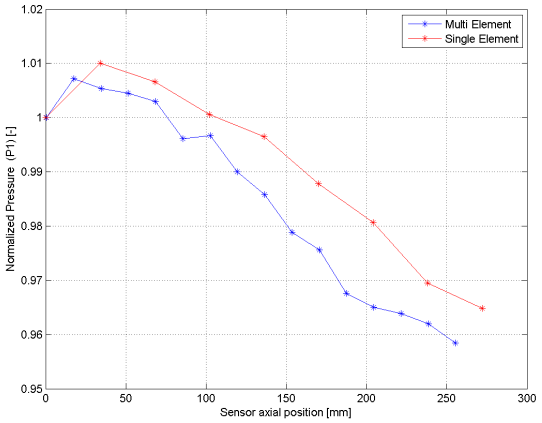

(b) Normalization respect p_1

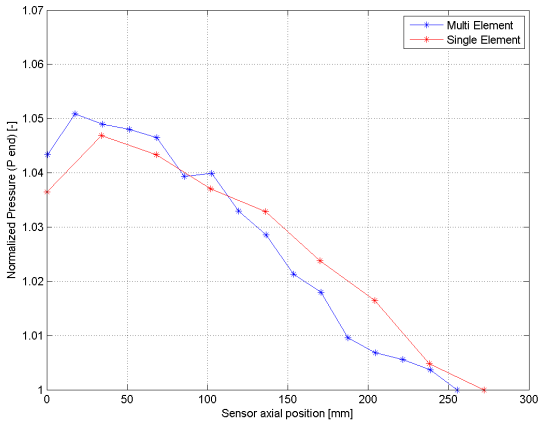

(c) Normalization respect p_{end}

According to Figures 5.3a, 5.4a, 5.5a, 5.6a, 5.7a, the flattening of the pressure is more evident in the multi-element combustion chamber. A flattening in the pressure distribution along the chamber axis indicates the end of combustion, which is presumed for all load points at the last transducer pressure (PC8 for the single-element combustion chamber and PC15 for the multi-elment one). In fact, it is possible to observe a variation of the pressure gradient along chamber axis. For both combustion chambers, a tendency of the pressure flattening is observed for changing chamber pressure and mixture ratio. In particular, increasing the pressure from 10 to 20 bar, the 'plateau' of the pressure is more visible. Also the mixture ratio influences the flattening of the pressure, but in the opposite trend. Increasing the mixture ratio, the end of combustion is moving further downstream. The flattening of the pressure is more pronounced and it occurs first for the multi-element combustion chamber, respect to the single-element one.

Comparing the two combustion chambers, as shown in Table 5.1, it is possible to denotes that the multi-element combustion chamber has a higher pressure decrease (dp/dz), which

Figura 5.5: Normalized pressure at 20 bar and O/F=2.6

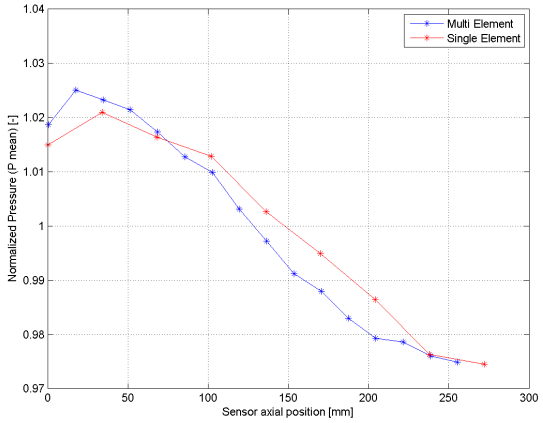

(a) Normalization respect p_{mean}

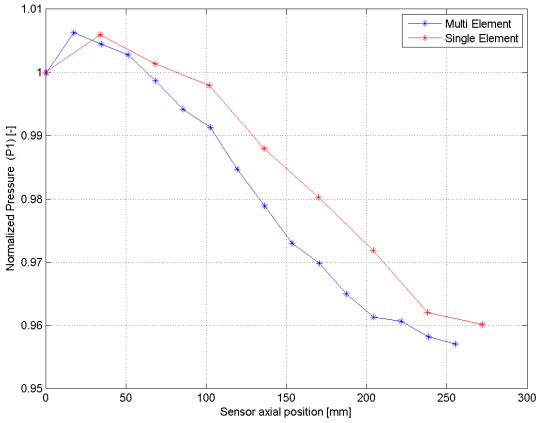

(b) Normalization respect p_1

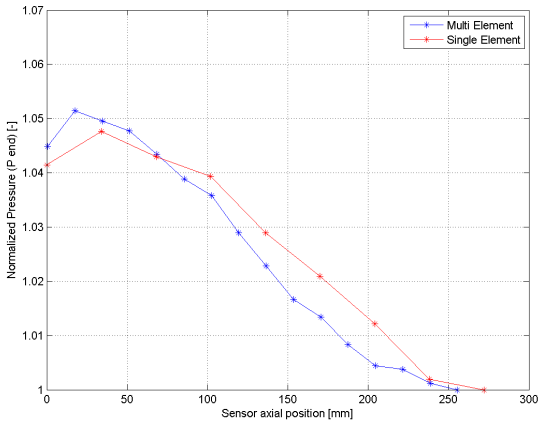

(c) Normalization respect p_{end}

consequently results in a higher hot gas velocity. This is compensated by the lower injection velocities for the multi-element chamber, yielding to the same combustion velocity in the end. For the single-element chamber, increasing the chamber pressure from 10 to 20 bar increases the pressure decay, which is defines ad the difference between the first pressure value (PC0) and the last pressure value (PC8), shown in Figures 5.3c, 5.4c, 5.5c, 5.6c, 5.7c. On the contrary, in the multi-element one, when increasing the chamber pressure, this effect does not really shown. Furthermore, increasing the mixture ratio a decrease in the pressure gradient dp/dz is visible, so the pressure decay is more evident in both combustion chambers.
Concluding, the pressure decay is more apparent in the multi-element combustion chamber to respect the single-element one, as shown in the pressure trend analysis and the recirculation zone is more pronounced in a single-element combustion chamber, due to the presence of the corners, which intensify the effect. Due to a larger recirculation zone, the residence time (See Equation 2.9) in the single-element combustion chamber increases.

In the Table 5.1, the pressure drop is reported. It is defined as the difference between the

Figura 5.6: Normalized pressure at 20 bar and O/F=3.0

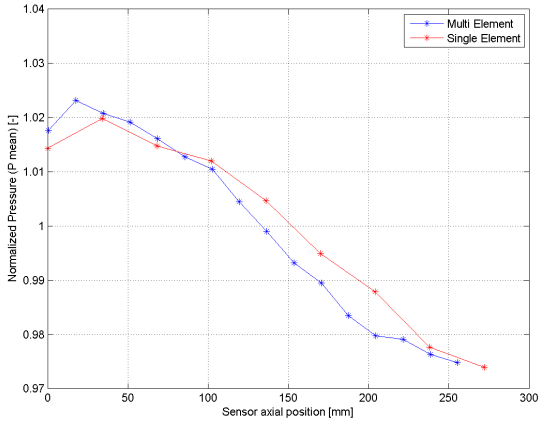

(a) Normalization respect p_{mean}

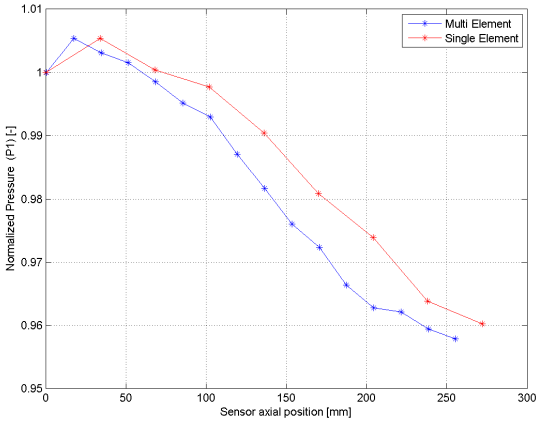

(b) Normalization respect p_1

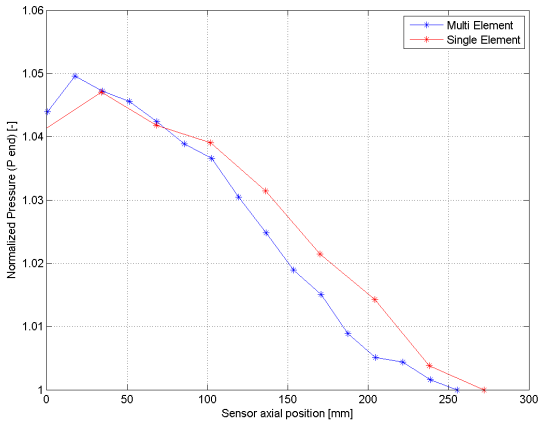

(c) Normalization respect p_{end}

Tabella 5.1: Pressure Drop

	10 - 2.6	**10 - 3.0**	**20 - 2.6**	**20 - 3.0**	**20 - 3.4**
Single Element	0,1407	0,0953	0,1169	0,1062	0,1328
Multi Element	0,0662	0,0697	0,117	0,099	0,08

maximum pressure value measured and the pressure value measured by the first transducer (PC0). The different conditions are shown. Increasing the mixture ratio, at 10 bar, the pressure drop decreases. At 20 bar, a lower difference exists between the two different combustion chambers.

Due to the different geometries, the single-element and the multi-element combustion chambers have a different characteristic velocity, which leads to a different combustion efficiency. In fact, the presence of five injector in the multi-element combustion chamber permits a higher mixing efficiency and a less influence of the corners in the flow behaviour.
Due to the different mass flow rate injected in the two combustion chambers, another possible

Figura 5.7: Normalized pressure at 20 bar and O/F=3.4

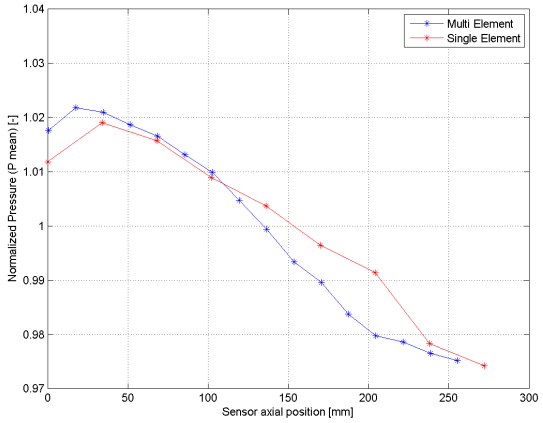

(a) Normalization respect p_{mean}

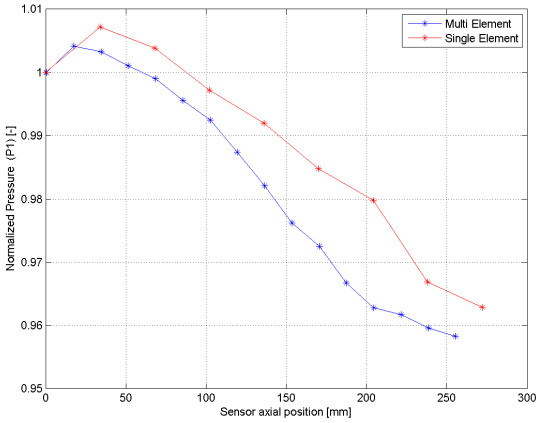

(b) Normalization respect p_1

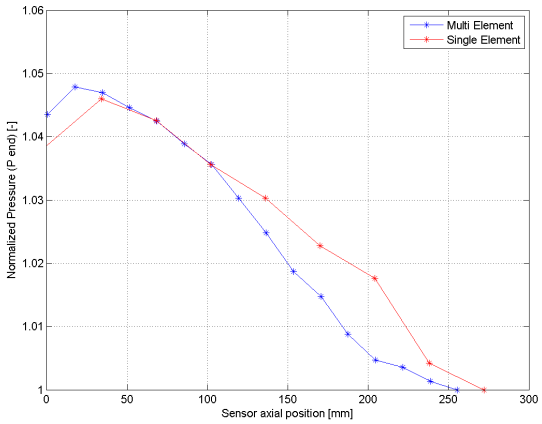

(c) Normalization respect p_{end}

normalization is given, in order to better understanding the pressure trend along the chamber axis. In the following Figures 5.8 and 5.9, the normalized pressure profile along chamber axis is reported, for different value of pressure and mixture ratio conditions: the pressure varies from 10 to 20 bar and mixture ratio from 2.6 to 3.4. The normalization is based on a correction of the chamber pressure as shown in the following Equation 5.1, according to the definition of the characteristic velocity, expressed by Equation 2.4.

$$p_{corr}(z) = p(z)\frac{(\dot{m}c^*)_{theo}}{(\dot{m}c^*)_{calc}} \tag{5.1}$$

According to the Equation 5.1, the corrected pressure of the two combustion chambers is calculated by the ratio between an ideal condition to a real one, which leads to an increasing of the chamber pressure trend, for the tests analyzed.

The Figures 5.8a and 5.8b report the corrected pressure along chamber axis for the two com-

Figura 5.8: Normalization respect to the mass flow rate

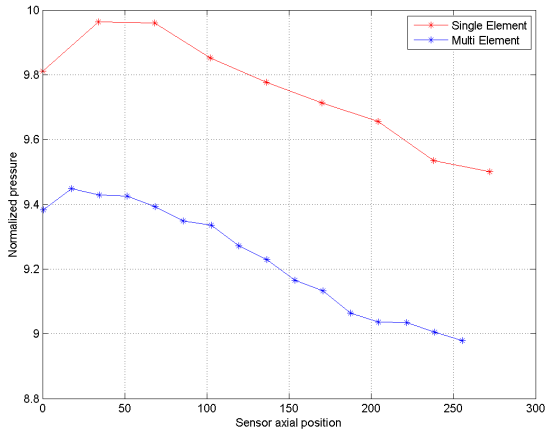

(a) Pressure of 10 bar and O/F=2.6

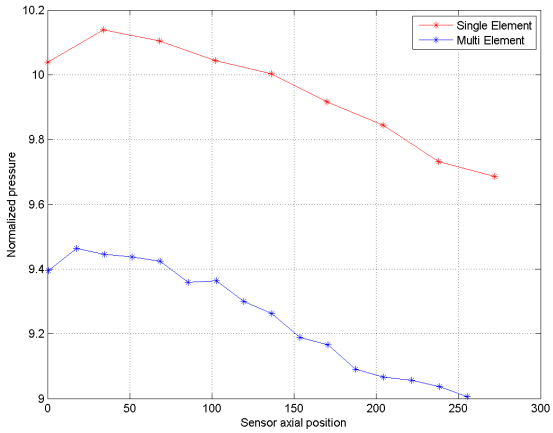

(b) Pressure of 10 bar and O/F=3.0

bustion chambers, considering a mixture ratio of 2.6 and 3.0 respectively and a pressure of 10 bar. In both load points, it is possible to observe a higher value of the chamber pressure for the single-element combustion chamber.

Figura 5.9: Normalization respect to the mass flow rate

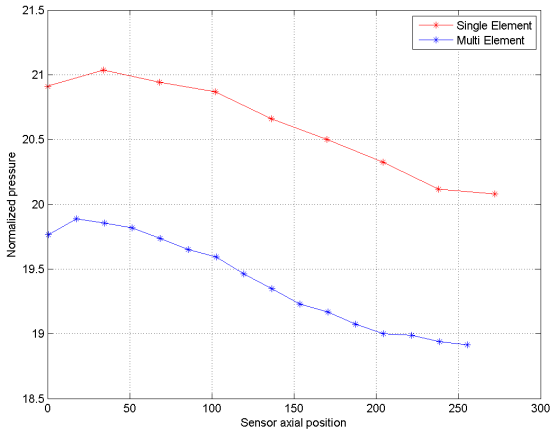

(a) Pressure of 20 bar and O/F=2.6

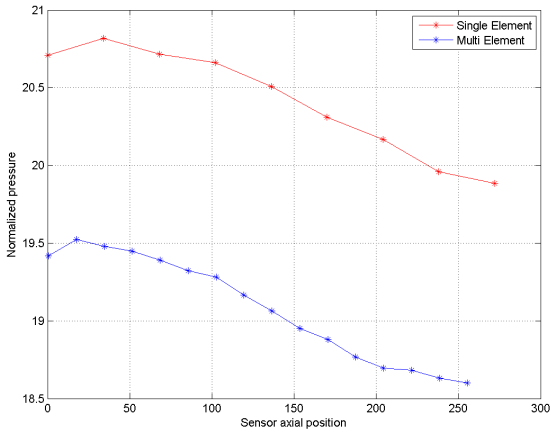

(b) Pressure of 20 bar and O/F=3.0

Increasing the mixture ratio, considering a constant pressure value, the difference between the chamber pressure values of the two combustion chambers increases. For the load point at 10 bar, increasing the mixture ratio, the chamber pressure increases for both combustion chambers. On the contrary, for a pressure equal to 20 bar, the pressure values along chamber axis decreases, when the mixture ratio increases, in the single-element and in the multi-element combustion chambers.

5.2 Temperature Trend along Chamber Axis

In this section, the temperature profile along the chamber axis is analysed. Although many thermocouples are mounted on the chamber surface, at different distances from the hot gas wall for the multi-element combustion chamber, for these examinations thermocouples positioned at 1mm distance from the hot gas on the upper side of the chambers are used, in order to compare the two hardware.

For capacitive cooled hardware, a higher initial temperature leads, for the same test duration, to a higher temperature level. Therefore looking at the temperature difference minimizes these influences. Along the chamber axis, a continuously rising temperature is observed, until the end of combustion is reached. In the last part, close to the nozzle, a flattening of the temperature curve can be identified, which indicates the completeness of the reaction process, as shown in Figure 5.10.

Figura 5.10: Temperature trend along chamber axis

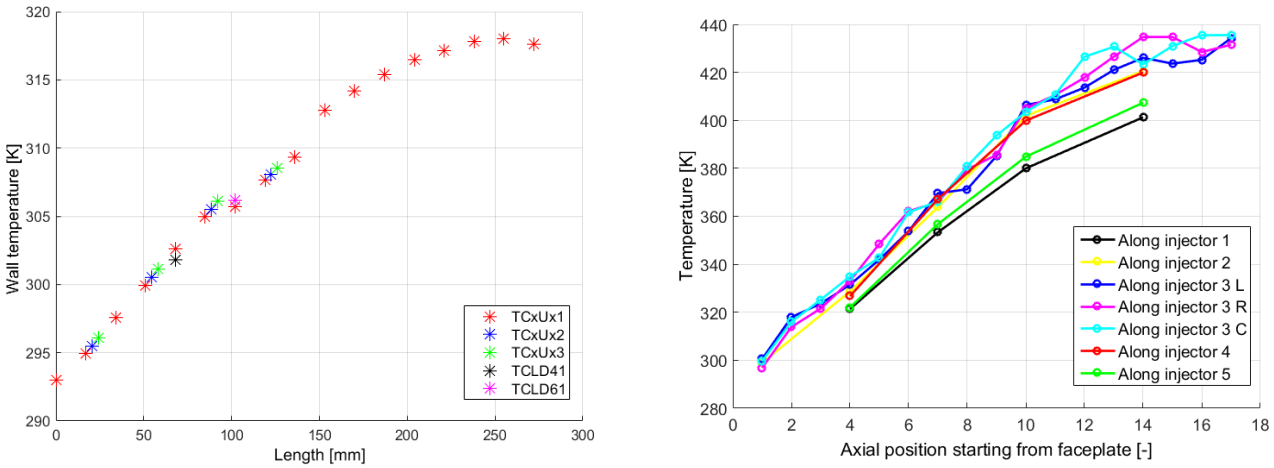

In Figure 5.10, the temperature distribution along chamber axis for the complete set of thermocouples situated in the first and second segments at 1 mm far from the hot gas wall is reported, considering a load point of 20 bar and O/F=2.6. The Figure situated on the left side concerns the single-element combustion chamber, instead the Figure on the right side, the multi-element one. It represents an example at 10 bar and O/F=2.6, where it is confirmed the expected temperature trend. In order to minimize the influence of the start-up transient, the temperature signals have been calculated as a mean value over a 0.5 s time interval, taken at 2/3 of the total run time. The run time is defined as the time duration, when both GCH4 and GOX propellant valves are fully opened.

In order to compare the two different combustion chambers, the temperature profile along the chamber axis refers to the injector situated in the middle position, along y axis, is chosen. In

Figura 5.11: Temperature trend at 10 bar and O/F=2.6

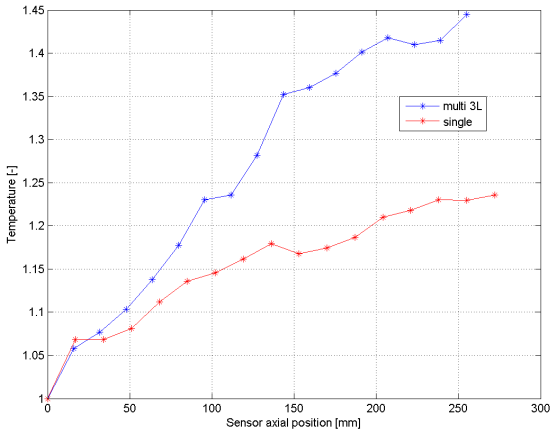

(a) 3L

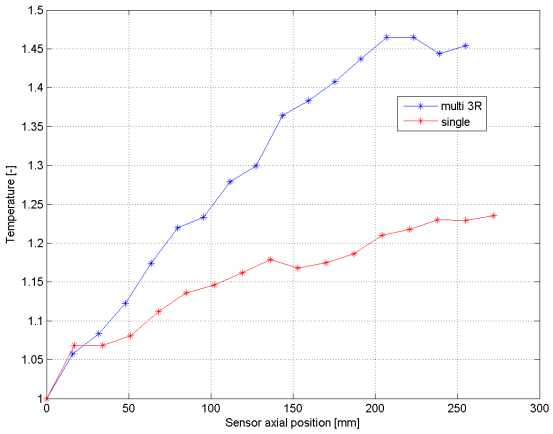

(b) 3R

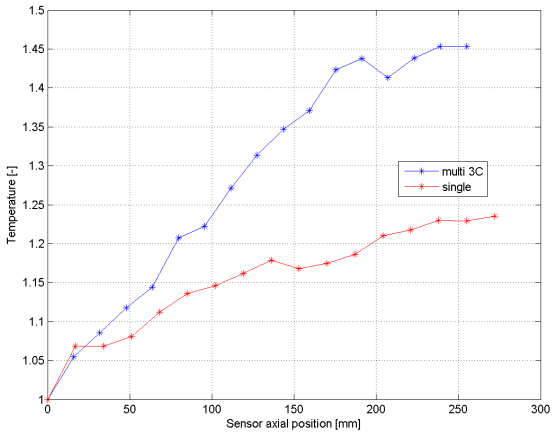

(c) 3C

particular, for the multi-element combustion chamber, has a great interested the temperature measured by the thermocouples, situated in the middle of the chamber and in the left and right side respect the middle one (TCXUXX3C01, TCXUXX3L01, TCXUXX3R01). For the single-element, the temperature profile regarding the only propellant injector, is analysed.
In the next Figures 5.11, 5.12, 5.13, 5.14 and 5.15, the temperature distribution is reported. Different values of temperature are achieved in the two combustion chambers: in particular, in the multi-element one, a higher temperature is reached respect to the single-element one. The difference between the final and the initial temperature is almost twice for the multi-element combustion chamber respect to the single-element one.
In each condition, for the last three thermocouples a clear flattening of the temperature is visible, for both chamber pressures, which indicates the end of the combustion process.
For the first load point (10 bar and O/F=2.6, shown in Figure 5.11), the temperature distribution, measured by the three different thermocouples (3L, 3C and 3R) is quite similar. It is characterized by an initial increasing of temperature along the chamber axis, which is simi-

Figura 5.12: Temperature trend at 10 bar and O/F=3.0

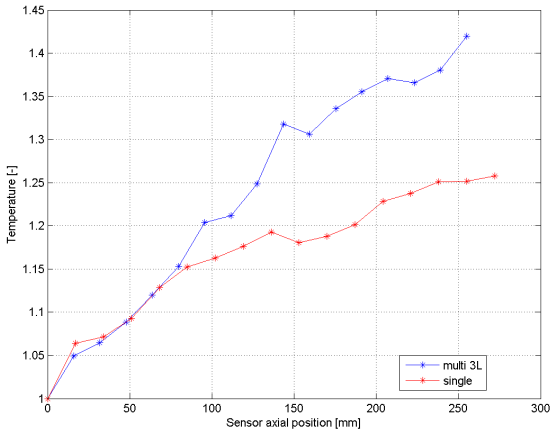

(a) 3L

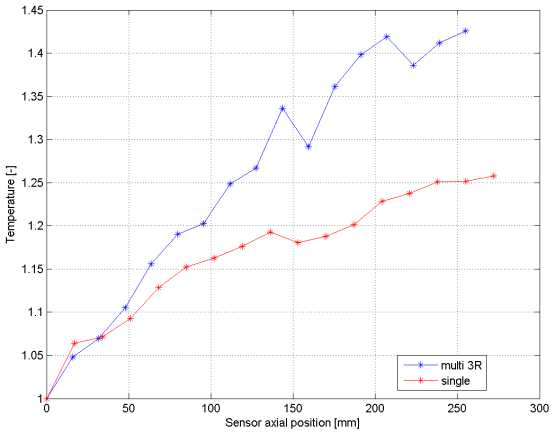

(b) 3R

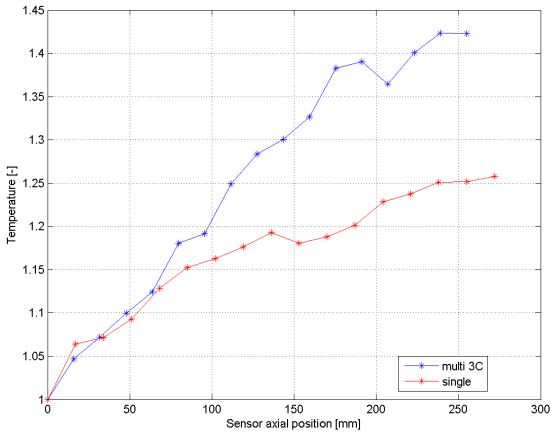

(c) 3C

lar with the one referred to the single-element combustion chamber. Then, the temperature increases more for the multi-element than for the single-element one. This increment of the temperature can be attributed to the presence of the flow, coming from the other injectors, due to the different number of injectors, which characterizes the multi-element combustion chamber. The flattening of the temperature is more visible for the thermocouples mounted in the middle position and in the right side.

Increasing the mixture ratio, from 2.6 to 3.0, maintaining the same pressure of 10 bar, the difference of the temperature, between the temperature measured by the first thermocouple and the one measured by last thermocouple, increases for the single-element combustion chamber and decreases for the multi-element one. For this load point, the temperature distribution of the multi-element combustion chamber follows the one of the single element one until the sixth sensor.

In addition, in this condition, a flattening of the temperature trend is visible just for the last

Figura 5.13: Temperature trend at 10 bar and O/F=2.6

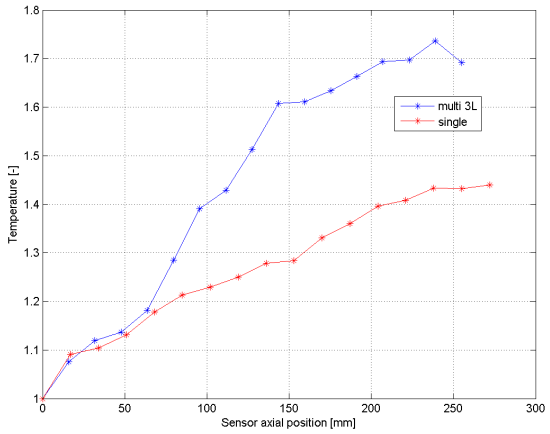

(a) 3L

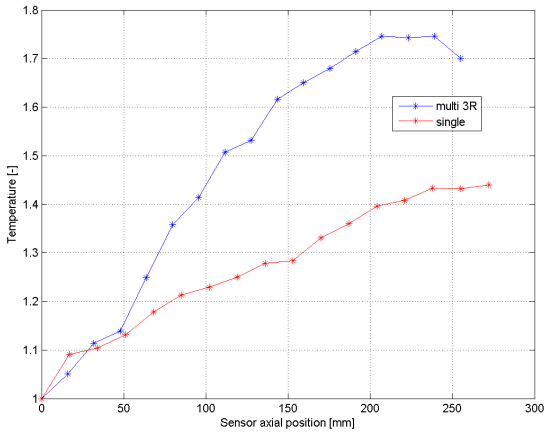

(b) 3R

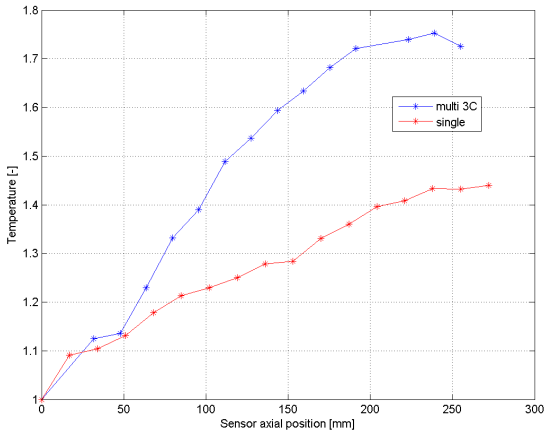

(c) 3C

thermocouples, so in the final part of the combustion chamber.
Comparing the temperature profile of the two combustion chambers at 20 bar, as shown in Figure 5.13, the temperature level seems to be the same for both chambers, until the fifth thermocouple. Due to a steeper increase in temperature over length happening in the following thermocouples, the multi-element combustion chamber achieves higher temperature level.
Increasing the chamber pressure from 10 to 20 bar, the temperature level increases, both for the two combustion chambers. For the last four thermocouples a clear flattening is observed in Figure 5.13, which indicates the end of combustion which appears further upstream and more pronounced for the multi-element combustion chamber. At 20 bar, also the temperature profile measured by the thermocouple situated on the left side (TCXUXX3L01), shows a 'plateau' at the end of chamber, as shown in Figure 5.13a.

The following load point (Pressure of 20 bar and O/F=3.0) is reported in Figure 5.14. As in the previous cases, it is possible to observe a temperature trend, which is similar between

Figura 5.14: Temperature trend at 10 bar and O/F=3.0

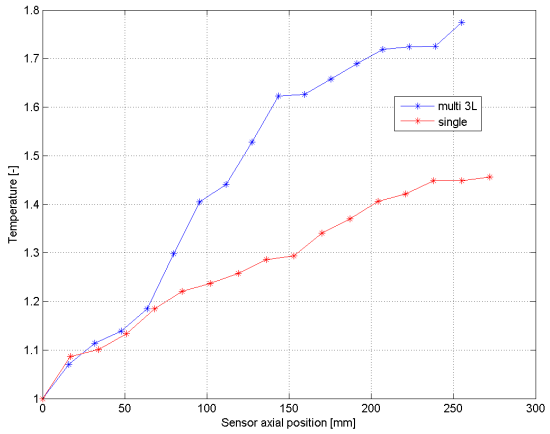

(a) 3L

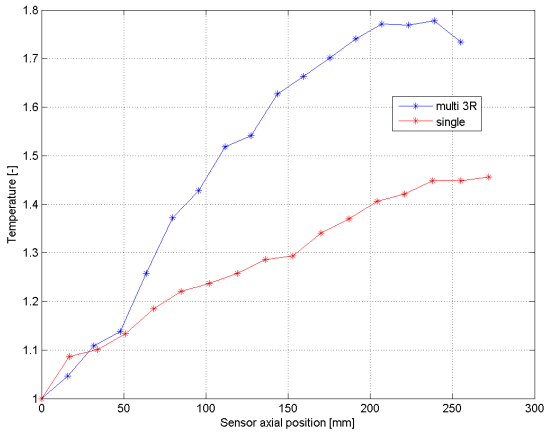

(b) 3R

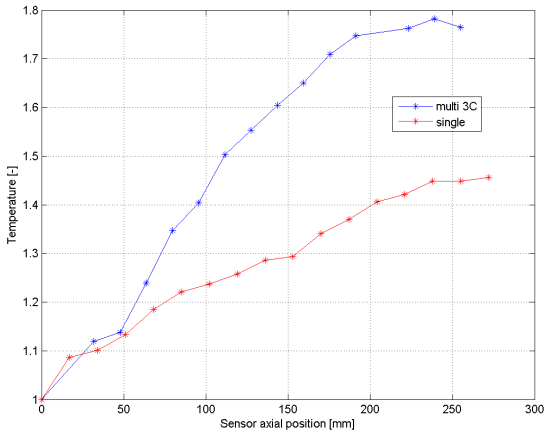

(c) 3C

the two combustion chambers until the fifth thermocouple. Then, the temperature gradient along the chamber axis increases more in the multi-element combustion chamber respect to the single-element one.

Increasing the mixture ratio from 2.6 to 3.0, confirmed by Figures 5.13a and 5.14a, the flattening of the temperature is not visible for the sensor mounted on the left side. The end of combustion is confirmed by the temperature distribution referred to Figures 5.14c and 5.14b, where a 'plateau' is visible. When comparing this flattening of the multi-element combustion chamber to the single element one, for both load points the flattening is more pronounced for the multi-element chamber.

Respect to the previous case, shown in Figure 5.13, a slight higher temperature level is achieved for a higher mixture ratio, for both combustion chambers, as demonstrated in Figures 5.14 and 5.15.

A higher temperature gradient over length dT/dz for the multi-element combustion chamber is expected. Therefore the second segment shows higher temperature levels and the earlier

completed combustion can be observed by the earlier flattening of the temperature profile.

Figura 5.15: Temperature trend at 10 bar and O/F=3.0

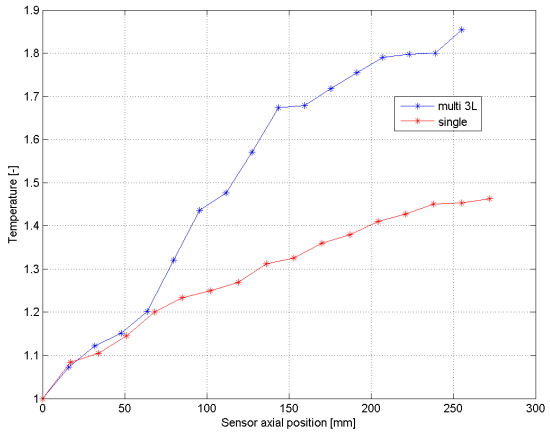

(a) 3L

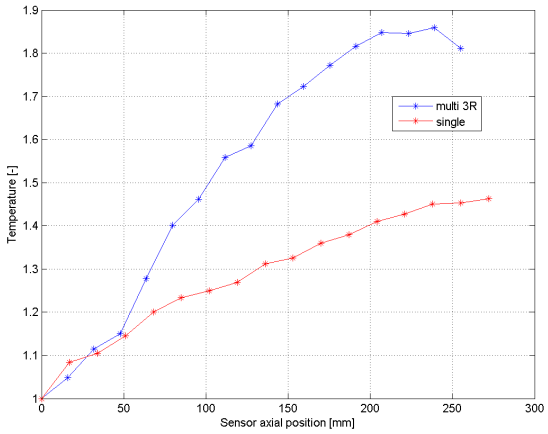

(b) 3R

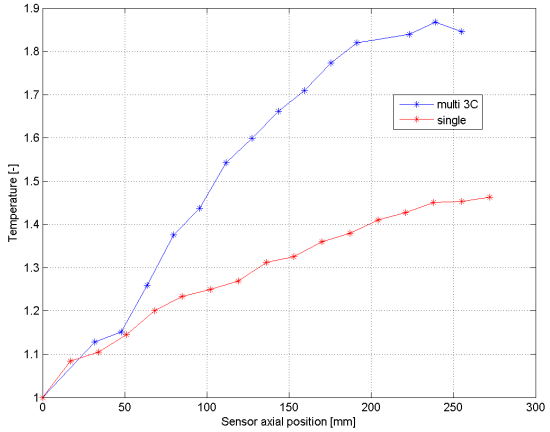

(c) 3C

To conclude, the last load point is shown in Figure 5.15. Also in this case, the multi-element combustion chamber achieve a higher temperature value.
The temperature profile between the single-element and the multi-element combustion chambers is similar in the first part of the chambers, close to the injectors. Moving along chamber axis, the temperature increases due to the hot flows coming from the five injectors, in the multi-element combustion chamber. A possible proof of the end of combustion is given by the flattening of the temperature trend, which is visible in Figures 5.15c and 5.15b. As for the central and right thermocouples, the temperature, measured by the thermocouples mounted in the left side respect to the middle injector, has a flattening trend, except for the last sensor.
Increasing the mixture ratio, maintaining the same chamber pressure, the temperature value increases, but the trend is similar, considering the same thermocouples.
The higher temperature gradient along the chamber axis dT/dz corresponds with the higher

pressure decay observed in the multi-element combustion chamber. The higher temperature level for the multi-element combustion chamber can be attributed to the number of injectors.

5.3 Temperature Trend along the Y-Axis

Figura 5.16: Temperature trend along y-axis at 10 bar and O/F=2.6

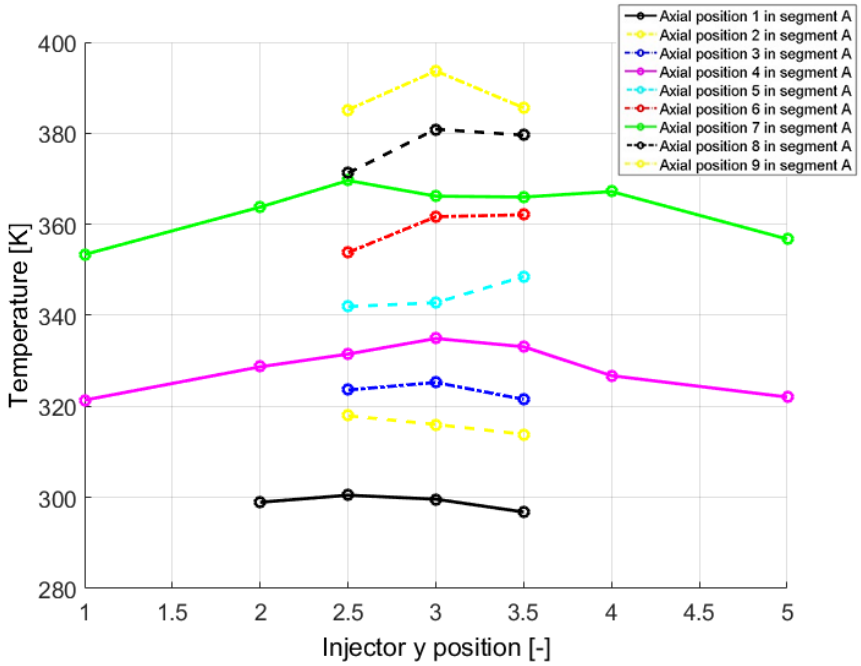

(a) First Segment

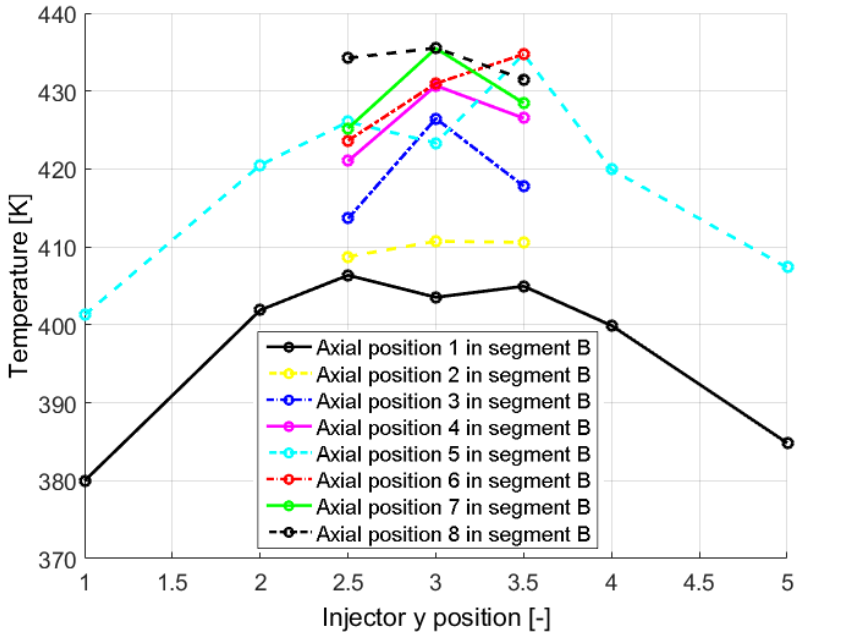

(b) Second Segment

In this section, the temperature profile along the y axis is reported, as shown in Figure 5.16. In this way it is possible to analyse the temperature profile for the multi-element combustion chamber and to investigate the influence of the injectors position and how the corners can have an impact on the flow.

Figura 5.17: Temperature trend along y-axis at 10 bar and O/F=3.0

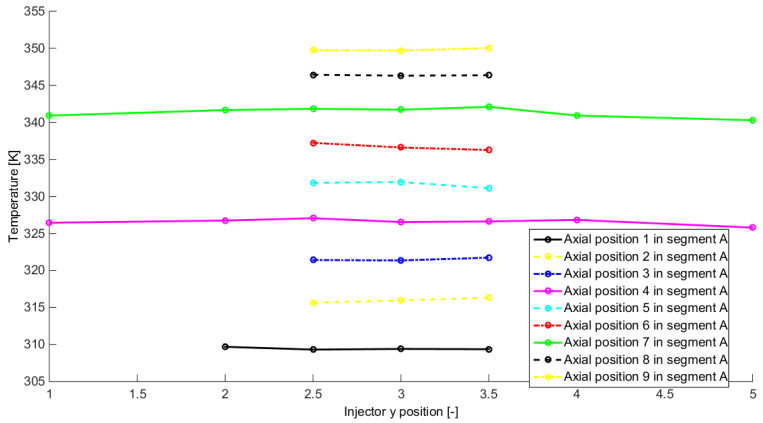

(a) First Segment

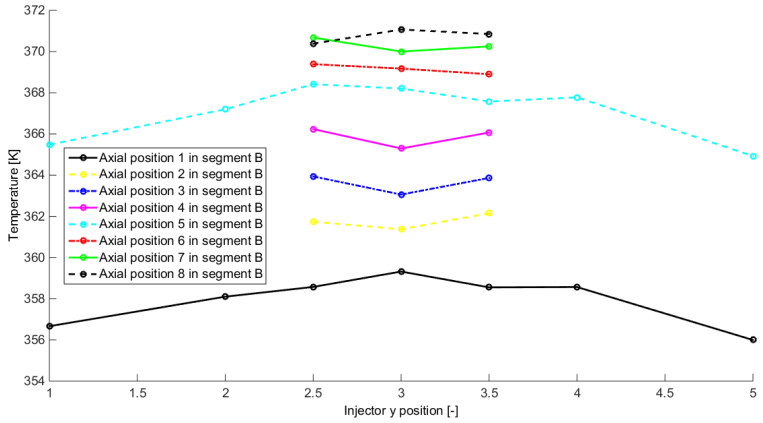

(b) Second Segment

In the Figure 5.16, the temperature trend of the multi-element combustion chamber along y axis is reported, considering a load point at 10 bar and mixture ratio equal to 2.6. In particular, it is possible to analyse the temperature behaviour, measured by each thermocouple, situated in the first 5.16a and in the second 5.16b segments.
Considering the Figure 5.16, the typical temperature profile, showed by the most thermocouples, is characterized by a higher temperature value in correspondence of the injector situated in the central position (3C) and a lower value, close to the chamber walls, corresponding to the first and the fifth thermocouples. This temperature trend along y axis is due to the capacitive nature of the combustion chamber. In fact, the flow situated in the middle position is surrounding by hot flow on the left and right side. Differently, the flow in correspondence of the extreme injectors, is closer to the chamber walls, which inhibit the combustion process.

The evaluation time considered for this analysis is 0.5 s. During the combustion process, the temperature trend along y axis will change, yielding to a flattening value, in order to reach a uniform temperature in the combustion chamber.
Approaching the end of the combustion process, the temperature difference between the temperature measured by the thermocouple situated in the central position and the one close to the wall become higher, as confirmed in the Figures 5.16a and 5.16b. In some part of the combustion chamber, (as for example in the first position of the second segment shown in Figure 5.16), the temperature peak along the y axis does not correspond to the central injector (3C), but to the injector situated on the left (3L) or right (3R) side, due to the presence of recirculation zone.
Increasing the chamber pressure, from 10 to 20 bar, as shown in Figure 5.17, maintaining the same mixture ratio, the difference between the temperature peak in correspondence of the middle injector and the temperature close to the walls is higher, in both segments.
The other load points are reported in the Appendix B.

5.4 Temperature Trend along Time

In this section, the temperature distribution during the whole test duration for both combustion chamber, is reported. In particular, the focus is based on the temperature, measured by the thermocouples positioned at 1 mm from the hot surface of the chamber along the chamber axis during firing.

For the temperature versus time trace, it is possible to identify two main temperature gradients. In the first second after ignition, the temperature profile has a steeper increase, as the thermal wave travels through the chamber wall. Then, a smoother temperature increase is observed, during the remaining running time.
The increasing of temperature ends when the temperature peak is reached, which indicates the end of the combustion process. After a strong initial cooling, indicated by a decreasing of the temperature distribution, a plateau temperature is reached.
Furthermore it can be noticed that the slope of the wall temperature versus time profiles decreases with time into the firing. The same trend could be identified in each temperature signal in the first and second chamber segments. The trend of the temperature during the test duration is shown in the Figures 5.18 and 5.19, for both combustion chambers.
It is reported only the plot for one load point, at 10 bar and mixture ratio equal to 2.6, considering the temperature measured by all thermocouples. For the single-element combustion chamber, it is shown additionally the readings of the thermocouples positioned on the external surface ('TCSU1S' and 'TCSU7S'), which present temperature not superior to 360K during the complete hot run and for the all different load points.

Figura 5.18: Temperature trend along time for Single-Element Combustion Chamber

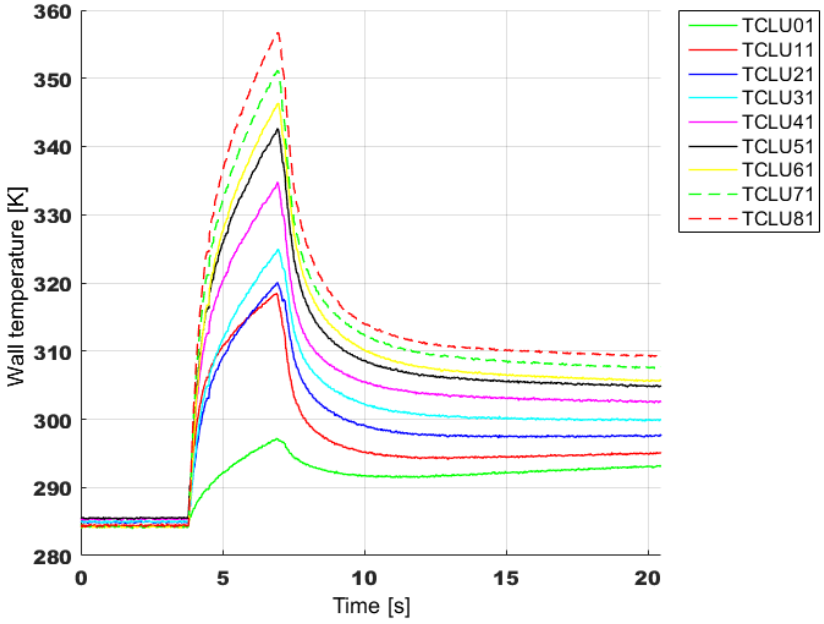

(a) Long Segment

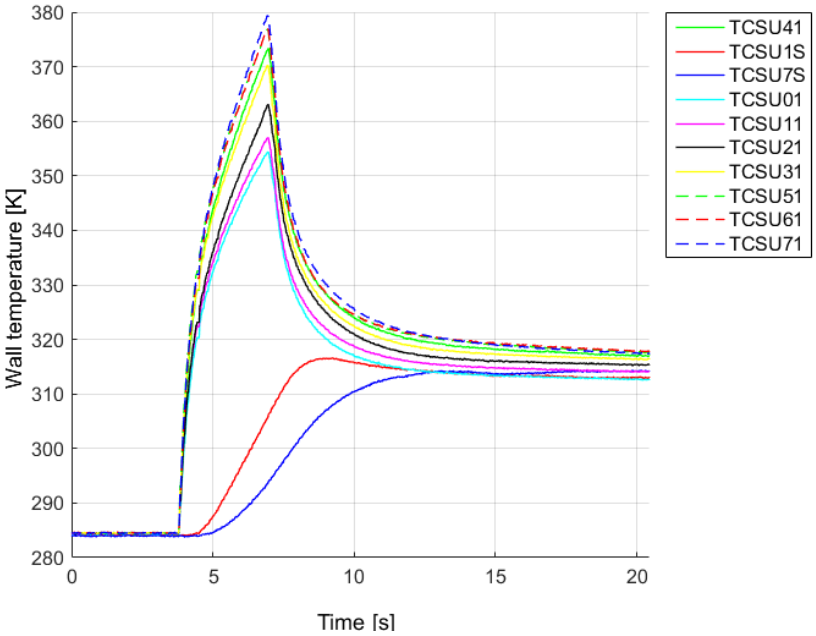

(b) Short Segment

At the starting time, the single-element combustion chamber shows a higher slope, as shown in Figure 5.20. After the thermal wave has come to the external wall, the slope tends to decrease constantly and reach lower values respect to the multi-element combustion chamber. This trend of the temperature profile appears in the first and second segments of the two combustion chambers. The temperature level achieved is higher for the multi-element combustion chamber respect to the single element one.

Figura 5.19: Temperature trend along time for Multi-Element Combustion Chamber

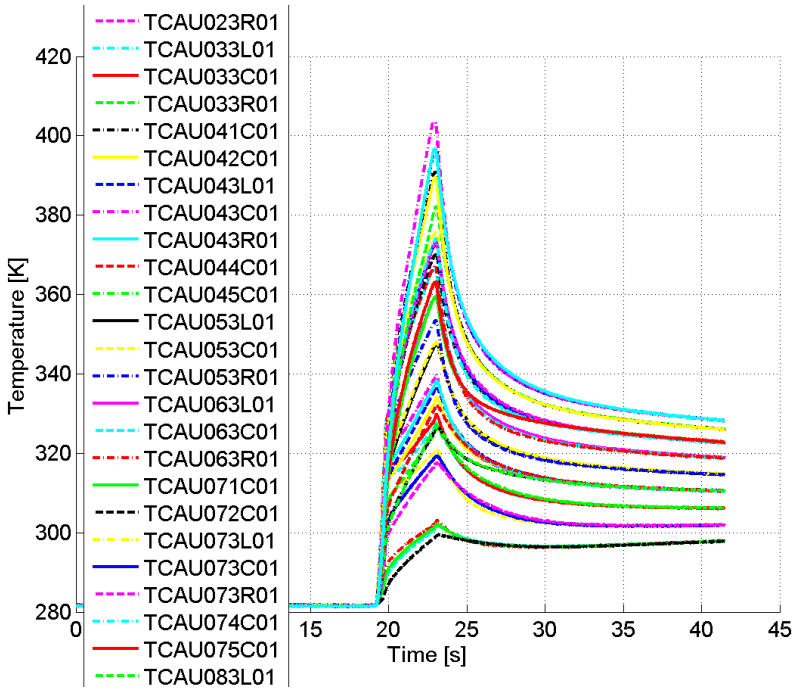

(a) First Segment

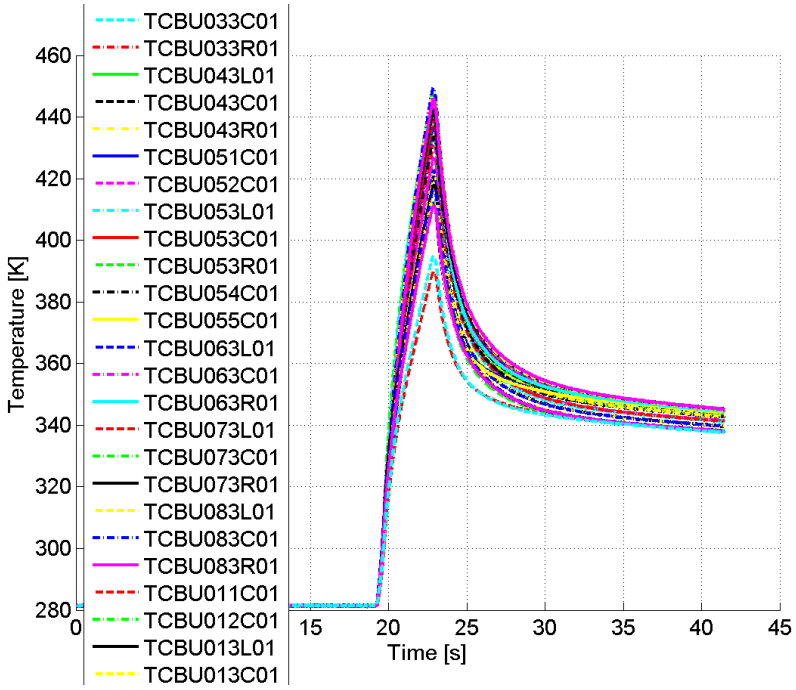

(b) Second Segment

Differently from the pressure trend along time, according to Figure 3.5, the temperature profile is not characterized by a 'plateau', which persists during the all burning time. This temperature behaviour is due to the nature of two capacitive combustion chambers because they are realized with copper free-oxygen, which is characterized by a higher thermal conductivity.

At the start-up, when the heat wave has not reached the external surface yet, the difference

in the slope of the temperature profile depends only on the different surface available. The single-element combustion chamber has more surface available, according to to the important parameter A/V which is higher respect the one of the multi-element combustion chamber, as calculated in the Table 4.1.
Later on, the steepness of the curve decreases down, due to the heavier mass of the single-element combustion chamber, which acts as a heat sink. The same difference is also visible after the shut-down. While in the single-element combustion chamber the temperature of the material cools down quickly, the wall of the multi-element one remains hotter.
In the next Figures 5.20 and 5.21, it is shown the trend of the temperature gradient, considering a pressure of 10 bar and a mixture ratio of 2.6 for the single-element and the multi-element combustion chambers. The total number of thermocouples, mounted at 1 mm from the hot wall, are reported in these plots: in the left one the thermocouples situated in the long segment are found and in the right one the thermocouples referred to the short segment.

The two main different steeper increases are confirmed in this Figure 5.20 and 5.21, where is visible a first higher gradient and a second lower gradient until the end of the burning. When the shut down occurs, a steeper decreases is present in both combustion chambers. This negative gradient represents the cooling of the the chamber walls.

The temperature profile and the temperature gradient over the time is reported in the following part of this section, considering the behaviour for each thermocouples, mounted at 1 mm from the hot wall in the single-element and in the multi-element combustion chambers. In order to compare the two different combustion chambers, it is necessary to make equal the starting time of combustion process, removing the initial constant temperature, which corresponds to the pre-burn operations.

In the following sections, the temperature and the gradient temperature for each thermocouple are considered. In order to compare the two different hardware, only the temperature measured by the thermocouple mounted in the middle plane is shown, for the multi-element combustion chamber. The cardinal number is referred to the position along the chamber axis, (as for example "1st" means the first position).

5.4.1 10 bar and O/F=2.6

In this subsection, it is shown the temperature and the gradient temperature profiles for each thermocouples, considering a pressure of 10 bar and mixture ratio of 2.6. It is considered the thermocouples mounted at 1 mm from the hot wall and situated in the middle position along the y axis, for the single-element and in the multi-element combustion chambers. For the single-element combustion chamber, the thermocouple is named with a string of four letters and 2 numbers (as for example, TCLU01). Instead, for a multi-element combustion chamber, the

Figura 5.20: Temperature Derivative trend along time for Single-Element Combustion Chamber

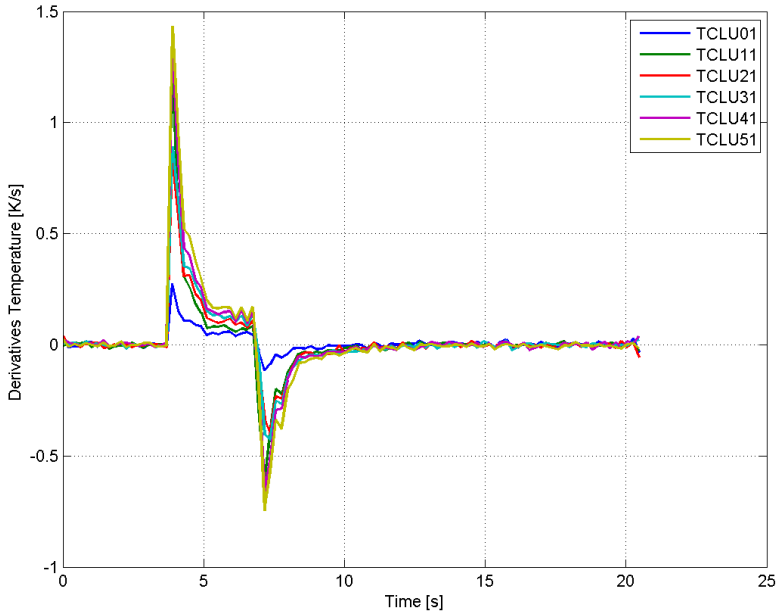

(a) Long Segment

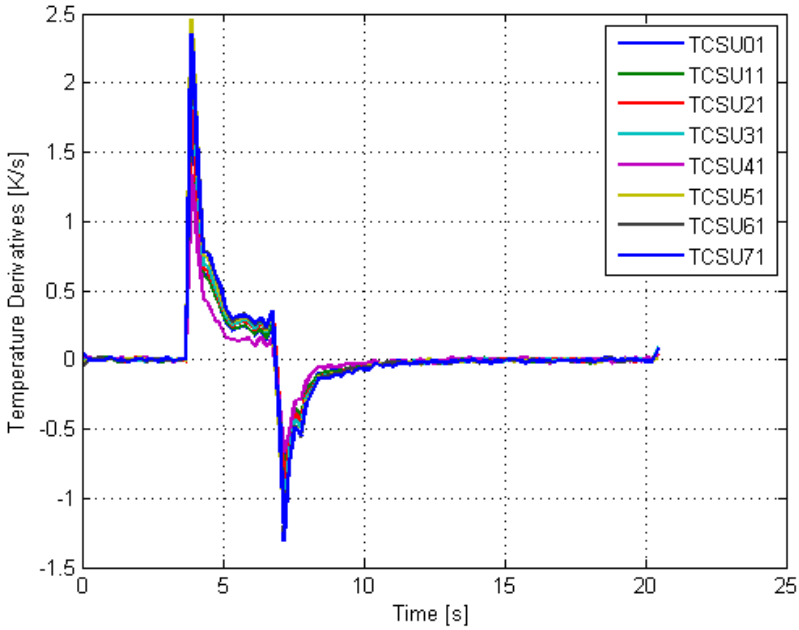

(b) Short Segment

name of each thermocouple presents five letters and five numbers (as for example TCAU013C01, See Nomenclature for the explanation).

In general, all thermocouples show a similar behaviour for all load points, which can be described by a first steep increase of temperature, then the temperature gradient flattens a bit until the shut-down of the chamber, indicated by the temperature peak. According to the following

Figura 5.21: Temperature Derivative trend along time for Multi-Element Combustion Chamber

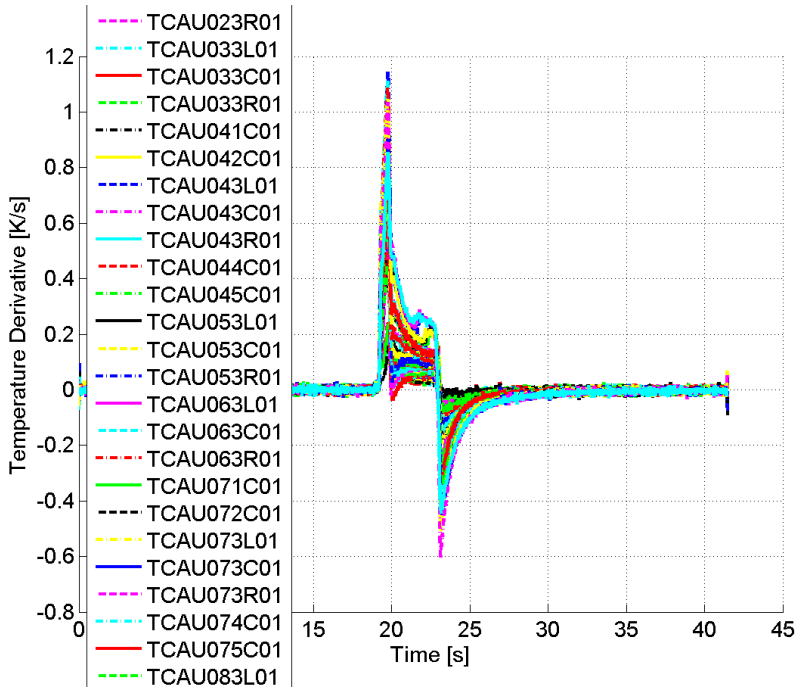

(a) First Segment

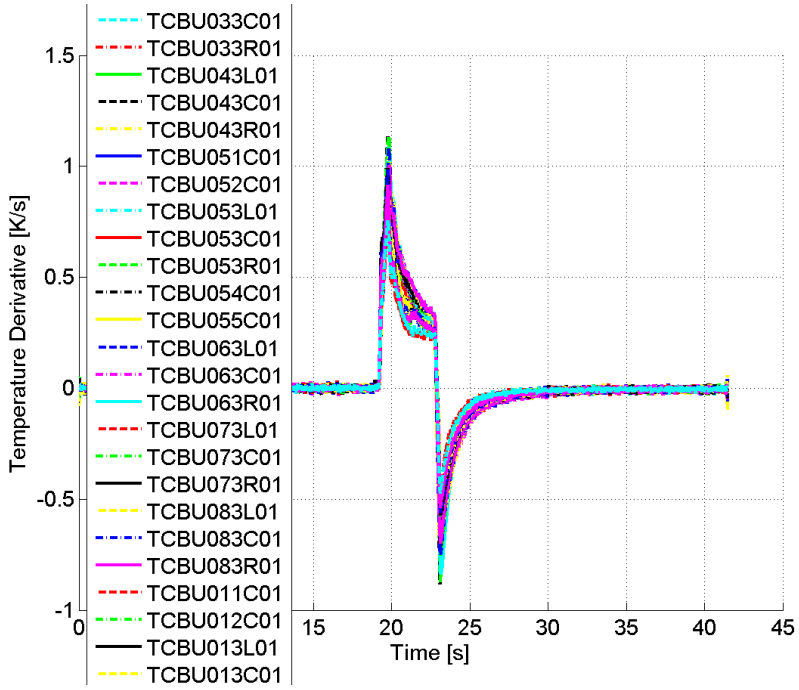

(b) Second Segment

Figures 5.22 and 5.23, it is evident a differences between the two combustion chambers, in terms of heat flux. Comparing the two combustion chambers, a higher chamber pressure results in a higher temperature.

At the start-up, a higher temperature gradient dT/dt characterizes the single-element combustion chamber, in according to the higher hot wall area. The same consideration is done for

Figura 5.22: 1st and 3rd thermocouples at 10 bar and O/F=2.6

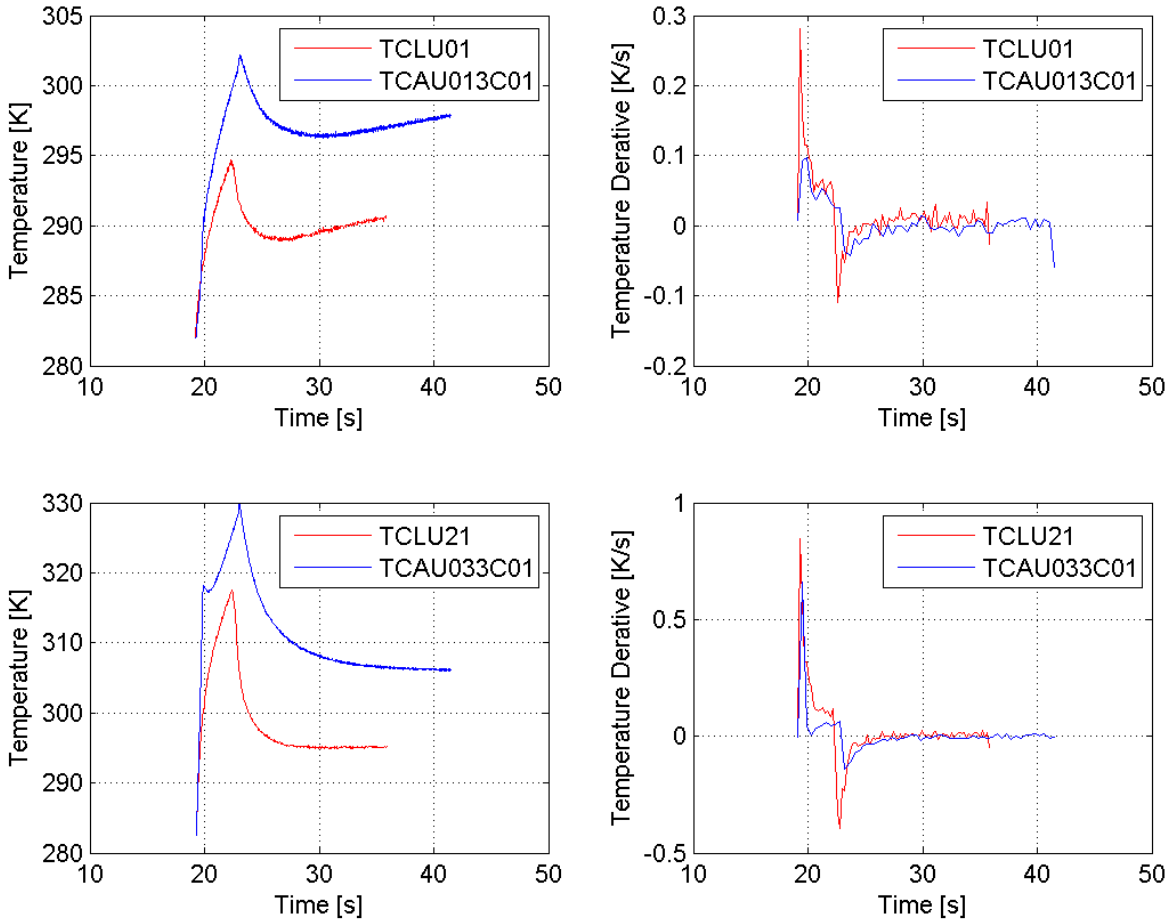

the shut down. Due to the higher area to volume ratio, the temperature of the single-element combustion chamber, acting as a heat-sink, at shut-down is lower than the one of the multi-element one. As a consequence, the higher negative temperature gradient, measured in the single-element combustion chamber, leads to a higher conductive heat transfer. Nevertheless, all temperature gradients approach zero with rising time.
For each thermocouples, the temperature gradient for the single-element combustion chamber is higher respect to the one of the multi-element combustion chamber.

In the Figure 5.22, the temperature measured by the first and the third thermocouples, mounted in the first segment is investigated, for both combustion chambers. It is possible to observe a higher temperature gradient (dT/dt) for the single-element combustion chamber, due to a higher value of A/V, as reported in the Table 4.1. This characteristic is a confirmation of the higher heat flux distribution presented in the single-element combustion chamber, respect to the multi-element one, according to Equation 2.17.
In addition, in the first thermocouple (TCLU01) of the single-element combustion chamber,

Figura 5.23: 4th and 5th thermocouples at 10 bar and O/F=2.6

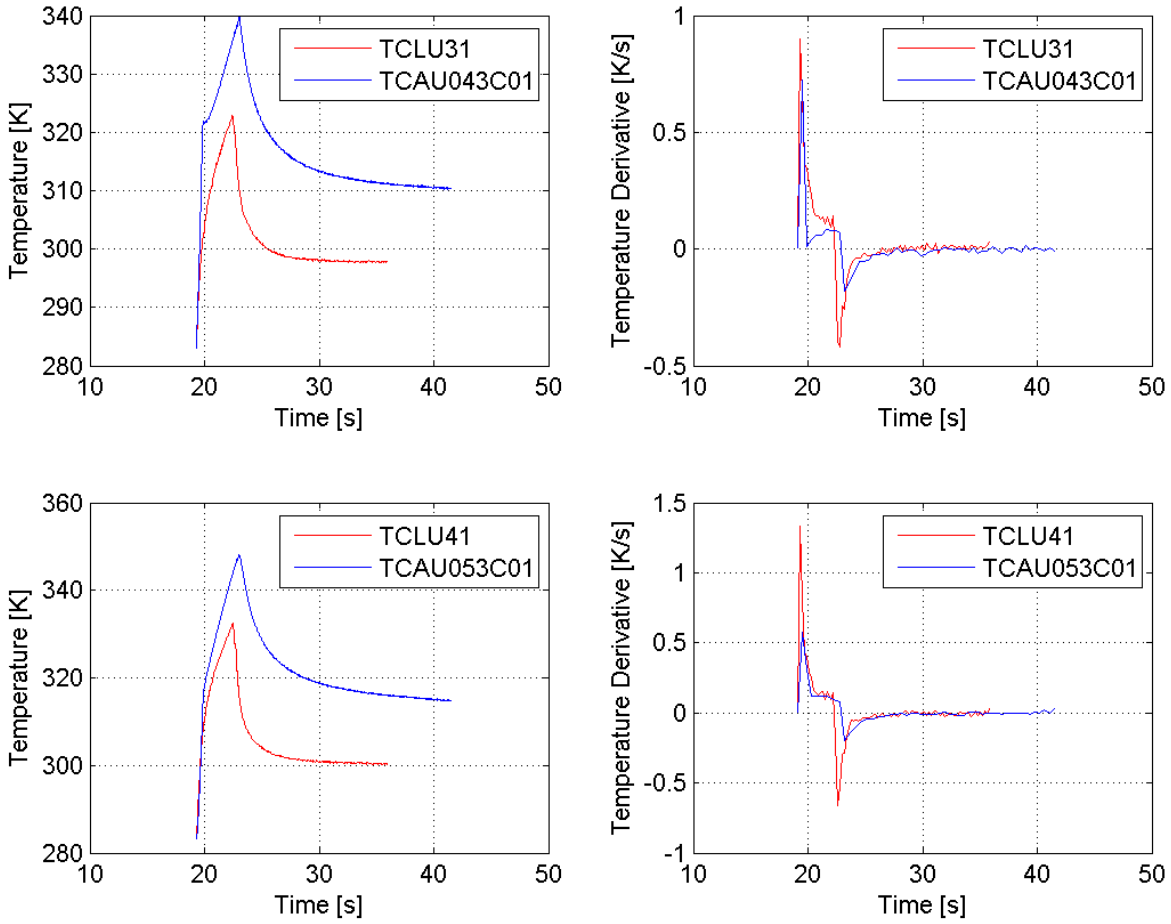

a higher differences in temperature slope is shown. In fact, the temperature derivative in the time switches from an initial peak (about 0.3 K/s) to a lower value (about 0.05 K/s), approaching to the value of the temperature derivative of the multi-element combustion chamber (TCAU013C01), as shown in 5.22. This difference in the temperature gradient of the single-element combustion chamber is observed also in the temperature trend over the time, thanks to a more roundness temperature trend over the time. As the heat wave reaches the external surface, the difference in temperature slope is a result of the transient ignition, which is different between the two combustion chambers.

When the shut-down occurs, represented by the temperature peak in the temperature profile over the time, the temperature gradient comes from positive to negative values, in order to dissipate the heat accumulated in the combustion chamber. In this situation, the heat flux is higher in the single-element combustion chamber, attested by the higher temperature slope in absolute term, due to a transient shut-down.
On the contrary, the temperature, measured by the third thermocouples (TCLU21 , TCAU033C01)

have a trend similar for both combustion chambers, in terms of temperature slope. In the multi-element combustion chamber, an edge in the temperature profile is evident. This edge is confirmed also in the temperature slope, thanks to a zero value of the dT/dt.

Figura 5.24: 1st and 2nd thermocouples in the second segment at 10 bar and O/F=2.6

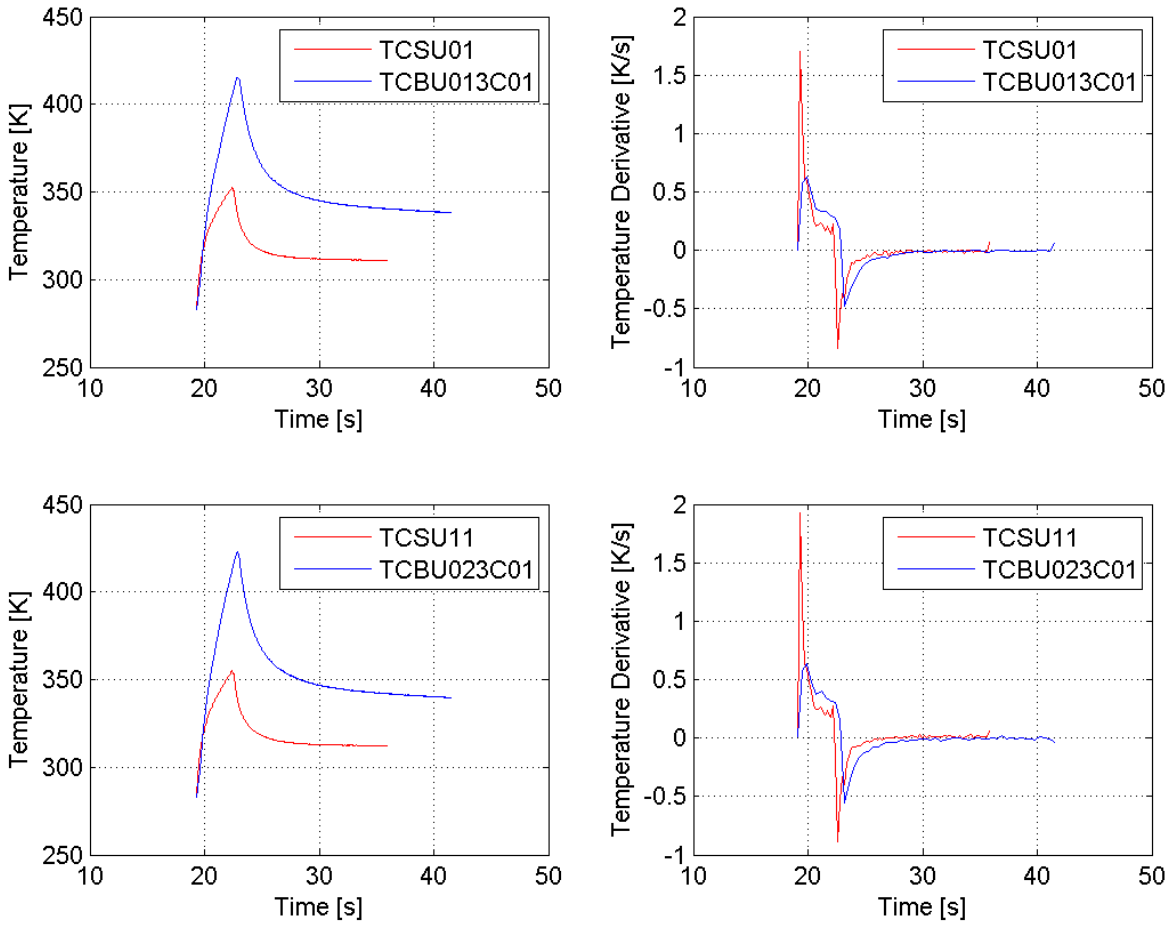

In Figure 5.24, the trend of the temperature and the temperature gradient is reported, referred to the first and second thermocouple, mounted in the second segment of the two combustion chambers.

5.4.2 10 bar and O/F=3.0

In this subsection is reported the temperature trend and the temperature slope for each thermocouples, mounted at 1 mm from the hot wall in the single-element and in the multi-element combustion chambers, considering a pressure of 10 bar and mixture ratio of 3.0.

Increasing the mixture ratio from a value of 2.6 to 3.0, maintaining a constant chamber pressure equal to 10 bar, the temperature profile become less roundness for both combustion chambers.

Figura 5.25: 1st and 3rd thermocouples at 10 bar and O/F=3.0

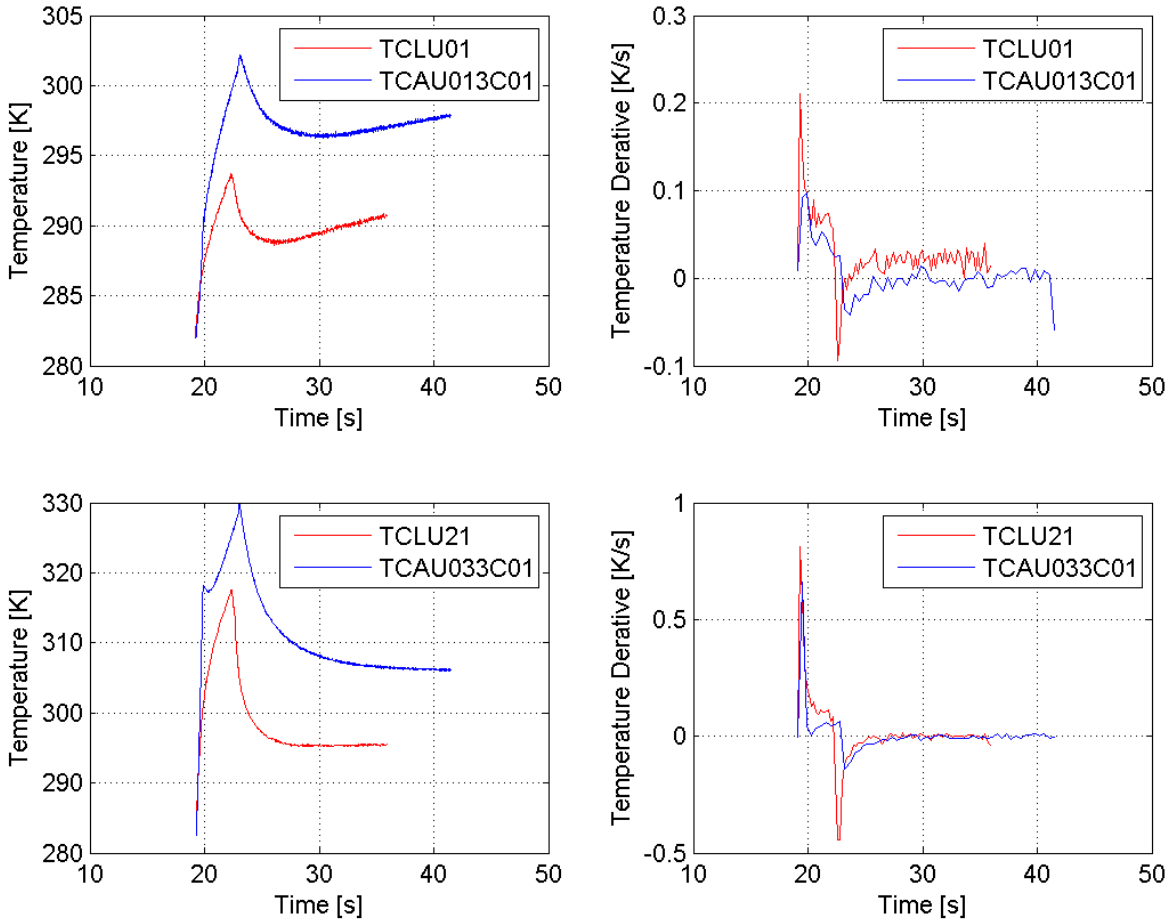

The roundness means a variation in the temperature slope, confirmed by a higher peak, followed by a lower dT/dt. In particular, for a mixture ratio equal to 3.0, the temperature gradient of the multi-element combustion chamber, measured by the first thermocouple, has a higher peak, respect to the load point at 10 bar and O/F=2.6.

The first two thermocouples show a lower value of the temperature gradient, both for the two combustion chambers, respect to the lower mixture ratio condition. In particular, for the single-element combustion chamber, a higher temperature slope respect to the one of the multi-element combustion chamber, is due to a lower V/A parameter, which means a faster heat flux dissipation. The higher temperature slope in the single-element combustion chamber is confirmed in the Figure 5.27, where the trend referred to the thermocouple situated in the second segment is reported, due to a lower value of the ratio between the chamber volume and the wall area. According to a lower value of V/A for the single-element combustion chamber, a higher dissipation of heat, represented by a higher peak in the temperature gradient along time, is confirmed also increasing the mixture ratio, as shown in the Figures presented in the

Figura 5.26: 4th and 5th thermocouples at 10 bar and O/F=3.0

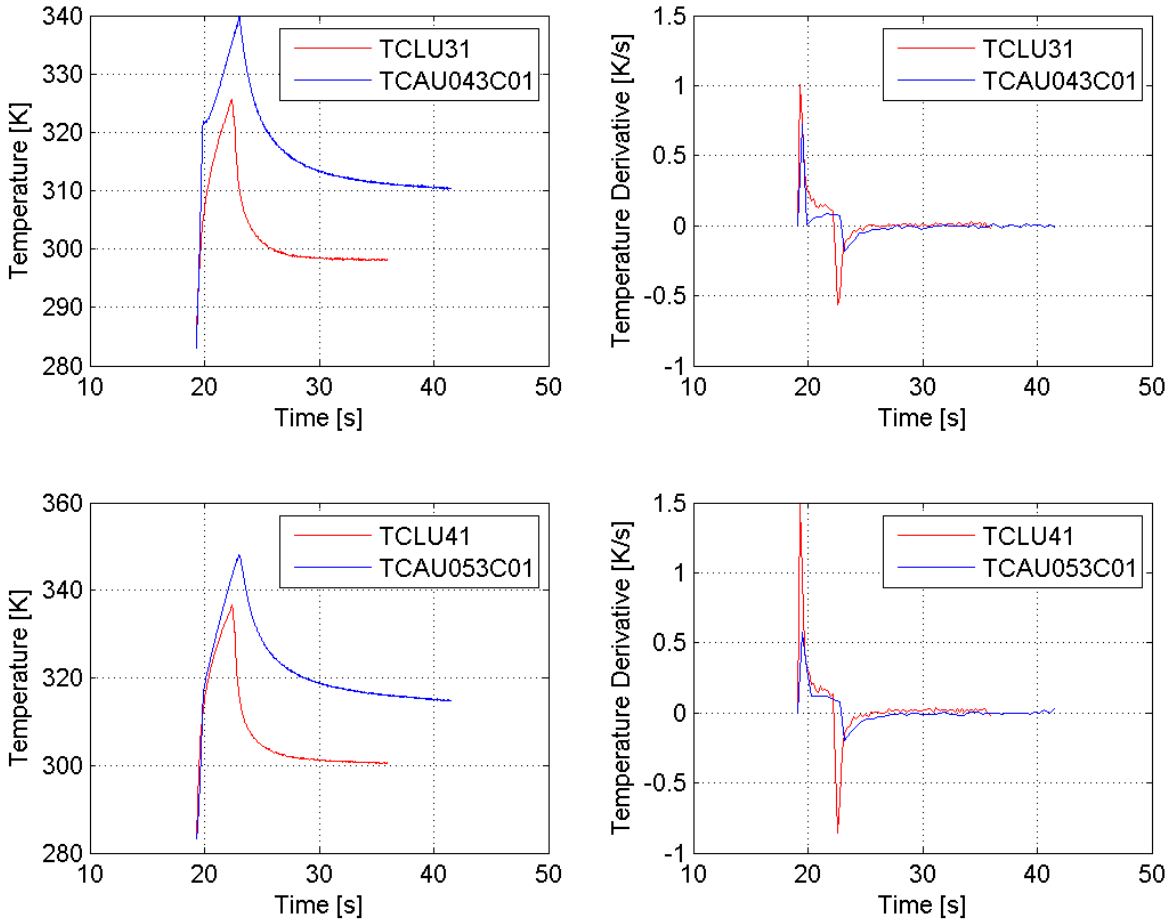

Appendix.
In the previous load point, at lower mixture ratio, a higher dT/dt for the multi-element combustion chamber is shown until the fourth thermocouple. Increasing the mixture ratio to a value of 3.0, the higher temperature gradient in the multi-element combustion chamber appears until the third thermocouple.

5.4.3 20 bar and O/F=2.6

In this subsection, it is reported the temperature and the gradient temperature profiles, measured by each thermocouples, situated at 1 mm from the hot wall. It is considered the load point at 20 bar and mixture ratio equal to 2.6, for both combustion chambers.

Increasing the chamber pressure, the more evident consequence is the lower variation of the temperature gradient related to the first thermocouples, situated in the multi-element combustion

Figura 5.27: 1st and 2nd thermocouples in the second segment at 10 bar and O/F=3.0

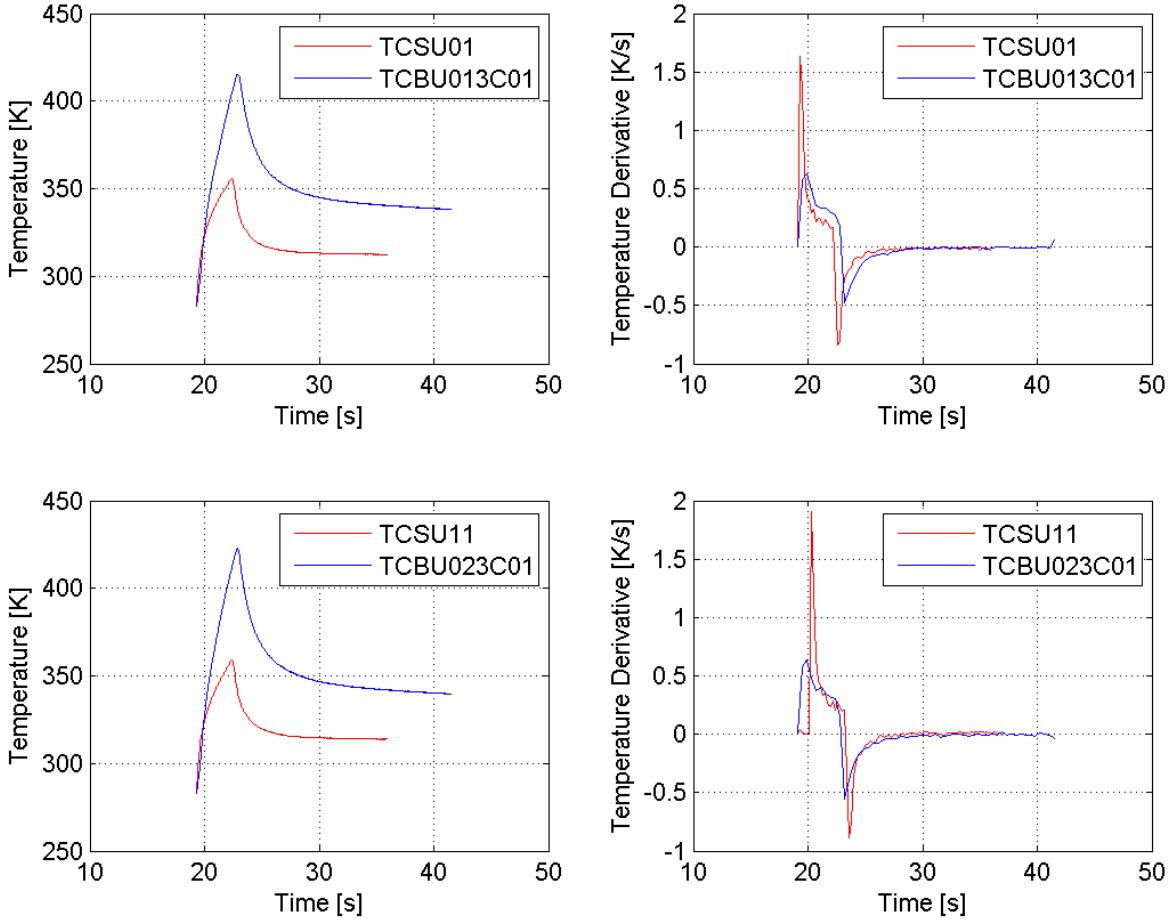

chamber. Nevertheless, in this combustion chamber, the edge in the temperature profile persists also in a higher pressure configuration, as shown in the Figure 5.28 for the third thermocouple.

As shown in the Figure 5.28, it is evident a higher temperature gradient (dT/dt) for the single-element combustion chamber, due to a higher value of A/V, as calculated in the previous chapter. For this reason, a higher heat flux distribution presented in the single-element combustion chamber, respect to the multi-element one, confirmed by Equation 2.17.
Increasing the chamber pressure from 10 to 20 bar, the difference in the temperature peak for the two combustion chambers is lower.
Comparing the two combustion chambers, a higher chamber pressure results in a higher temperature, which means a higher temperature gradient. In fact, in the single-element combustion chamber, the peak in the temperature gradient reaches a value, which is higher respect to the load point at lower chamber pressure. In addition, the peak value of the temperature gradient is increasing along the single-element combustion chamber, as shown in Figures 5.28 and 5.29 and in the Figures reported in the Appendix. This difference in the temperature gradient of the

Figura 5.28: 1st and 3rd thermocouples at 20 bar and O/F=2.6

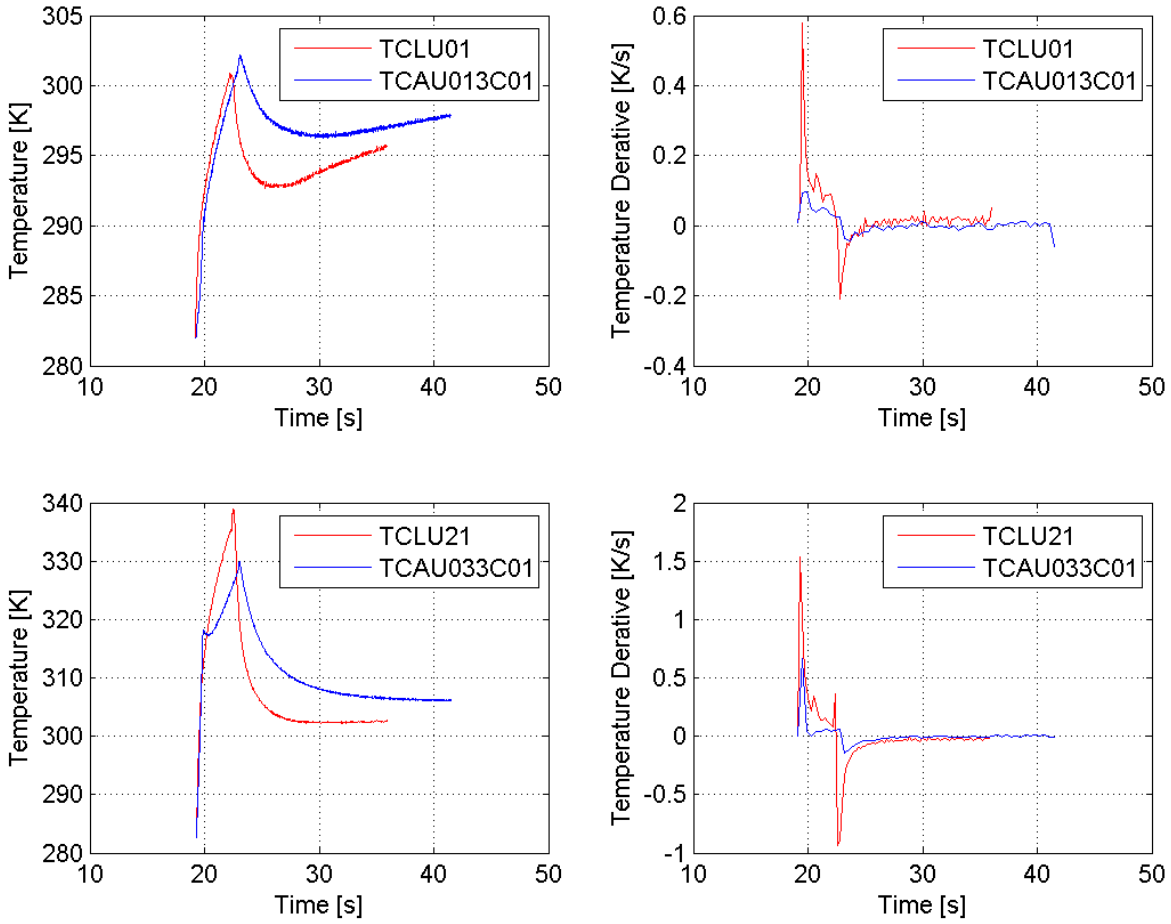

single-element combustion chamber permits to the heat wave to reach the external surface in a lower time. In addition, this difference is confirmed by the different masses that each injector can see, which is higher for the single-element one, thanks to a higher value of A/V.

At the shut down, the same consideration can be done. The heat accumulated in the combustion chamber has to be dissipated and, as a consequence, the temperature slope becomes negative. Also in this situation, the heat flux is higher in the single-element combustion chamber, due to the higher negative temperature slope.

In the Figure 5.30, the temperature profile and the temperature derivative versus time are represented, referring to the values measured by the first thermocouple situated in the second segment. The higher value of V/A for the multi-element combustion chamber is confirmed also by the Figure 5.30. When in the single-element combustion chamber the combustion process ends, the combustion continues for the multi-element combustion chamber. In fact, the temperature peak occurs before for the single-element combustion chamber.

Figura 5.29: 4th and 5th thermocouples at 20 bar and O/F=2.6

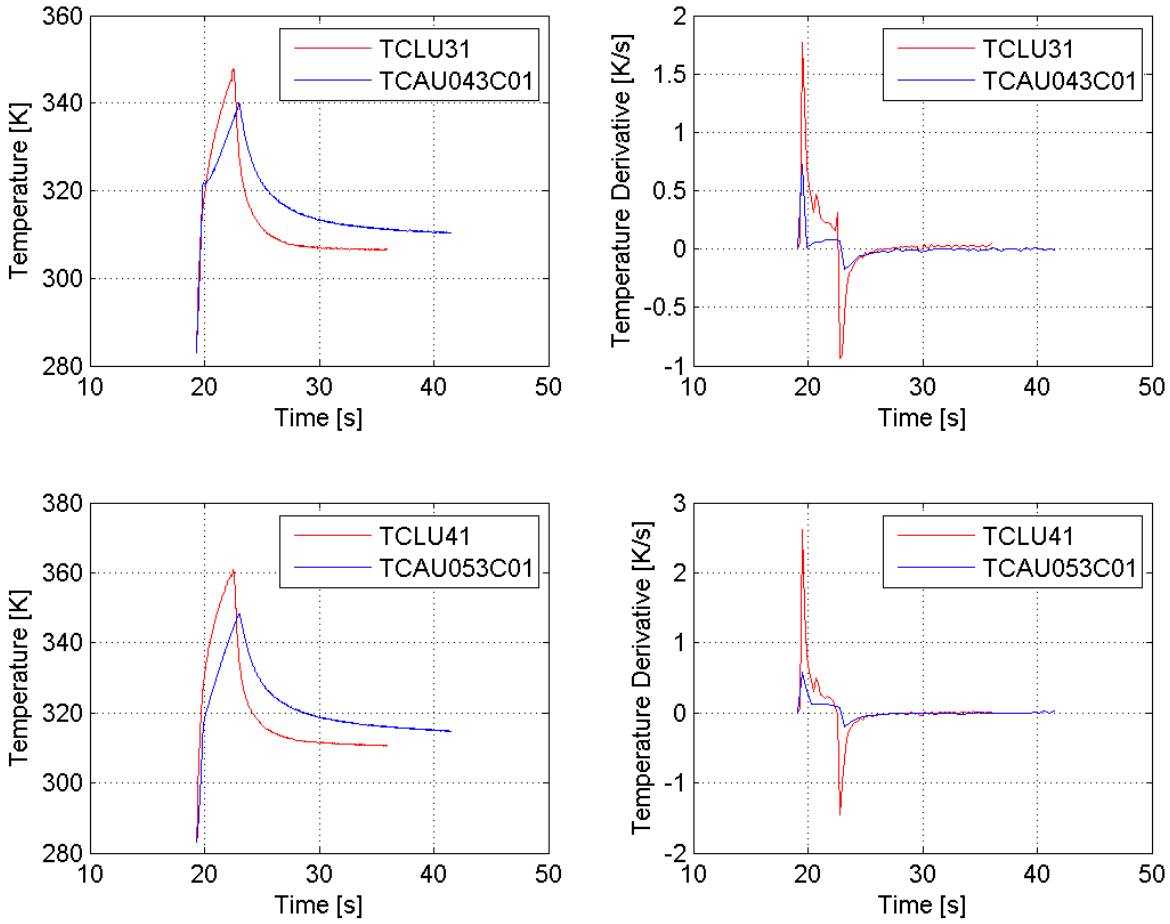

5.4.4 20 bar and O/F=3.0

In the following subsection, for both combustion chambers, it is reported the temperature and the gradient temperature profiles for each thermocouples, mounted at 1 mm from the hot wall. The load point considered is characterized by a pressure of 20 bar and a mixture ratio of 3.0.

For a constant chamber pressure of 20 bar, increasing the mixture ratio, from 2.6 to 3.0, as in the lower pressure condition, the temperature profile become less roundness for both combustion chambers. The roundness implies a variation in the temperature slope, confirmed by a peak, followed by a lower value of dT/dt. In particular, increasing the chamber pressure, the temperature gradient of the multi-element combustion chamber, measured by the first thermocouple, has a higher peak. On the contrary, in the single-element combustion chamber, increasing the mixture ratio, maintaining a constant chamber pressure, the peak in the temperature slope is lower. Comparing the temperature gradient along time of the two different combustion chambers in Figures 5.31 and 5.32, the higher temperature slope for the single-element combustion

Figura 5.30: 1st and 2nd thermocouples in the second segment at 20 bar and O/F=2.6

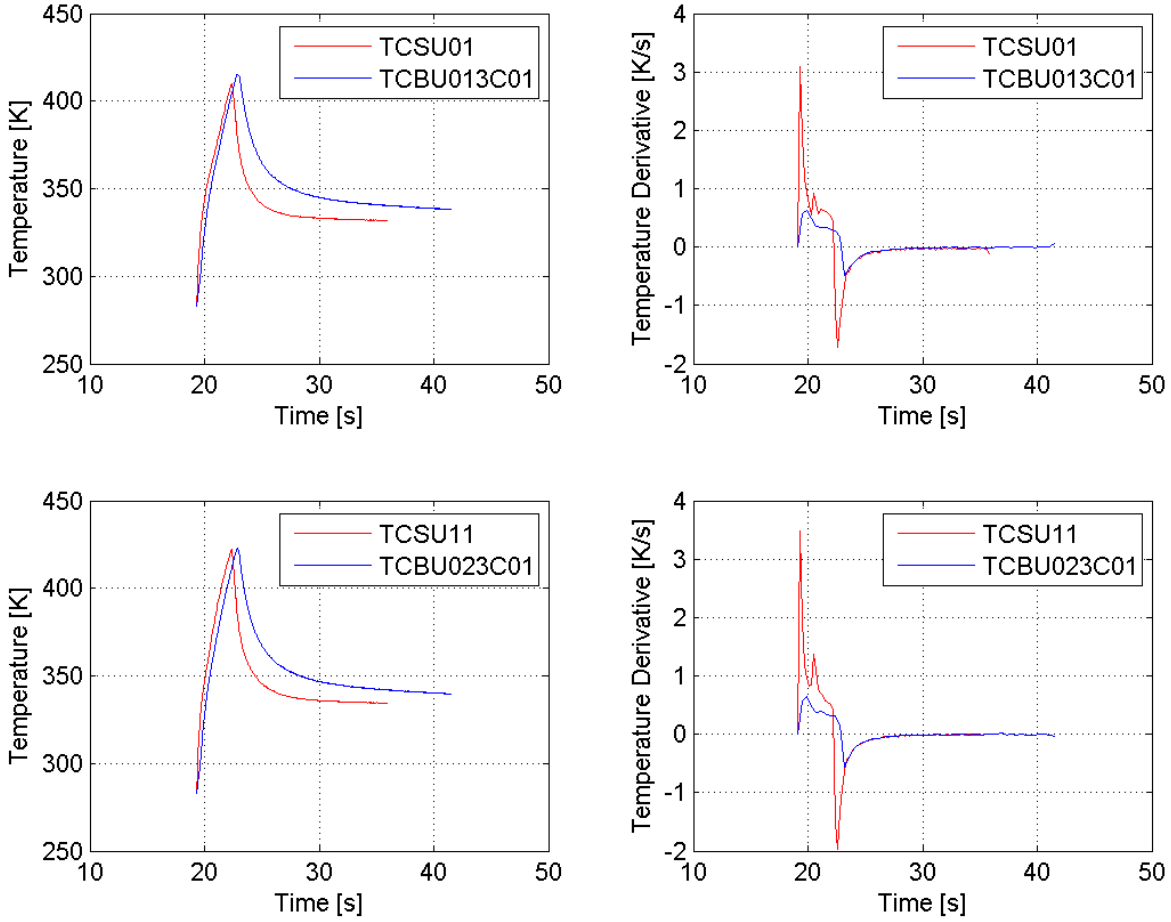

chamber represents a higher dissipation of heat, according to the Equation 2.17, related to the heat transfer. This is confirmed also by the value of the volume to area ratio (V/A), which is higher for the multi-element combustion chamber, due to the geometry of the two hardware. This difference in the temperature gradient related to both combustion chambers, is presented for all thermocouples, mounted along chamber axis, as shown in the Figures reported in Appendix. In the previous load point, at lower mixture ratio, a higher dT/dt for the multi-element combustion chamber is shown respect to the one examined.

In addition, it is possible to observe an edge in the temperature profile in the multi-element combustion chamber, shown in the third and fourth thermocouples (TCAU033C01 and TCAU043C01). As a consequence of this edge, in the temperature slope, a zero value of the dT/dt is presented for the multi-element combustion chamber. This means that the heat transfer is approaching to zero. According to Equation 2.17, in correspondence of the edge, the flux temperature is approximately equal to the wall temperature, due to the presence of five flows in the multi-element combustion chamber. In fact, increasing the mixture ratio, the edge is more evident. Progressing to the end of the chamber, the edge in the temperature profile of the multi-element

Figura 5.31: 1st and 3rd thermocouples at 20 bar and O/F=3.0

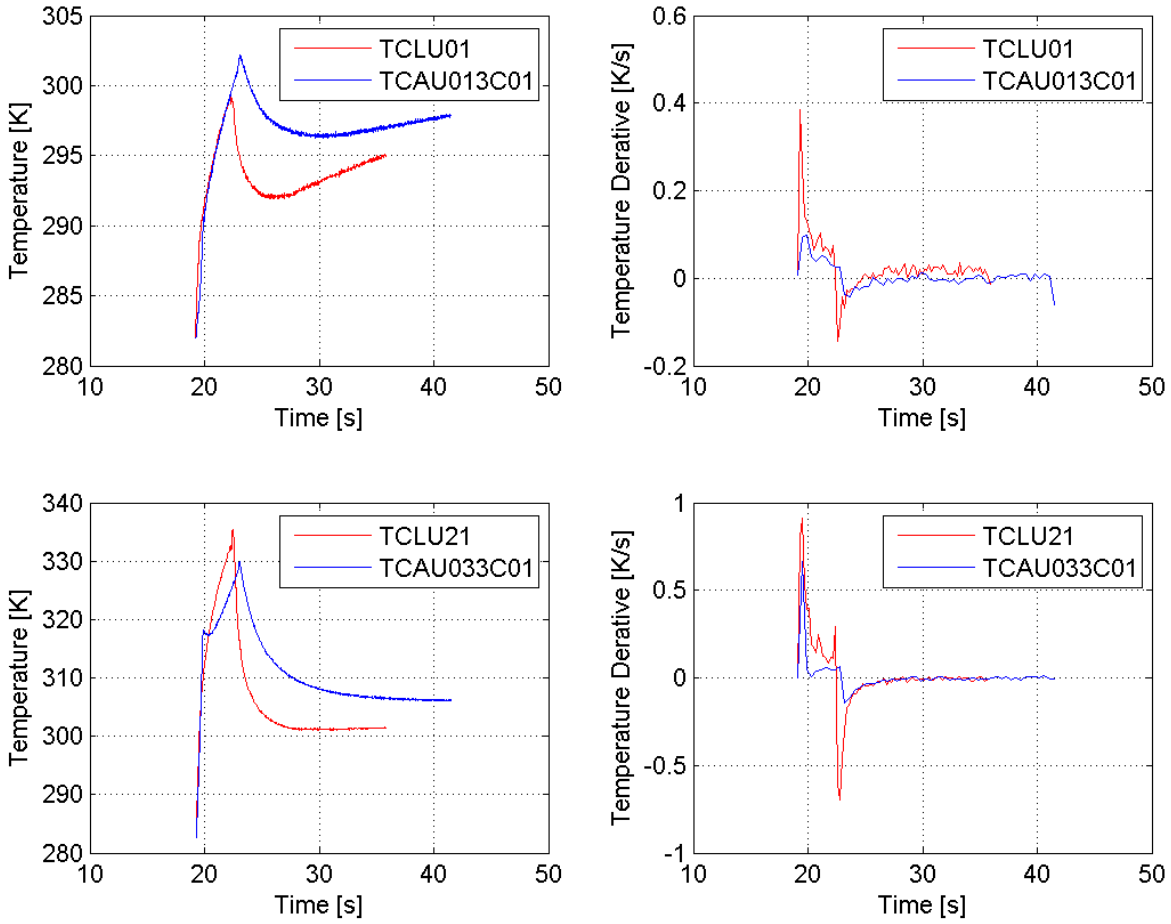

combustion chamber is extinguished, as confirmed by the Figure 5.33, where the thermocouples in the second segment are considered.

5.4.5 20 bar and O/F=3.4

In this subsection, it is shown the temperature and the gradient temperature profiles for each thermocouples, mounted at 1 mm from the hot wall in the single-element and in the multi-element combustion chambers, considering a pressure of 20 bar and mixture ratio of 3.4.

Increasing the mixture ratio from 3.0 to 3.4, in the single-element combustion chamber, the peak in the temperature gradient reaches a value, which is lower respect to the two previous load point for the first thermocouple. On the contrary, according to the other thermocouple, shown in the Figures 5.34 and 5.35, due to a higher value of A/V, it is possible to observe a higher temperature gradient (dT/dt) for the single-element combustion chamber, as demonstrated also in the previous load points. As a consequence, in the single-element combustion

Figura 5.32: 4th and 5th thermocouples at 20 bar and O/F=3.0

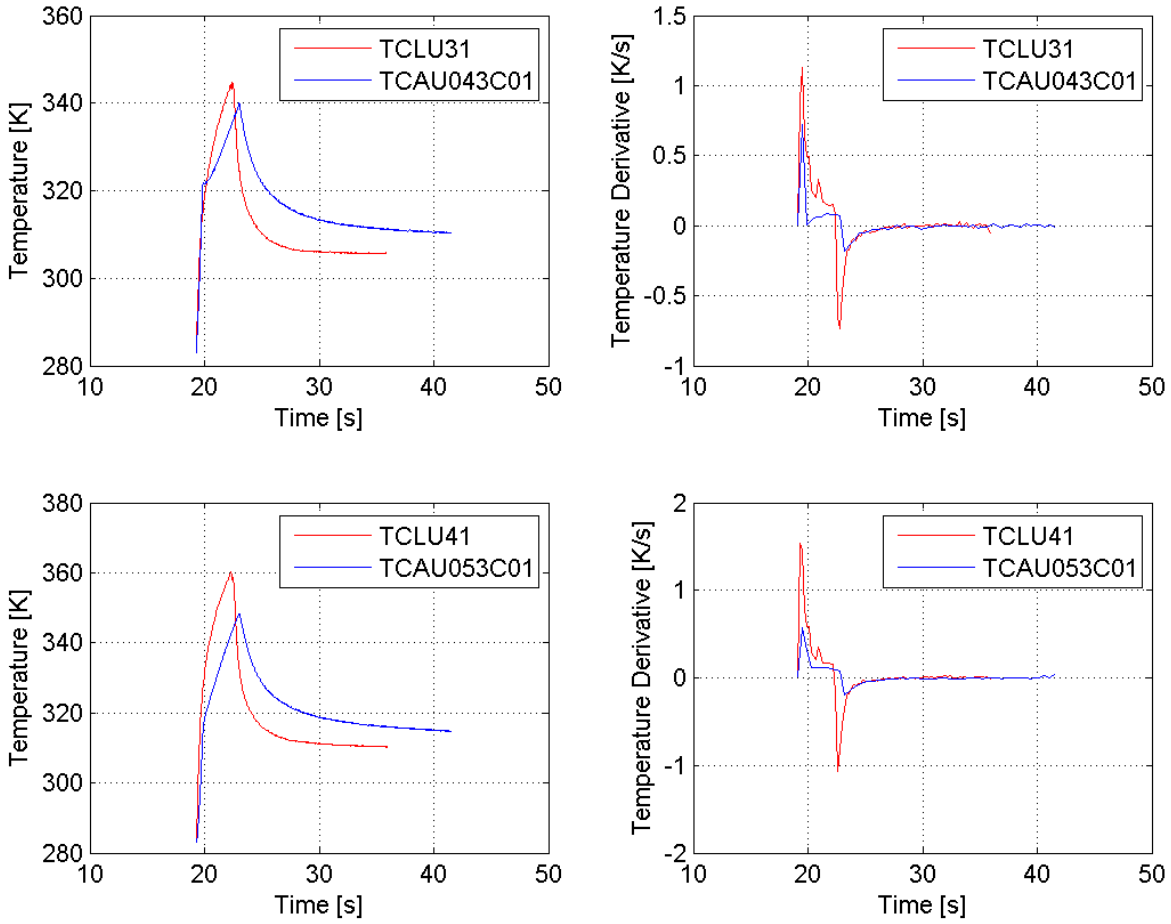

chamber, respect to the multi-element one, a higher heat flux distribution is presented, verified by Equation 2.17 (See more details in Appendix). The difference in the heat flux distribution is due to a difference in the temperature gradients between the two combustion chambers. For this reason, in the single-element combustion chamber the heat wave can reach the external surface in a lower time, in according to a higher value of V/A, which characterizes the multi-element combustion chamber.
For the same reason, at the shut down, represented by the peak in the temperature profile along time, the temperature slope has a higher negative value, increasing the mixture ratio.

This difference in the temperature gradient of the single-element combustion chamber is observed also in the temperature trend over the time, thanks to a more roundness temperature trend over the time. In fact, increasing the mixture ratio, maintaining a constant chamber pressure equal to 20 bar, the roundness in the temperature profile become lower for both combustion chambers. This means a variation in the temperature slope, confirmed by a higher peak, followed by a lower dT/dt. The roundness decreases along chamber axis, as confirmed

Figura 5.33: 1st and 2nd thermocouples in the second segment at 20 bar and O/F=3.0

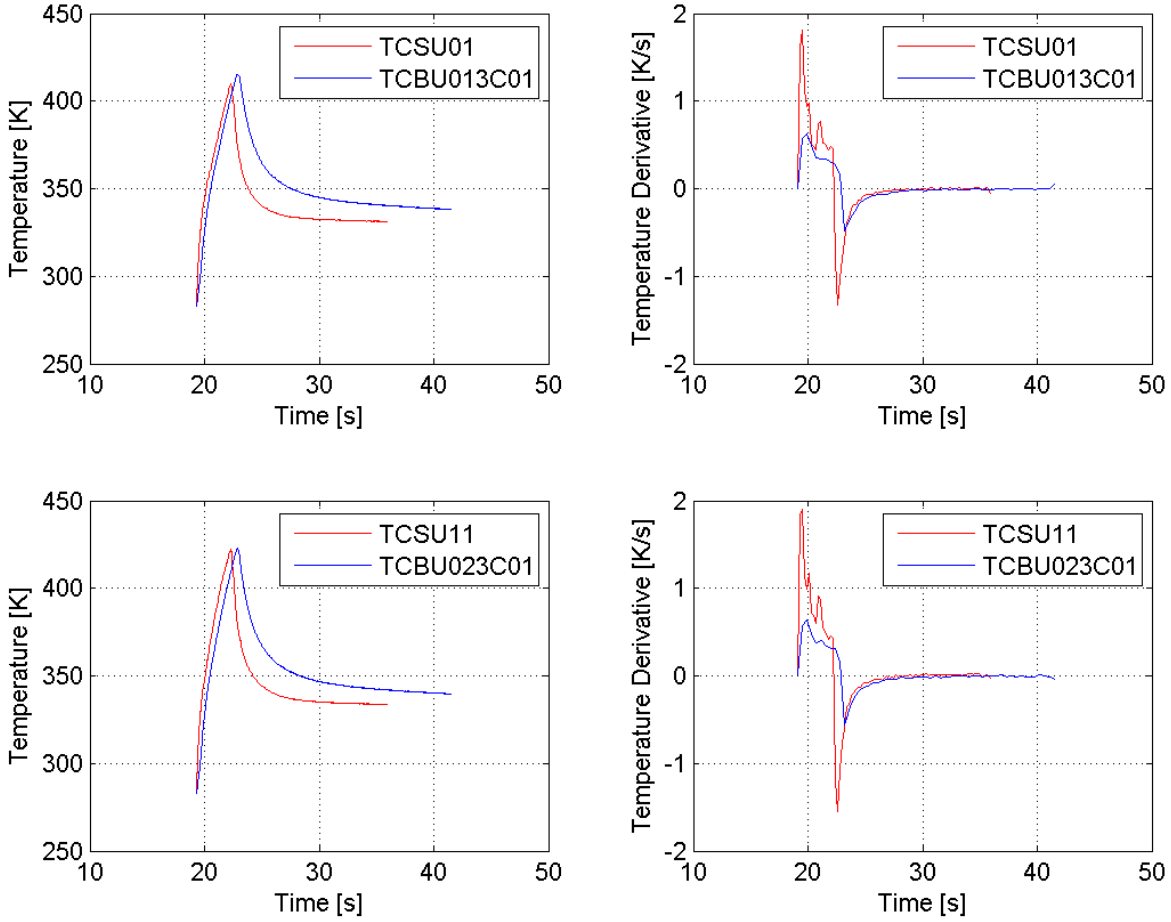

by the temperature and the temperature gradient profile reported in the Figure 5.36 and in the Figures in the Appendix A.

5.5 Combustion Efficiency

In this section, in order to give a complete comparison, an overview about the performances of the two rocket combustion chamber is reported.

The combustion efficiency, defined in Equation 2.6, is an important parameter used to quantify the efficiency of a combustion chamber. The combustion efficiency is defined as the ratio between the real characteristic velocity c_{calc} and the ideal one c_{theo}, (for more details see Equation 2.4). In the following Table 5.2, it is possible to know the real and ideal characteristic velocities and the combustion efficiency for both combustion chambers. The calculated parameters are

Figura 5.34: 1st and 3rd thermocouples at 20 bar and O/F=3.4

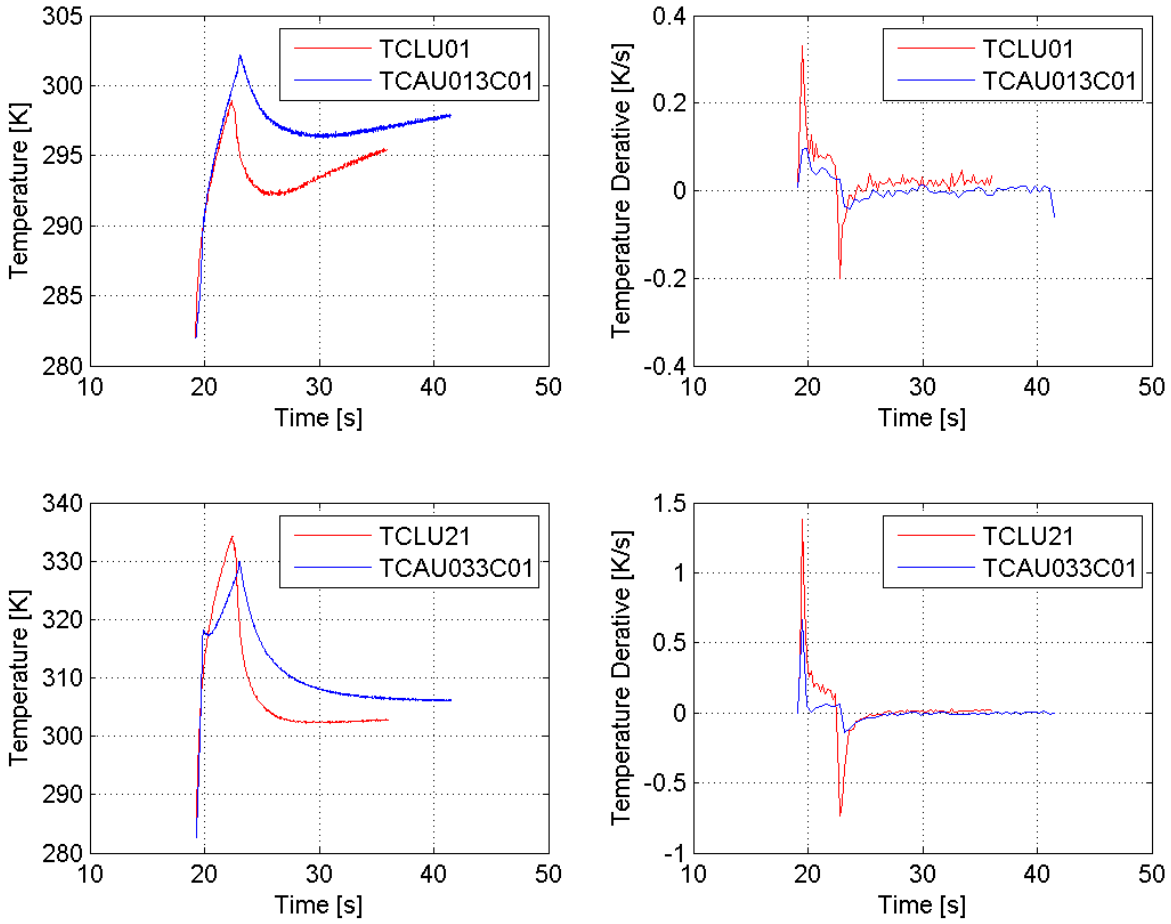

obtained, varying the pressure from 10 to 20 bar and the mixture ratio from 2.6 to 3.4. In this way, five load points are reported.

	$c^*_{theo,s}$	$c^*_{calc,s}$	$c^*_{theo,m}$	$c^*_{calc,m}$	η_s	η_m
10 bar						
O/F=2.6	1880,255	1738,665	1864,957	1809,398	0,9247	0,9702
O/F=3.0	1844,205	1736,277	1840,449	1811,201	0,9415	0,9841
20 bar						
O/F=2.6	1890,033	1783,698	1891,022	1803,850	0,9435	0,9539
O/F=3.0	1873,162	1774,952	1855,183	1811,617	0,9476	0,9765
O/F=3.4	1836,303	1773,385	1834,204	1799,808	0,9657	0,9812

Tabella 5.2: Efficiency of the two combustion chambers

In order to simplify the calculation, the approach used to calculate the characteristic velocity and the combustion efficiency for the two combustion chambers is based on the assumption of

Figura 5.35: 4th and 5th thermocouples at 20 bar and O/F=3.4

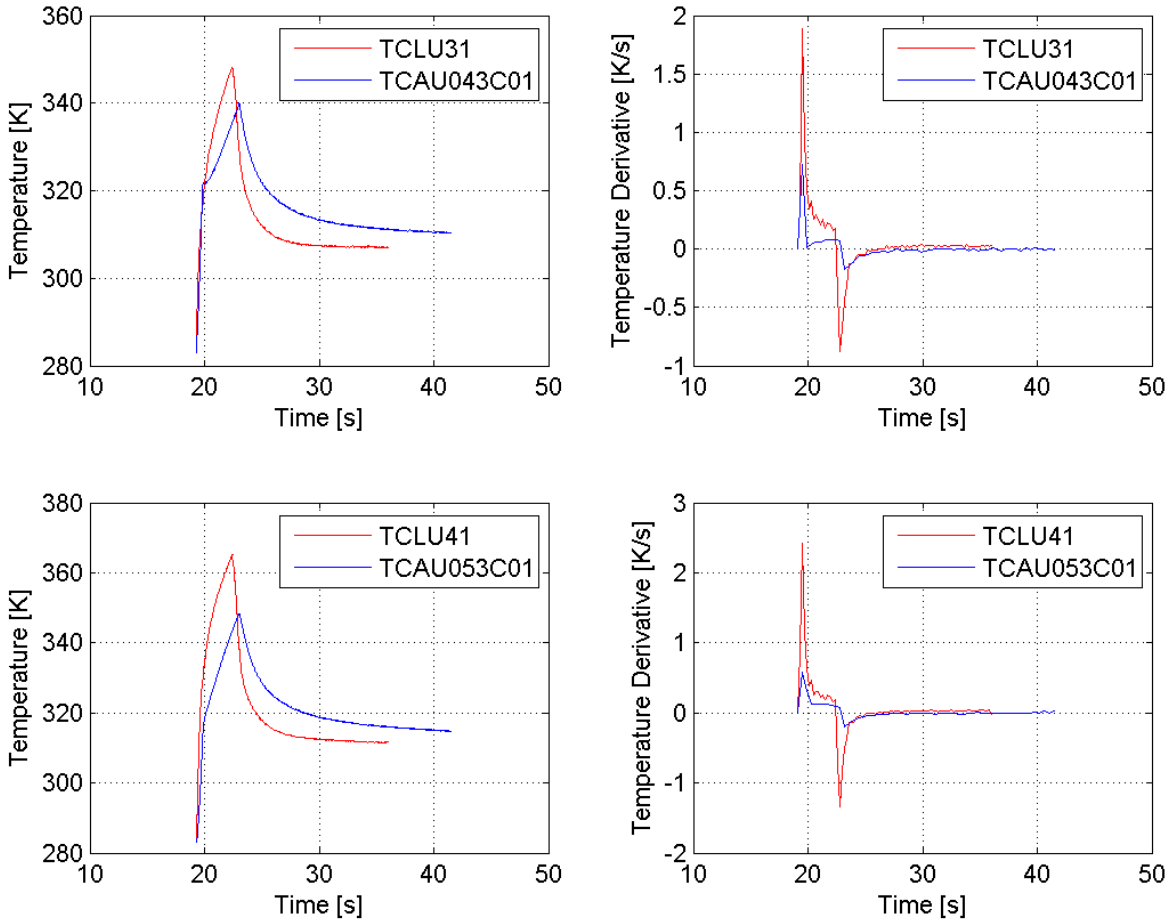

an adiabatic wall, so it is named "AW". In this way, the heat flux to the wall is not considered and as a consequence, the combustion efficiency is lower. Also the boundary layer in the throat area is not considered in the evaluation of the combustion efficiency. Without this correction, the values of the combustion efficiency obtained is higher, due to the proportionality of the characteristic velocity with the nozzle throat area, as shown in Equation 2.4.
In order to estimate the characteristic velocity, the chemical equilibrium compositions and properties of the propellant are calculated by the NASA Computer program CEA (Chemical Equilibrium with Applications). This program, developed by Bonnie J. McBride and Sanford Gordon [11], considers thermodynamic states, theoretical rocket performance, Chapman-Jouguet detonations, and shock-tube parameters for incident and reflected shocks.

In Figures 5.37 and 5.38, the values of the calculated combustion efficiency are reported, in order to compare the two rocket combustion chambers. In particular, in the Figures 5.37a and 5.37b, it is possible to find the combustion efficiency, varying the mixture ratio from 2.6 to 3.0 in the first case and from 2.6 to 3.4 in the second case, maintaining a constant pressure of 10

Figura 5.36: 1st and 2nd thermocouples in the second segment at 20 bar and O/F=3.4

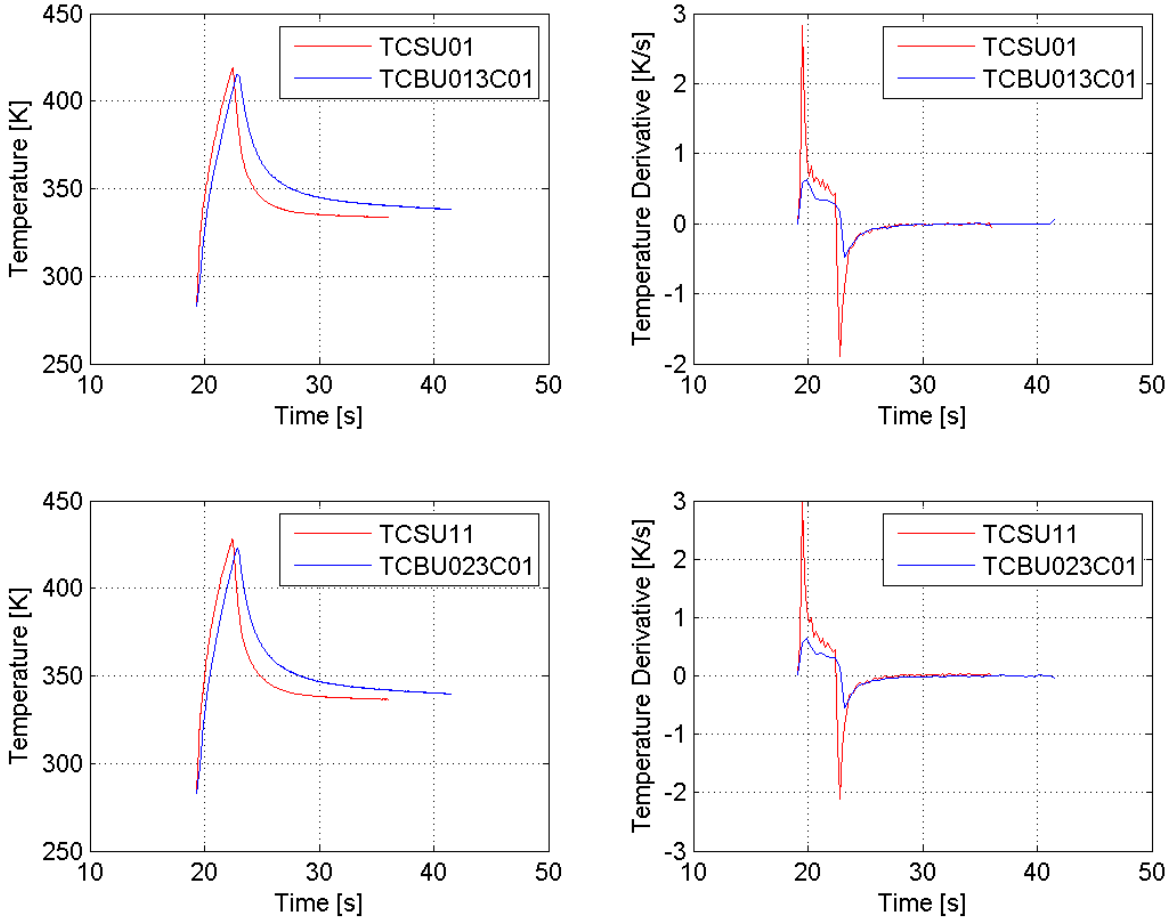

and 20 bar respectively. On the contrary, maintaining a constant mixture ratio of 2.6 or 3.0, it is considered the combustion efficiency, as a function of chamber pressure, as shown in Figures 5.38a and 5.38b.

Considering the same mass flow rate, chamber pressure and combustion temperature, also the ratio between the mass flow rate and the throat area ratio ($\dot{m}/A_{th}$) will be the same. As a consequence, the ideal characteristic velocity would be the same, according to Equation 2.4 and also the combustion efficiency would be the same, as shown in Equation 2.6.

As shown in Figures 5.37, keeping the chamber pressure constant and increasing the mixture ratio, the combustion efficiency of the two combustion chambers increases. A decrease in the mixture ratio means a higher quantity of fuel, which causes an increment in the ratio between the chamber temperature and the molar mass ($\sqrt{T_c/M_m}$). According to the definition of the ideal characteristic velocity, represented by Equation 2.5, assuming a constant specific heat ratio, it is possible to confirm that the theoretical characteristic velocity increases with the decreasing of the mixture ratio, as shown in Table 5.2. An increment in the characteristic velocity causes an increment in the residence time, in accordance with Equation 2.10, which

Figura 5.37: Combustion efficiency at different mixture ratio

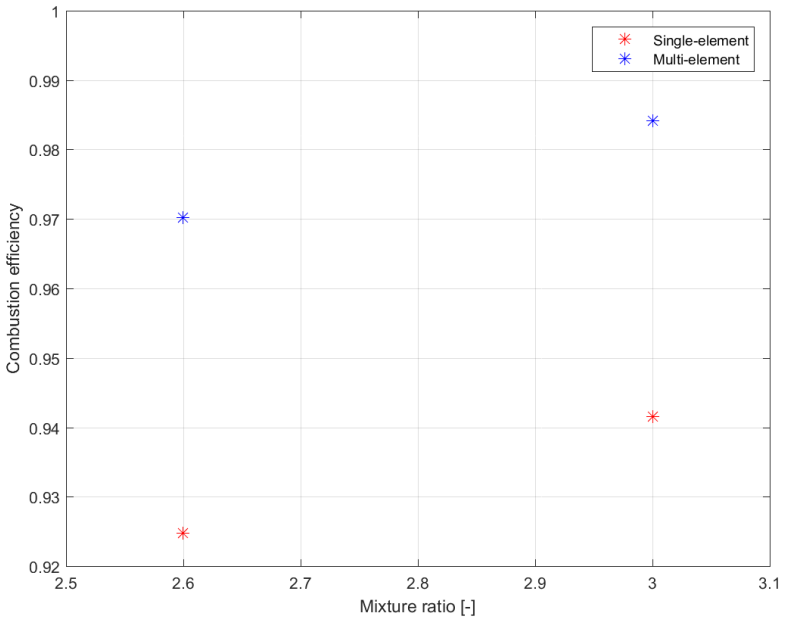

(a) Pressure = 10 bar

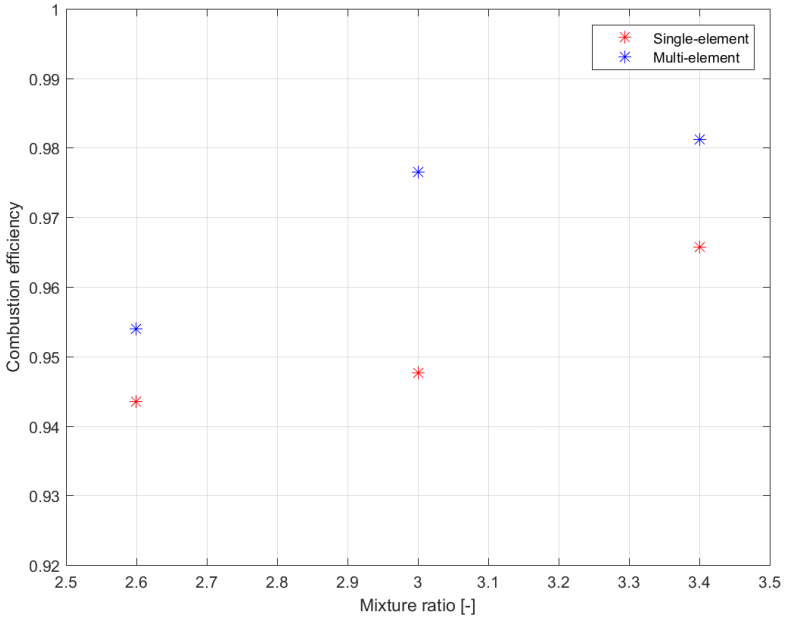

(b) Pressure = 20 bar

leads a higher mixing efficiency and, as a consequence, a higher combustion efficiency.
In the second condition shown in Figures 5.38, increasing the chamber pressure, the combustion efficiency increases, in a condition of constant chamber pressure, if the single-element combustion chamber is analysed. On the contrary, for the multi-element combustion chamber, increasing the mixture ratio, the combustion efficiency decreases, maintaining a constant cham-

Figura 5.38: Combustion efficiency at different chamber pressure

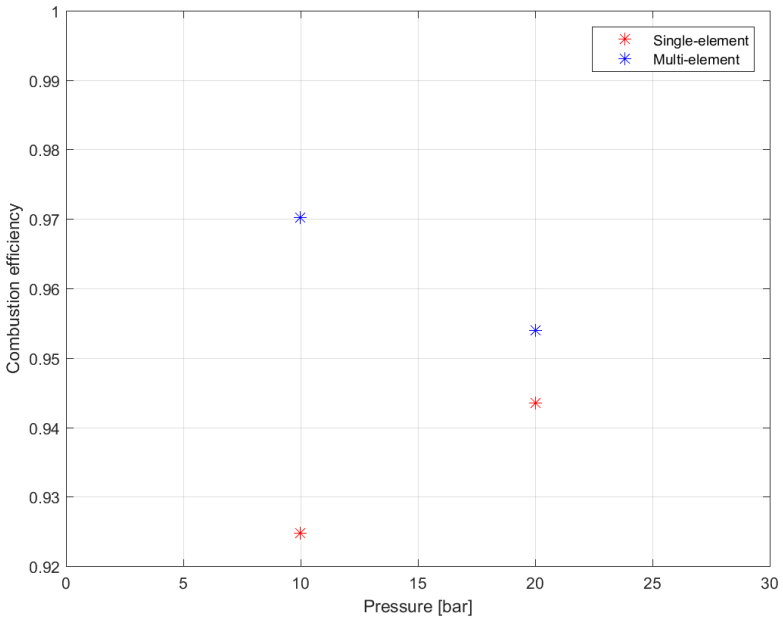

(a) O/F = 2.6

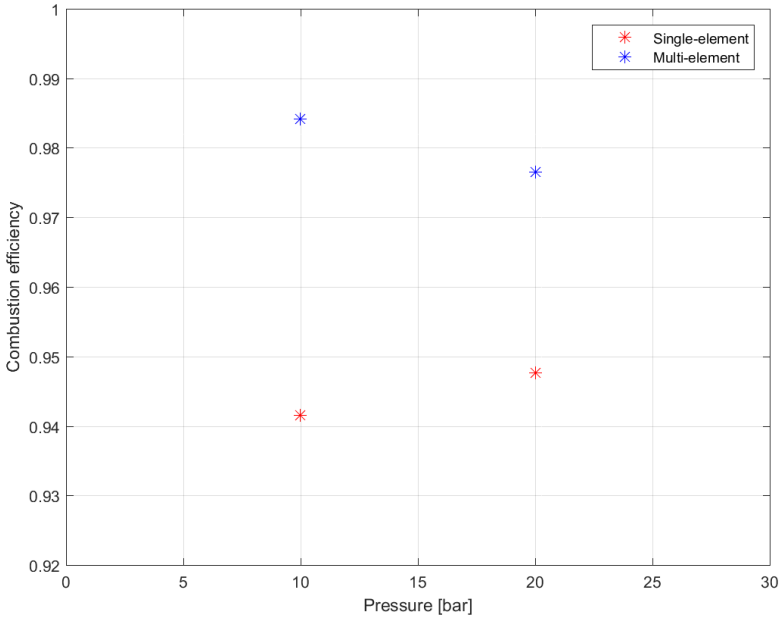

(b) O/F = 3.0

ber pressure. For the all load points, the combustion efficiency is higher for the multi-element combustion chamber, respect to the single-element one, due to a less influence of the corners in the mixing of the propellant.

Capitolo 6

Conclusion

In the “Lehrstuhl für Turbomaschinen und Flugantriebe" (LTF), two different rocket combustion chambers are tested, varying the chamber pressure from 10 to 20 bar and the mixture ratio from 2.6 to 3.4. In this way, it is possible to have a better understanding of the injection and combustion processes and to predict the pressure, temperature and heat flux behaviour, considering the gaseous propellant combination methane-oxygen. The two subscale combustion chambers designed and tested are: a single-element and a multi-element ones, which differ in the number of injectors. In fact, the single-element one has one injector, instead the multi-element one has five injectors.
Despite the same injector geometry is used in both combustion chambers, the two hardware differ in their cross section: the single-element combustion chamber has a square cross section and the multi-element has a rectangular cross section. The contraction ratio between the two combustion chambers is maintained constant to assure similarity of the combustion process. Other parameters, as characteristic length, diameter hydraulic, chamber volume to wall area ratio are different, due to the different geometries of the two combustion chambers. The results obtained by the two hardware are compared, in order to understand the combustion process and the interaction between the injectors.
Considering the pressure trend along chamber axis, the end of the combustion processes is more pronounced in the multi-element combustion chamber. Thanks to the presence of the corners, which influence the single-element combustion chamber because are closer to the injector, the recirculation zone is more evident, respect to the multi-element combustion chamber.
In according to the temperature trend versus time, the combustion process is achieved towards the end of the chamber. The two combustion chambers reach a different value of temperature, during the combustion process. In particular, the multi-element one is characterized by a higher value of temperature, which leads to a higher temperature drop, due to the presence of five injectors. In the single-element combustion chamber, the temperature profile versus time has a more roundness trend, due to more chamber walls presented. In fact, the ratio between the

chamber volume and the wall area (V/A) is lower for the single-element combustion chamber. For this reason, despite the same amount of energy per unit volume is introduced into the systems, the two combustion chambers have a different thermal response in time.
Due to the capacitive nature of the two combustion chambers, the typical temperature profile along y axis is characterized by a higher temperature value approaching the middle position and a lower value close to the chamber walls. In fact, the flow situated along the central injector is surrounding by hot flow on the left and right side and by the walls on the top and on the bottom. Differently, the flow, in correspondence of the extreme injectors, is surrounding by the wall for three sides and just, in one side, it meets another hot flow.
Concluding, the multi-element combustion chamber is characterized by a higher combustion efficiency, due to the presence of more injectors, which give a better mixing efficiency, respect to the single-element combustion chamber, for all pressure and mixture ratio values.
In order to better understanding the combustion process, the influence of the injectors, it is possible to extend this work with numerical simulations, where the heat flux profile is investigated, in a future work.

Appendix A

Temperature Trend and Temperature Derivative along Time

A.1 10 bar and OF=2.6

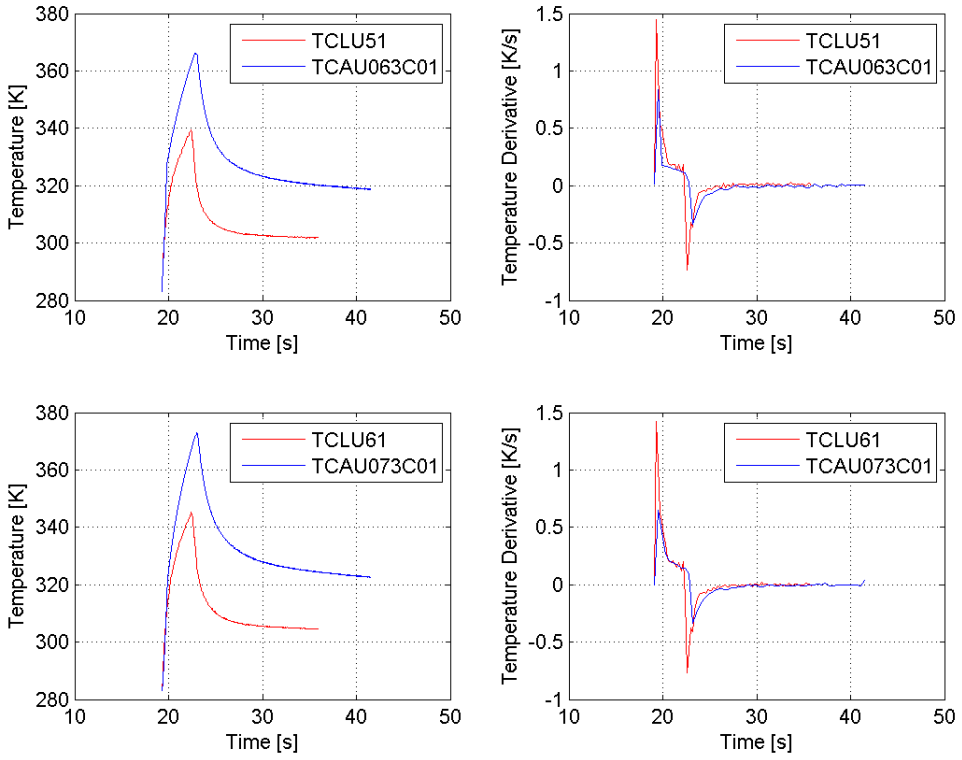

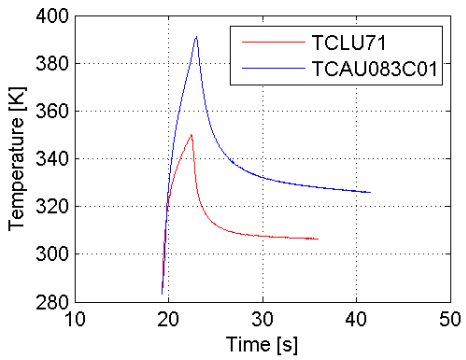
TCLU71
TCAU083C01
Temperature [K]
Time [s]

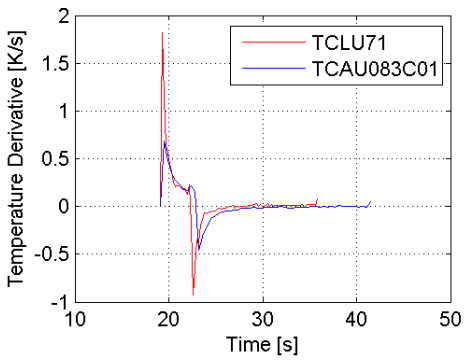
TCLU71
TCAU083C01
Temperature Derivative [K/s]
Time [s]

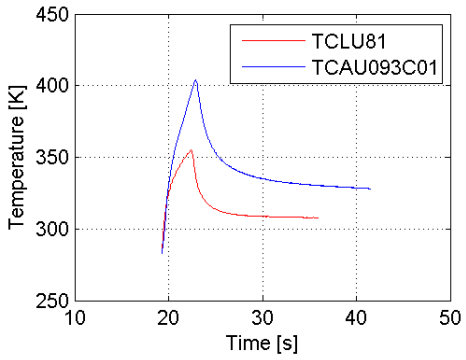
TCLU81
TCAU093C01
Temperature [K]
Time [s]

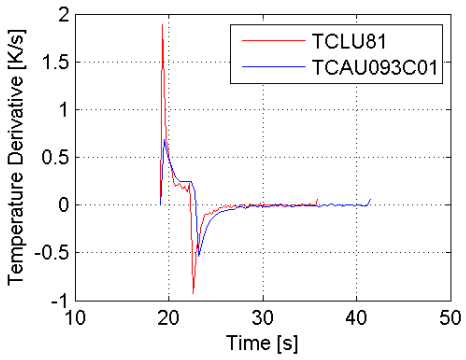
TCLU81
TCAU093C01
Temperature Derivative [K/s]
Time [s]

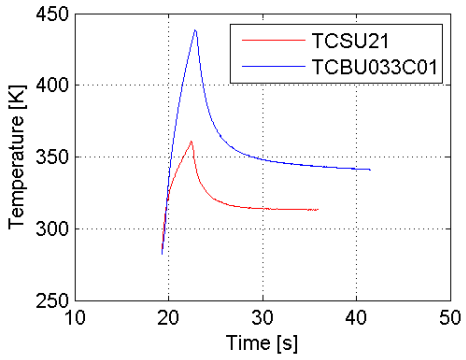
TCSU21
TCBU033C01
Temperature [K]
Time [s]

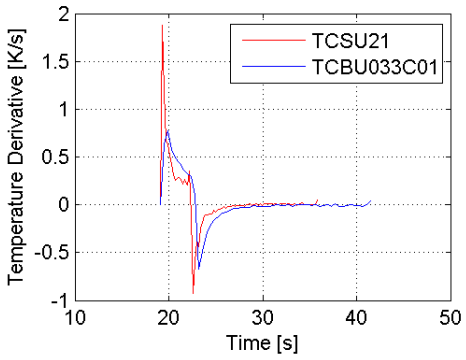
TCSU21
TCBU033C01
Temperature Derivative [K/s]
Time [s]

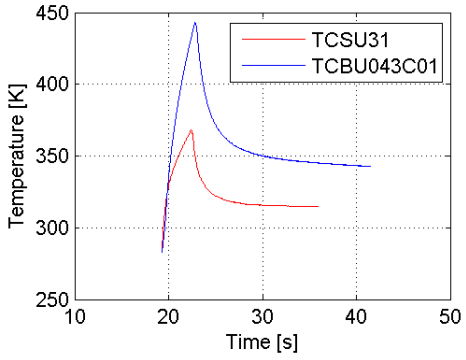
TCSU31
TCBU043C01
Temperature [K]
Time [s]

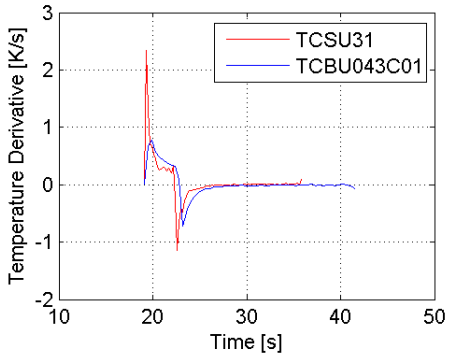
TCSU31
TCBU043C01
Temperature Derivative [K/s]
Time [s]

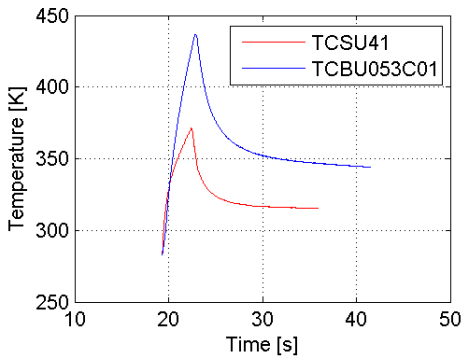
TCSU41
TCBU053C01
Temperature [K]
Time [s]

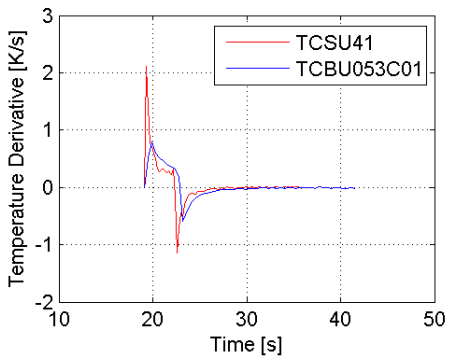
TCSU41
TCBU053C01
Temperature Derivative [K/s]
Time [s]

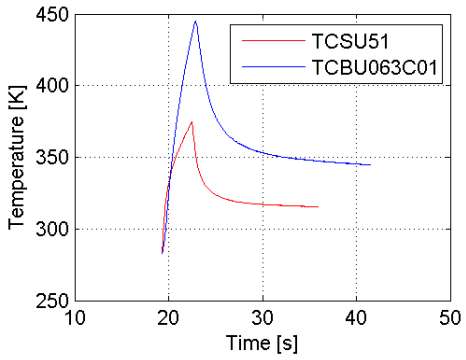
TCSU51
TCBU063C01
Temperature [K]
Time [s]

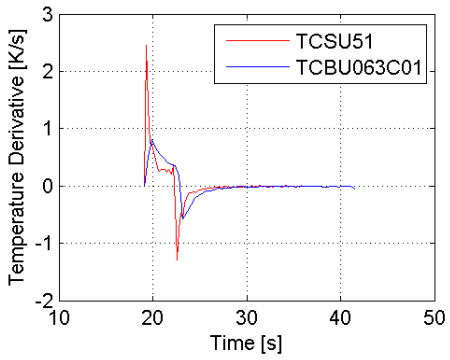
TCSU51
TCBU063C01
Temperature Derivative [K/s]
Time [s]

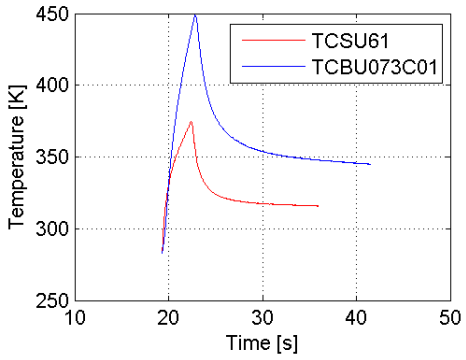
TCSU61
TCBU073C01
Temperature [K]
Time [s]

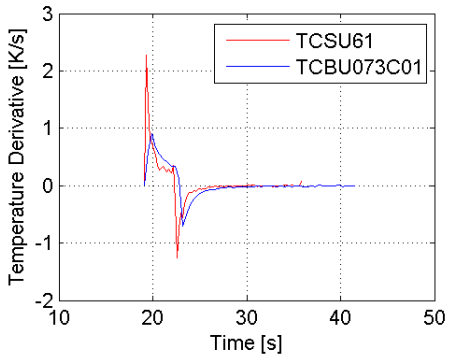
TCSU61
TCBU073C01
Temperature Derivative [K/s]
Time [s]

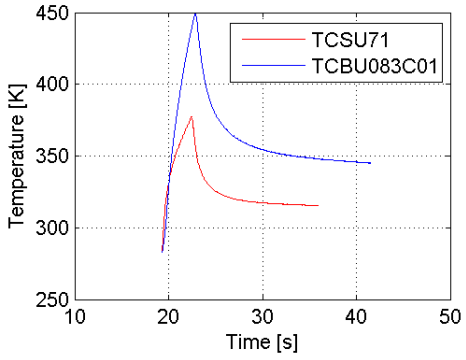
TCSU71
TCBU083C01
Temperature [K]
Time [s]

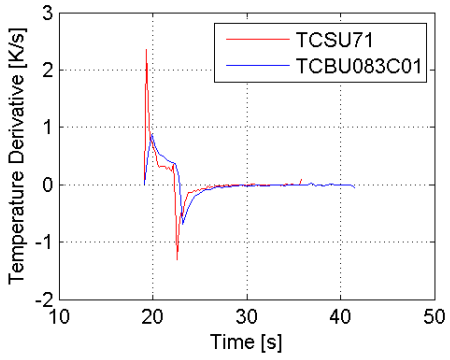
TCSU71
TCBU083C01
Temperature Derivative [K/s]
Time [s]

A.2 10 bar and OF=3.0

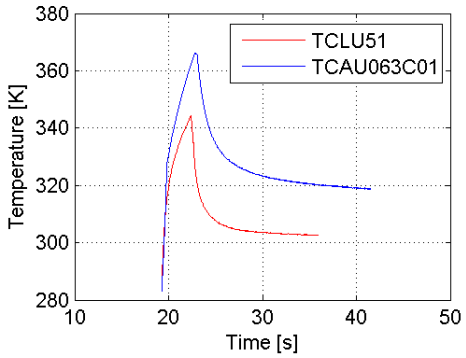

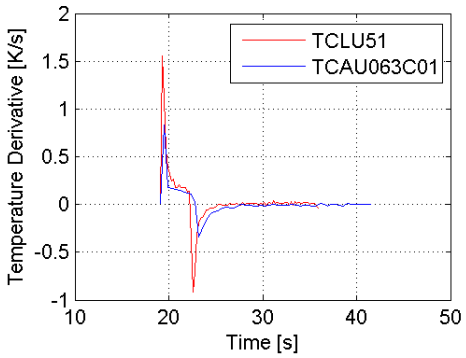

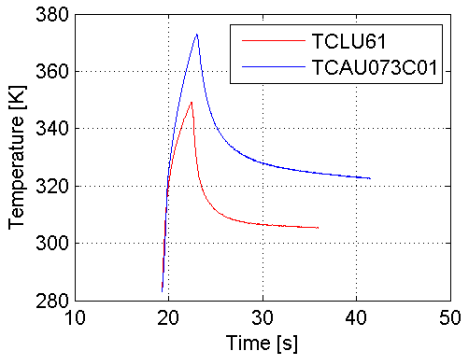

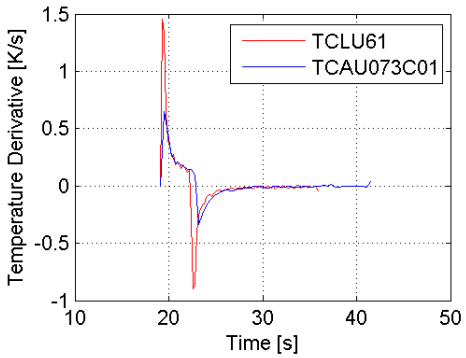

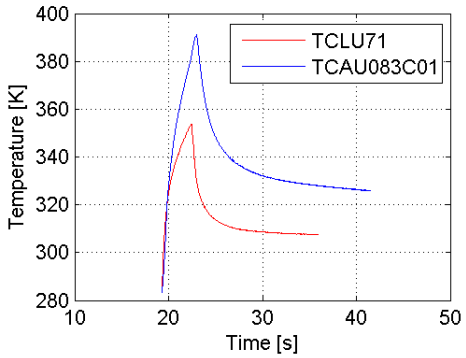

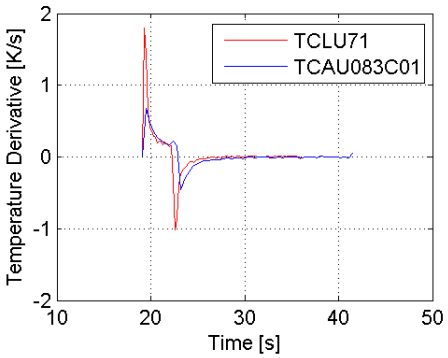

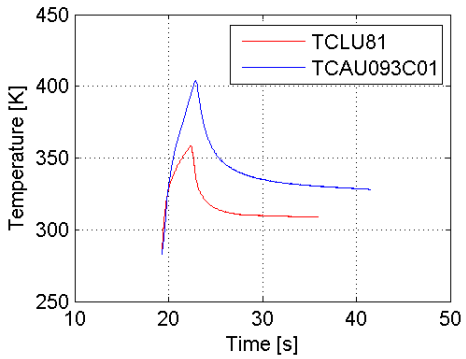

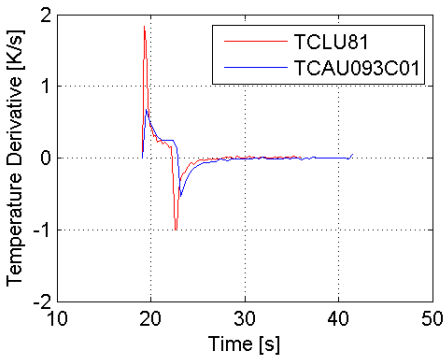

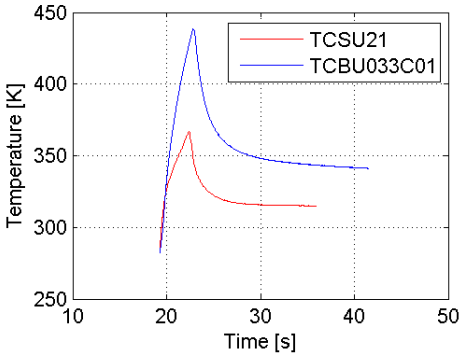
TCSU21
TCBU033C01
Temperature [K]
Time [s]

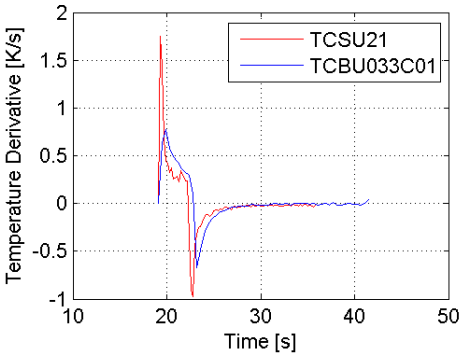
TCSU21
TCBU033C01
Temperature Derivative [K/s]
Time [s]

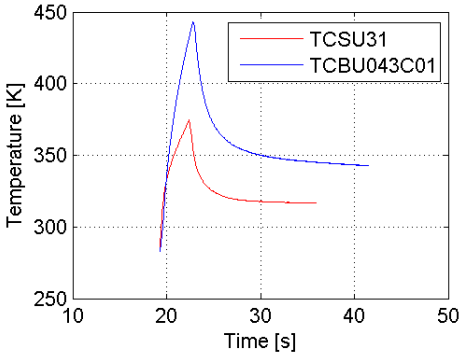
TCSU31
TCBU043C01
Temperature [K]
Time [s]

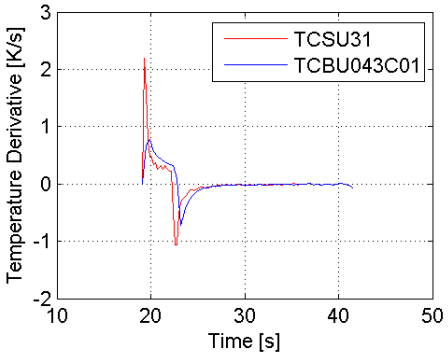
TCSU31
TCBU043C01
Temperature Derivative [K/s]
Time [s]

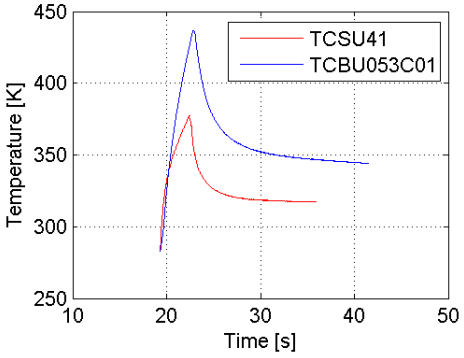
TCSU41
TCBU053C01
Temperature [K]
Time [s]

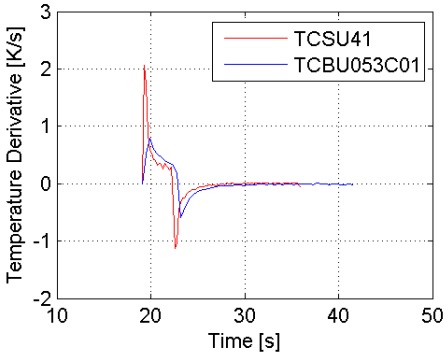
TCSU41
TCBU053C01
Temperature Derivative [K/s]
Time [s]

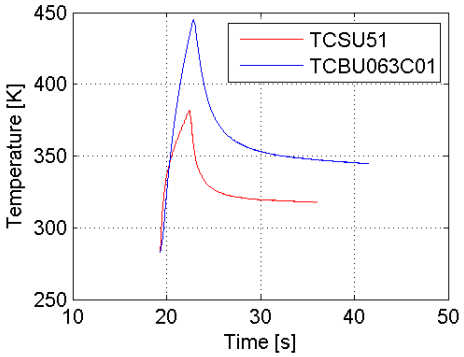
TCSU51
TCBU063C01
Temperature [K]
Time [s]

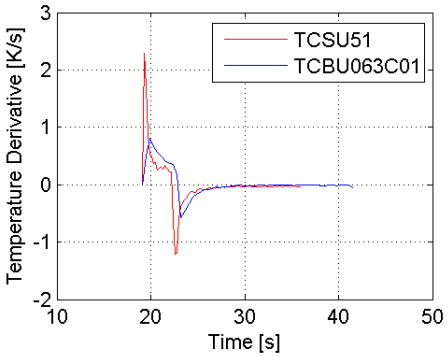
TCSU51
TCBU063C01
Temperature Derivative [K/s]
Time [s]

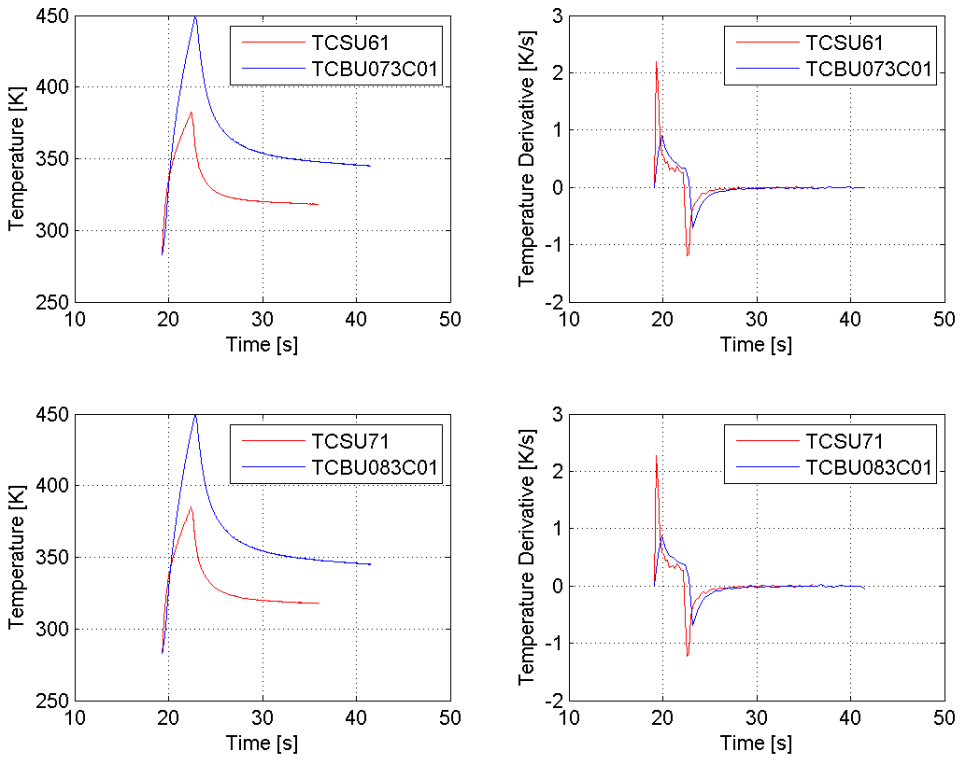

A.3 20 bar and OF=2.6

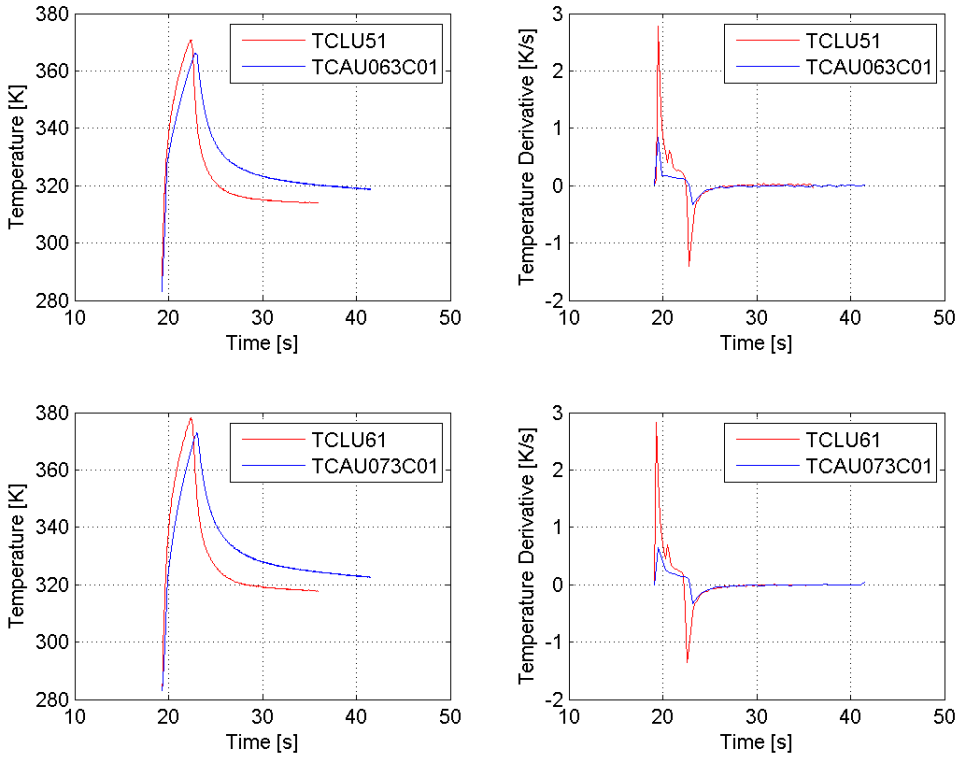

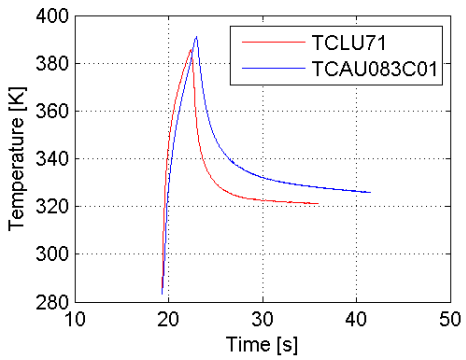
TCLU71
TCAU083C01
Temperature [K]
Time [s]

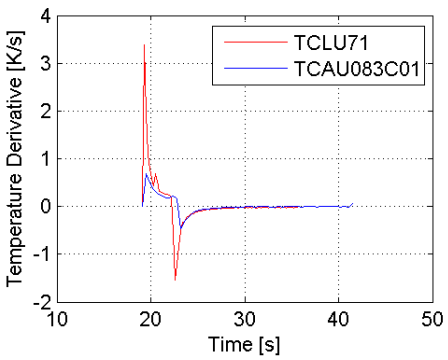
TCLU71
TCAU083C01
Temperature Derivative [K/s]
Time [s]

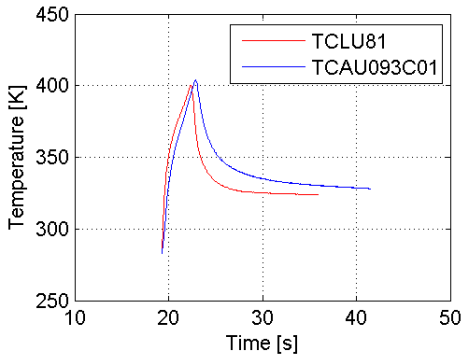
TCLU81
TCAU093C01
Temperature [K]
Time [s]

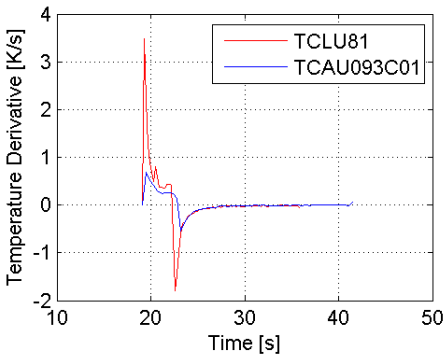
TCLU81
TCAU093C01
Temperature Derivative [K/s]
Time [s]

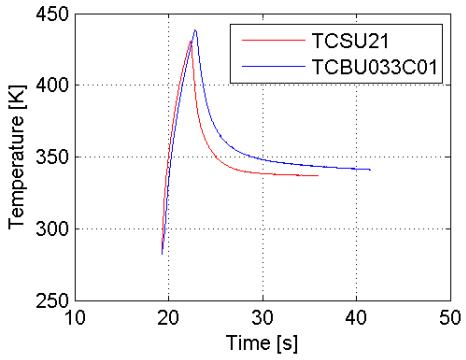
TCSU21
TCBU033C01
Temperature [K]
Time [s]

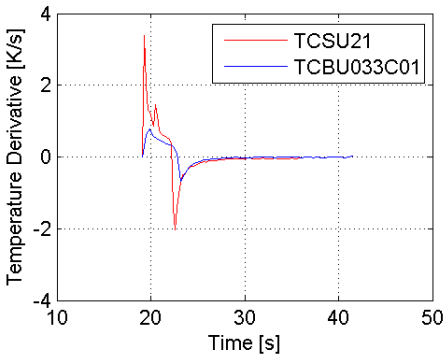
TCSU21
TCBU033C01
Temperature Derivative [K/s]
Time [s]

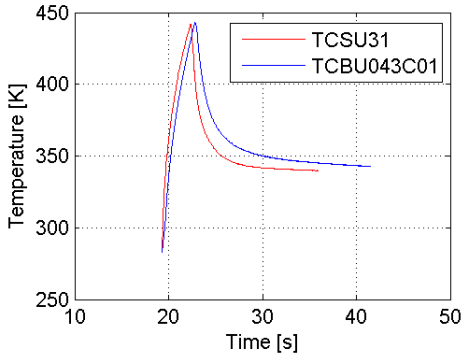
TCSU31
TCBU043C01
Temperature [K]
Time [s]

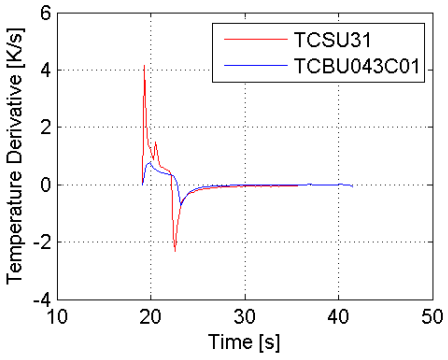
TCSU31
TCBU043C01
Temperature Derivative [K/s]
Time [s]

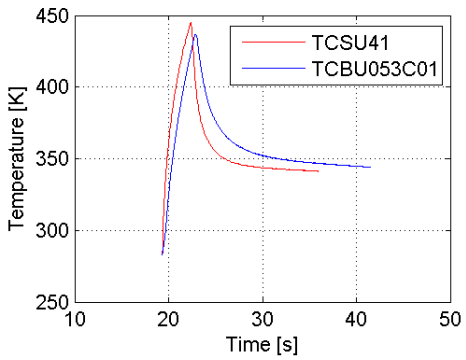
TCSU41
TCBU053C01
Temperature [K]
Time [s]

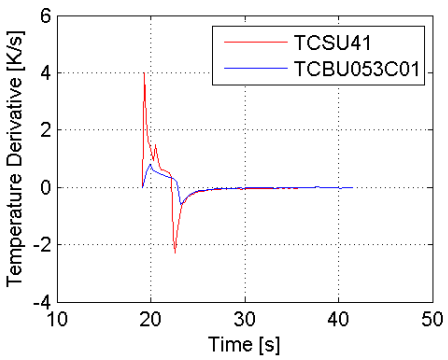
TCSU41
TCBU053C01
Temperature Derivative [K/s]
Time [s]

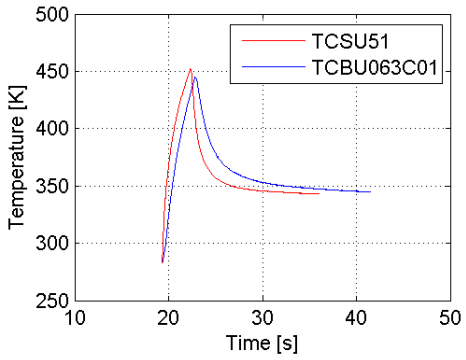
TCSU51
TCBU063C01
Temperature [K]
Time [s]

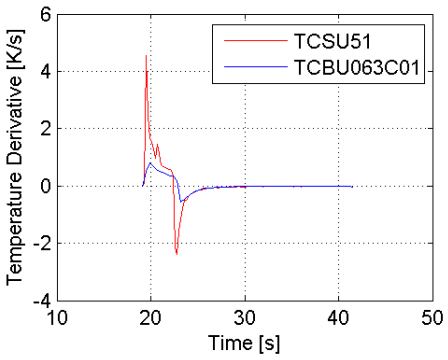
TCSU51
TCBU063C01
Temperature Derivative [K/s]
Time [s]

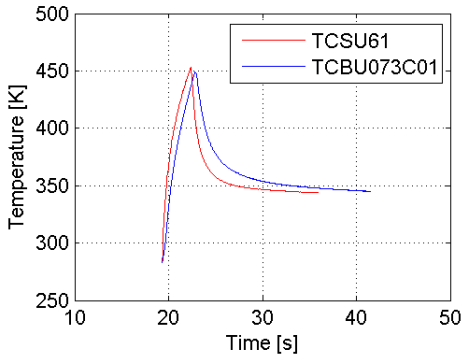
TCSU61
TCBU073C01
Temperature [K]
Time [s]

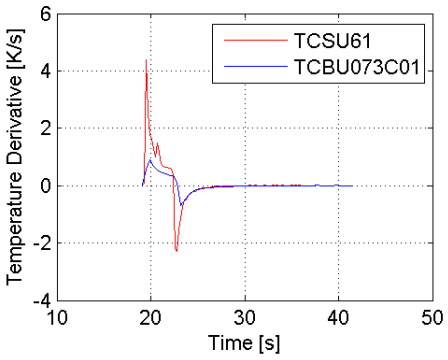
TCSU61
TCBU073C01
Temperature Derivative [K/s]
Time [s]

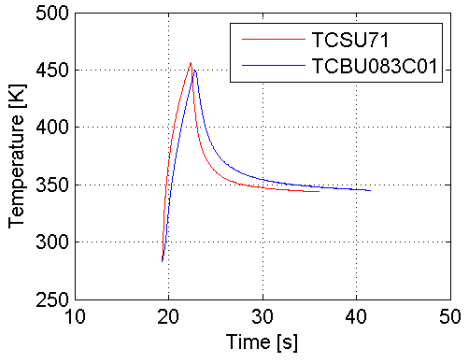
TCSU71
TCBU083C01
Temperature [K]
Time [s]

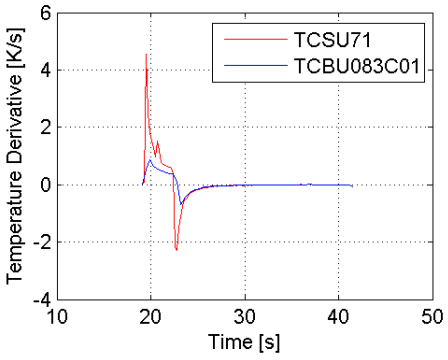
TCSU71
TCBU083C01
Temperature Derivative [K/s]
Time [s]

A.4 20 bar and OF=3.0

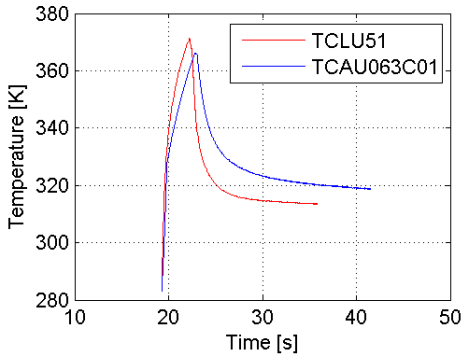

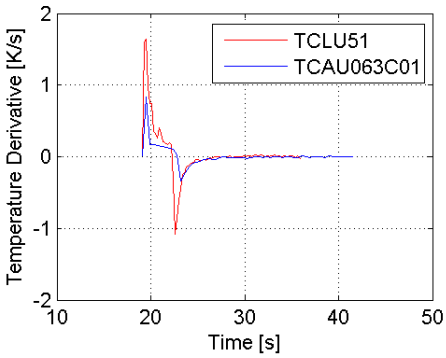

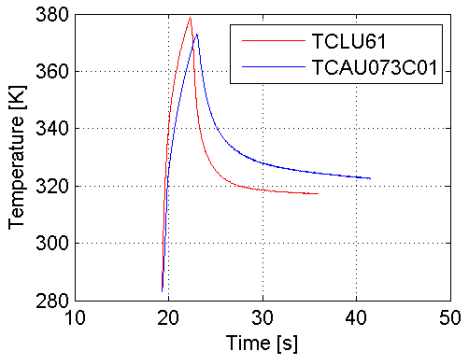

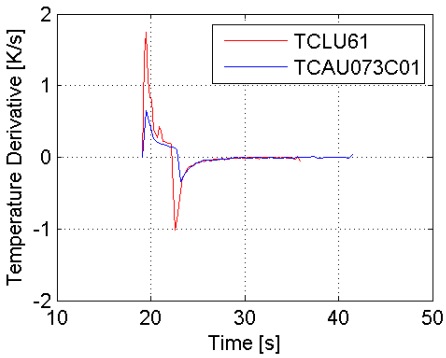

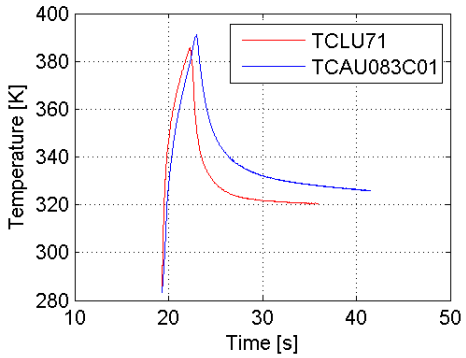

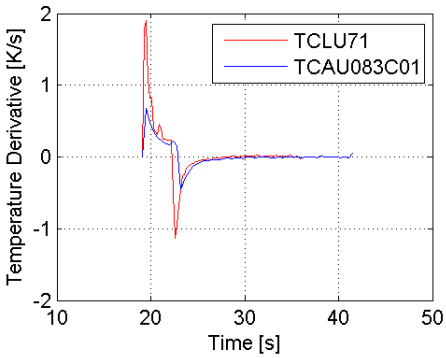

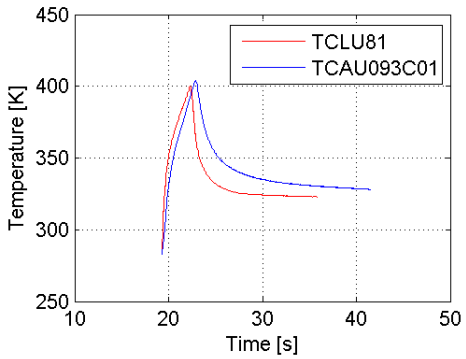

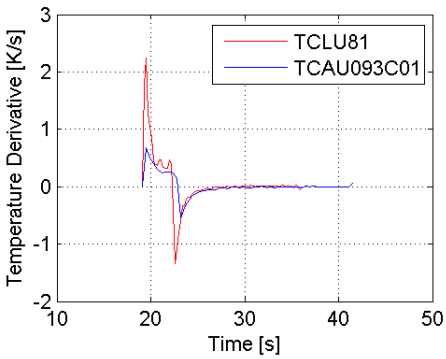

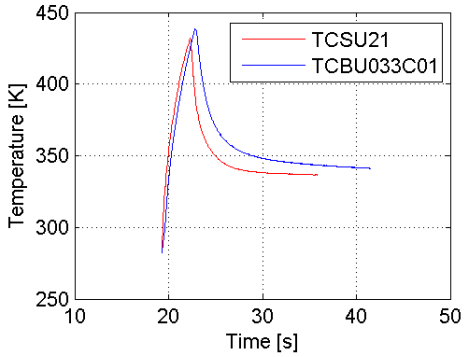
TCSU21
TCBU033C01
Temperature [K]
Time [s]

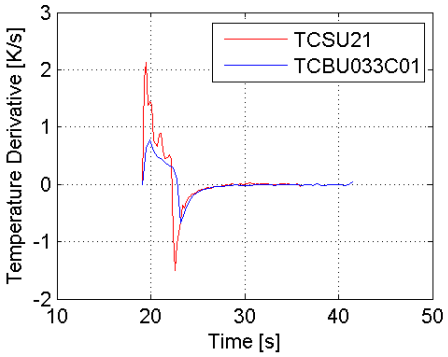
TCSU21
TCBU033C01
Temperature Derivative [K/s]
Time [s]

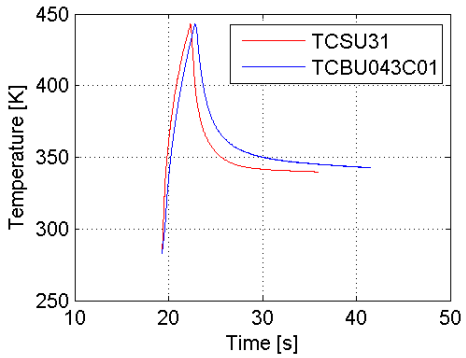
TCSU31
TCBU043C01
Temperature [K]
Time [s]

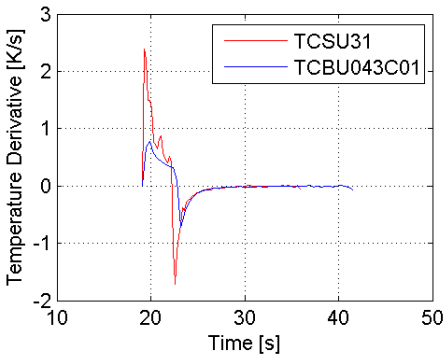
TCSU31
TCBU043C01
Temperature Derivative [K/s]
Time [s]

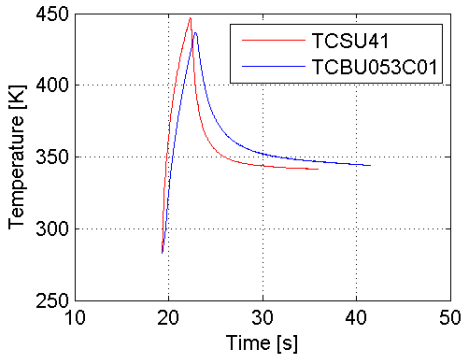
TCSU41
TCBU053C01
Temperature [K]
Time [s]

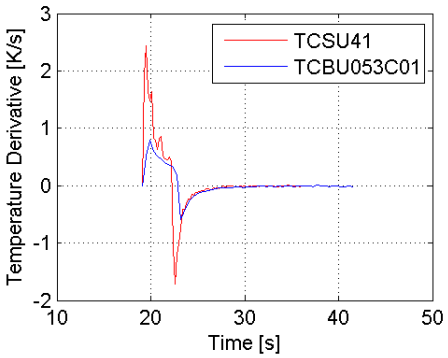
TCSU41
TCBU053C01
Temperature Derivative [K/s]
Time [s]

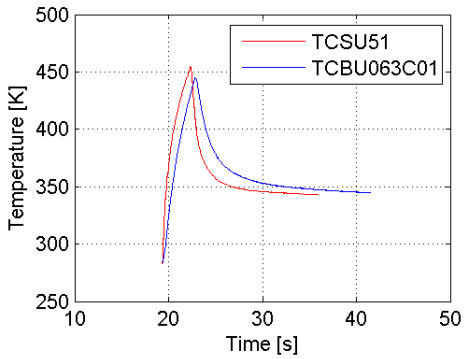
TCSU51
TCBU063C01
Temperature [K]
Time [s]

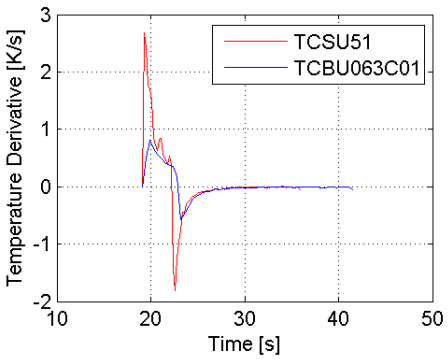
TCSU51
TCBU063C01
Temperature Derivative [K/s]
Time [s]

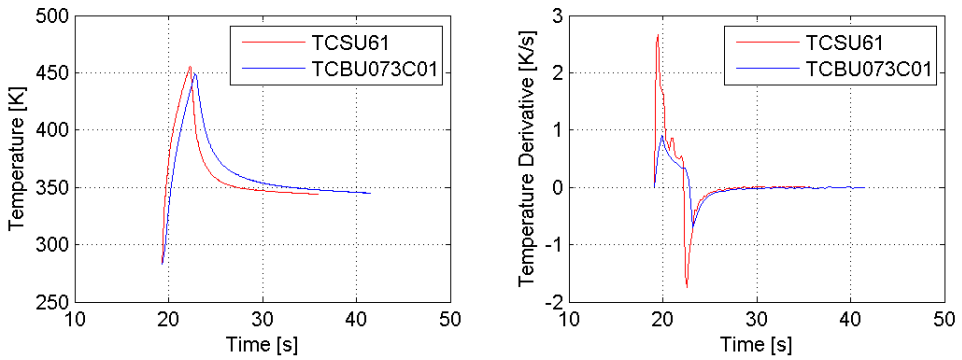

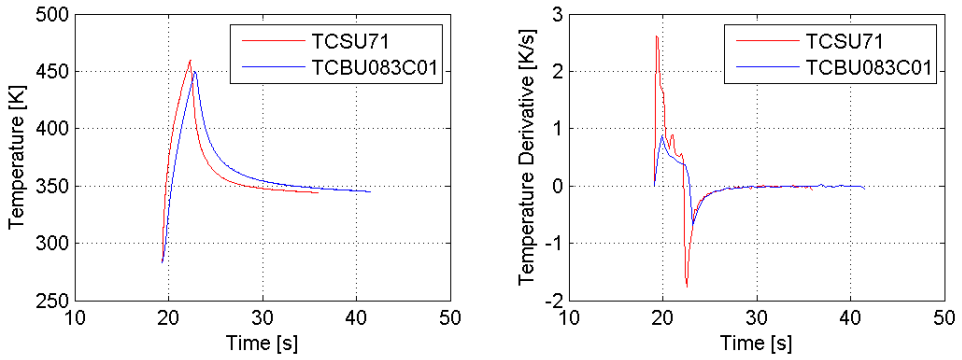

A.5 20 bar and OF=3.4

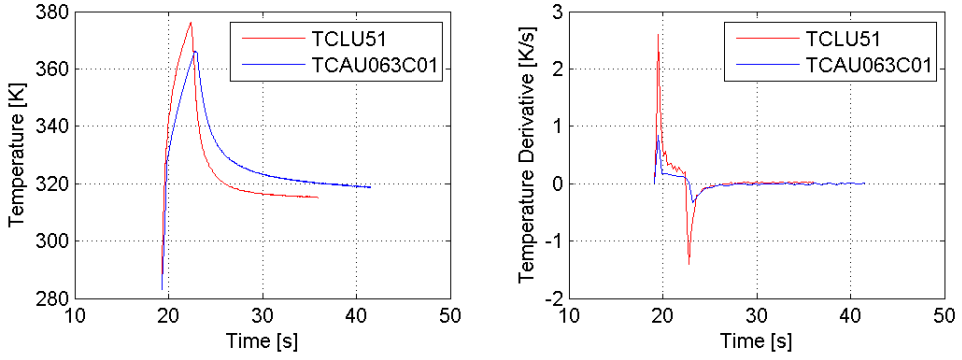

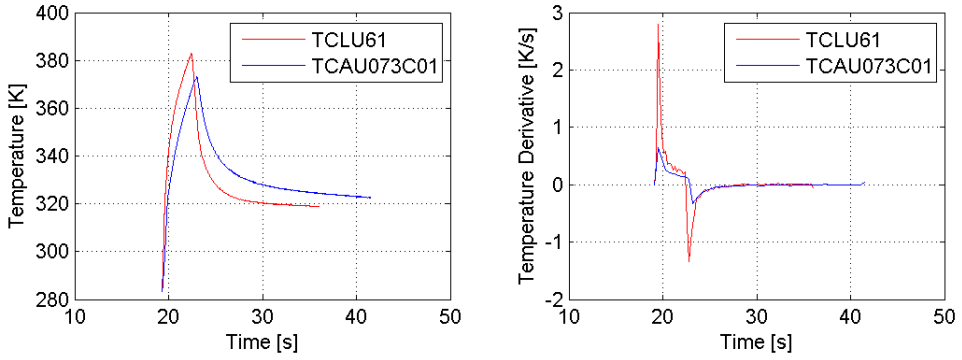

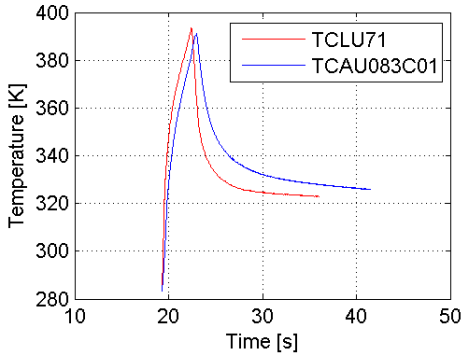
TCLU71
TCAU083C01
Temperature [K]
Time [s]

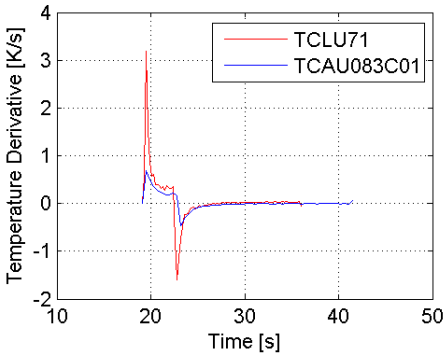
TCLU71
TCAU083C01
Temperature Derivative [K/s]
Time [s]

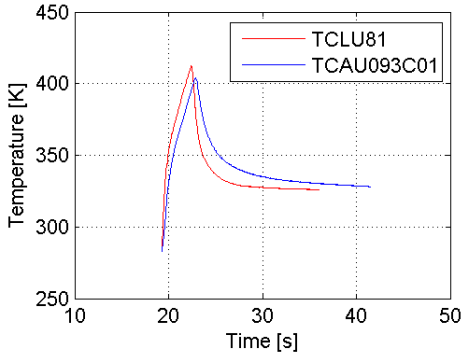
TCLU81
TCAU093C01
Temperature [K]
Time [s]

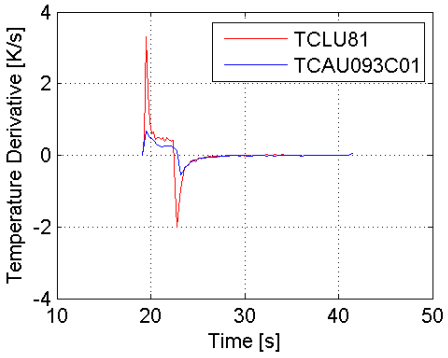
TCLU81
TCAU093C01
Temperature Derivative [K/s]
Time [s]

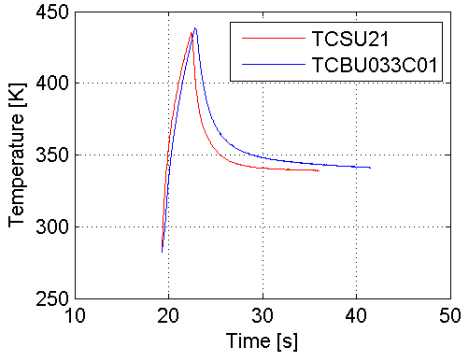
TCSU21
TCBU033C01
Temperature [K]
Time [s]

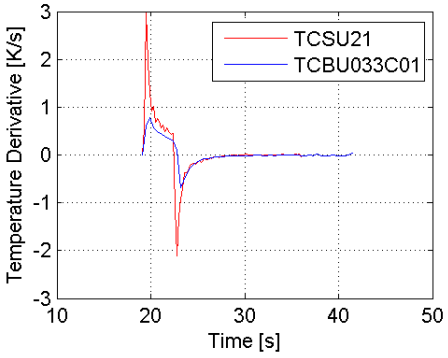
TCSU21
TCBU033C01
Temperature Derivative [K/s]
Time [s]

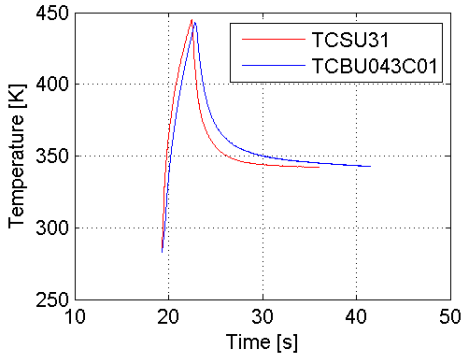
TCSU31
TCBU043C01
Temperature [K]
Time [s]

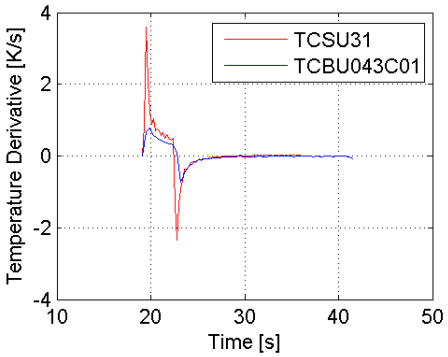
TCSU31
TCBU043C01
Temperature Derivative [K/s]
Time [s]

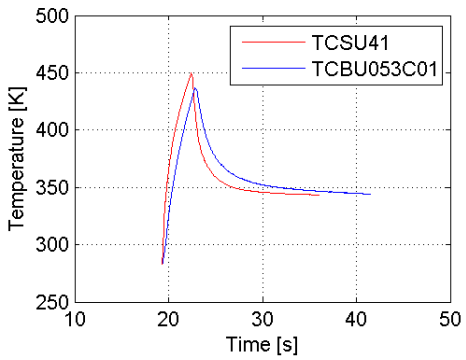
TCSU41
TCBU053C01
Temperature [K]
Time [s]

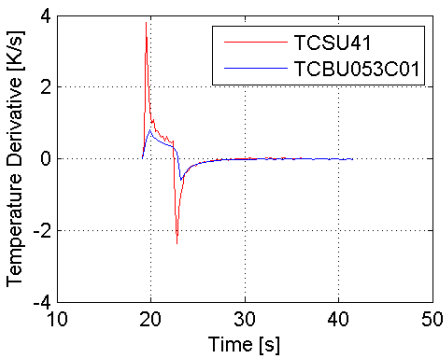
TCSU41
TCBU053C01
Temperature Derivative [K/s]
Time [s]

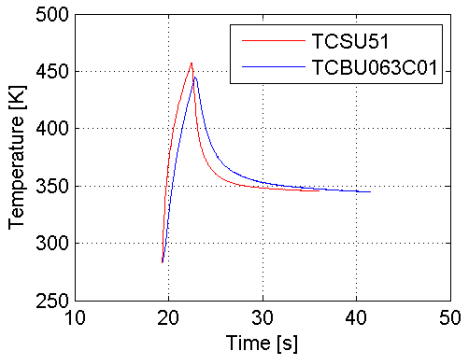
TCSU51
TCBU063C01
Temperature [K]
Time [s]

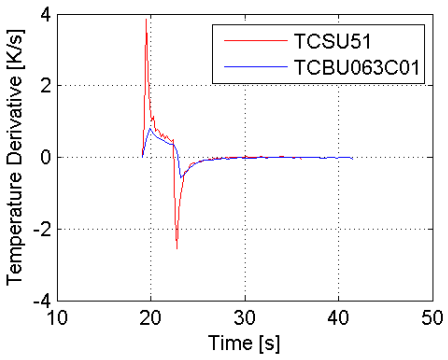
TCSU51
TCBU063C01
Temperature Derivative [K/s]
Time [s]

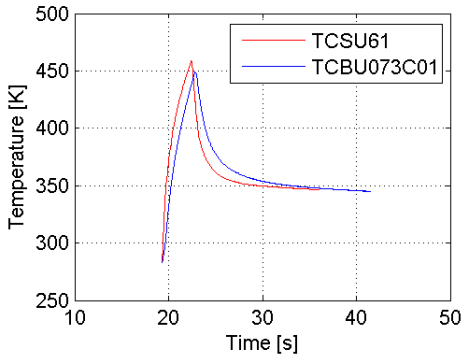
TCSU61
TCBU073C01
Temperature [K]
Time [s]

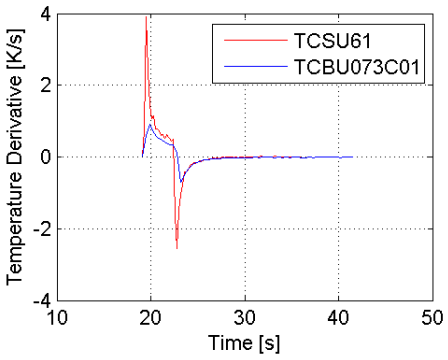
TCSU61
TCBU073C01
Temperature Derivative [K/s]
Time [s]

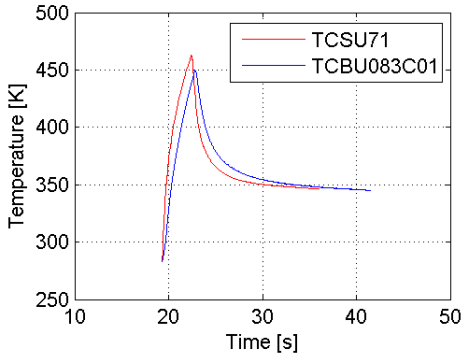
TCSU71
TCBU083C01
Temperature [K]
Time [s]

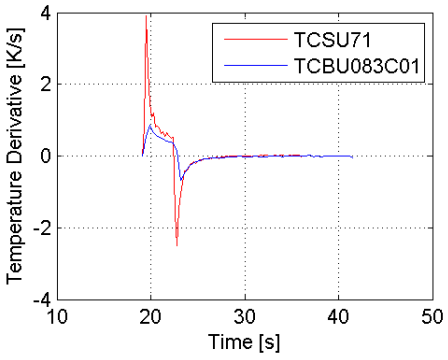
TCSU71
TCBU083C01
Temperature Derivative [K/s]
Time [s]

Appendix B

Temperature Trend along Y-Axis

B.1 20 bar and O/F=2.6

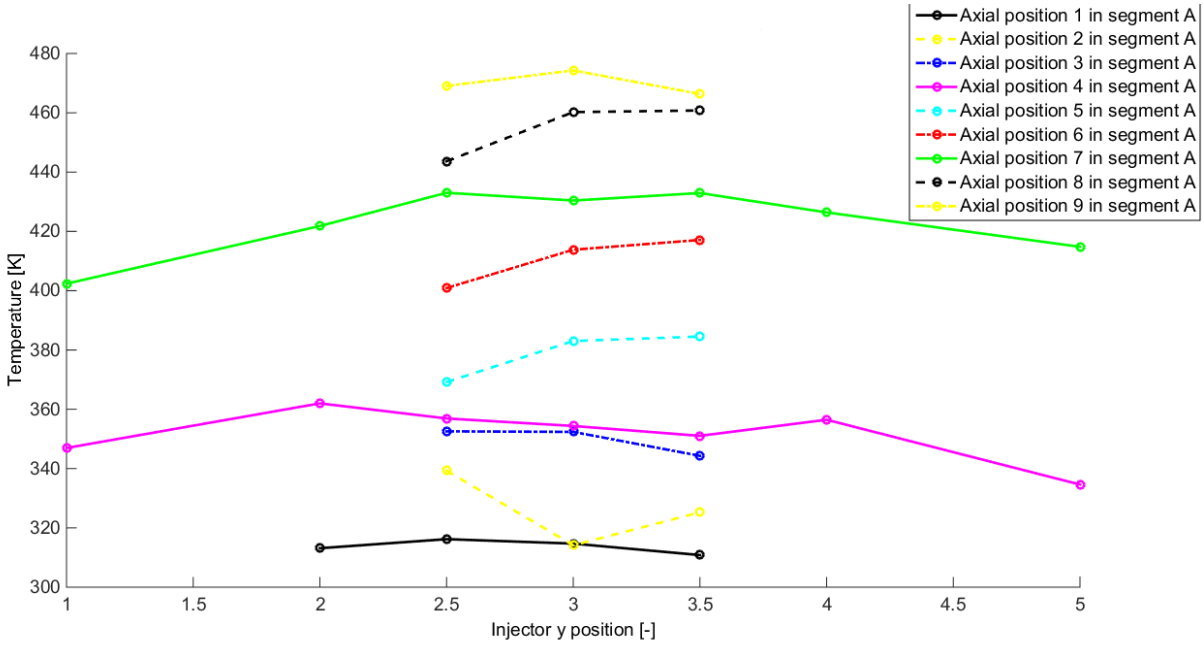

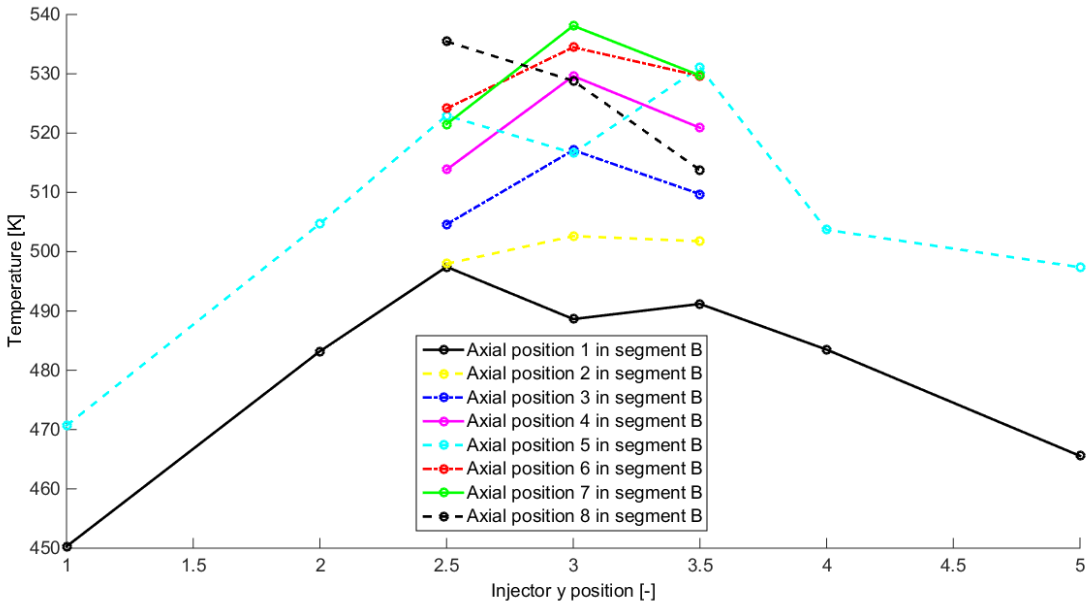

B.2 20 bar and O/F=3.0

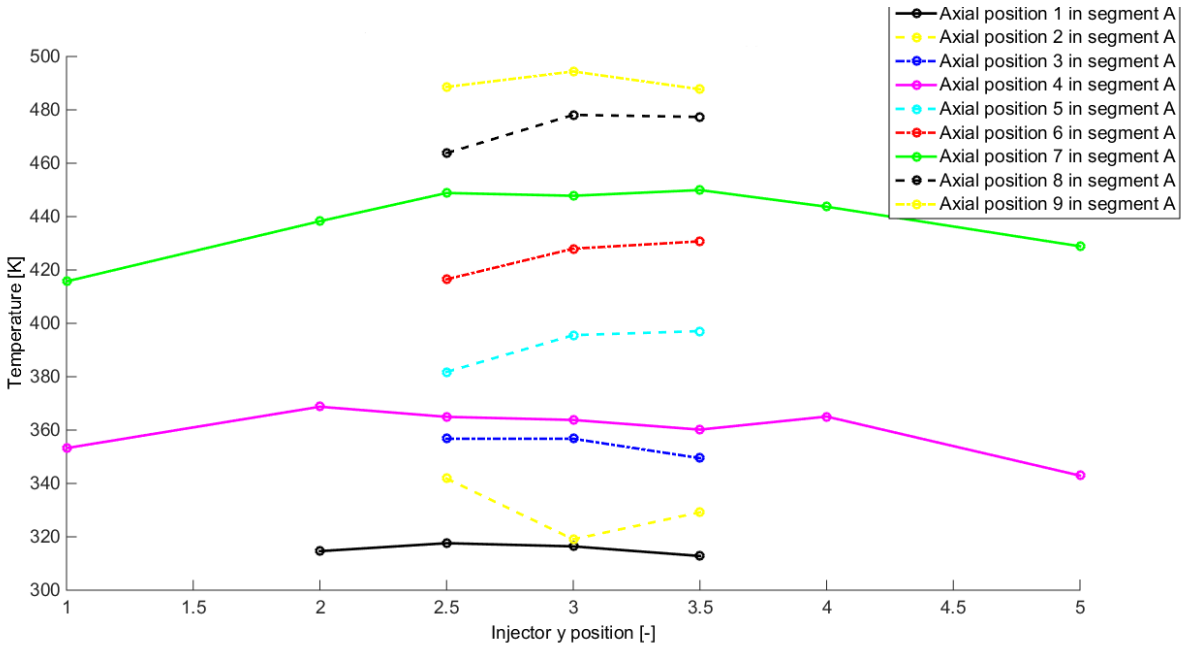

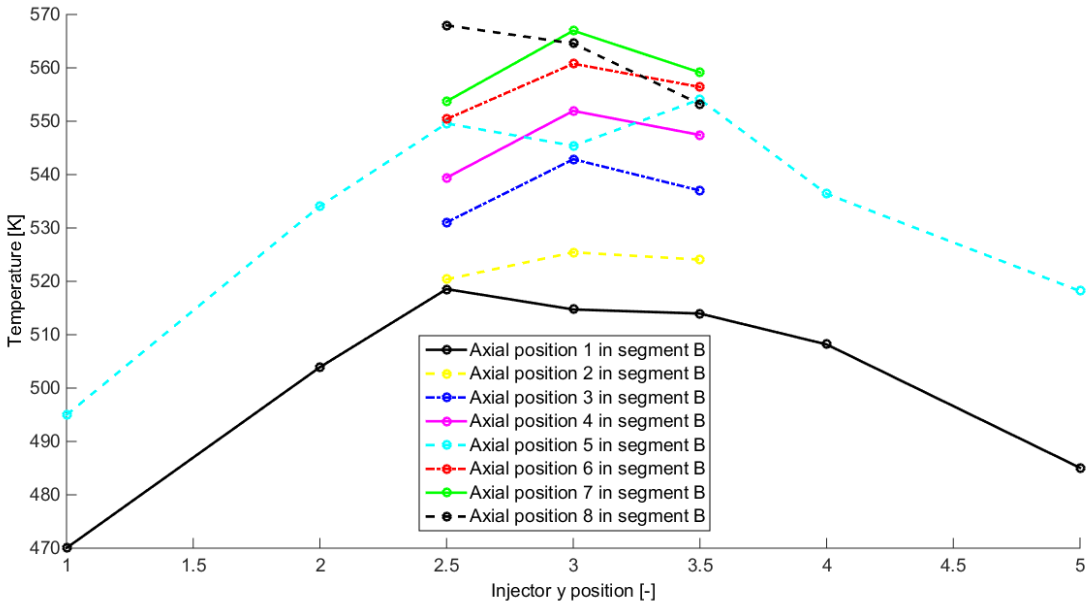

B.3 20 bar and O/F=3.4

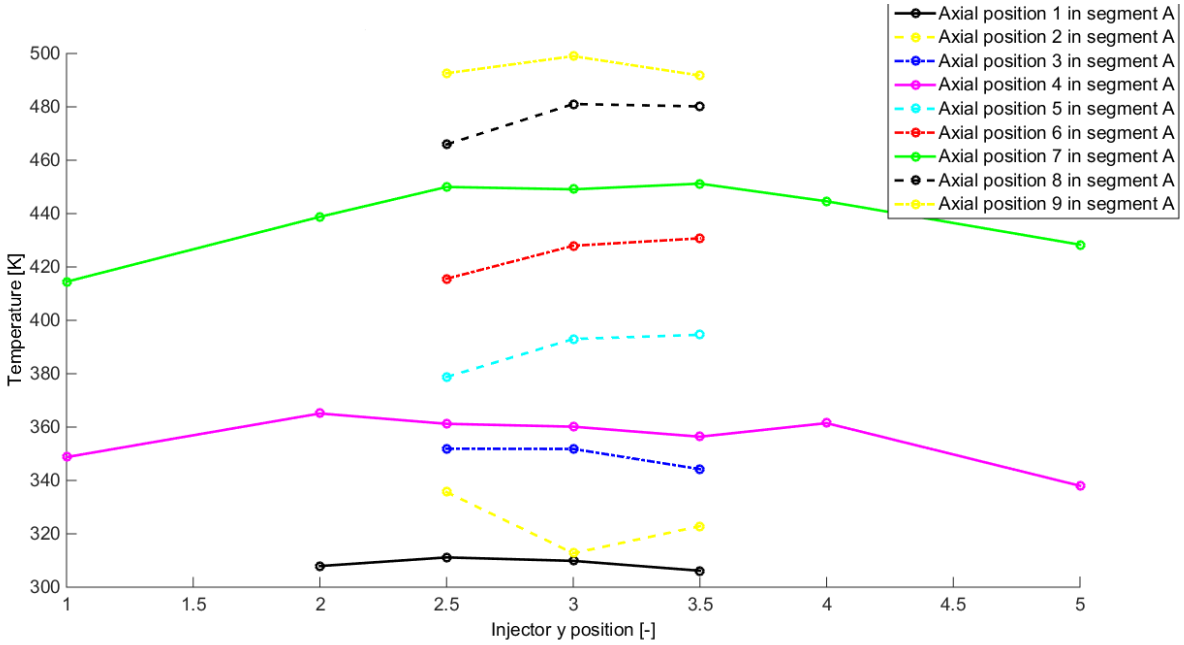

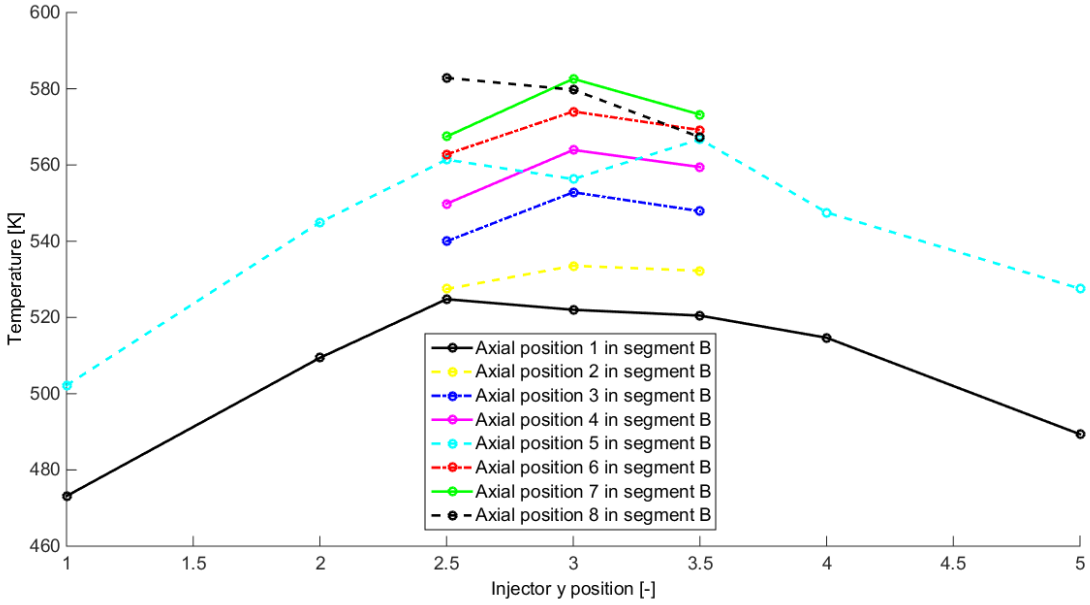
600
580
560
540
520
500
480
460
Temperature [K]
1
1.5
2
2.5
3
3.5
4
4.5
5
Injector y position [-]
Axial position 1 in segment B
Axial position 2 in segment B
Axial position 3 in segment B
Axial position 4 in segment B
Axial position 5 in segment B
Axial position 6 in segment B
Axial position 7 in segment B
Axial position 8 in segment B

Bibliografia

[1] G. P. Sutton, O. Biblarz, Rocket Propulsion Elements, 7th Edition, John Wiley & Sons, 2001;

[2] M.P. Celano, S. Silvestri, G. Schlieben, C. Kirchberger, and H. J. Haidn, Injector Characterization for a GOX-GCH4 Single Elelment Combustion Chamber, Eucass 2013;

[3] Jannaf Rocket Engine Performance Prediction and Evaluation Manual, Johns Hopkins University, 1975;

[4] S. Silvestri, M. P. Celano, G. Schlieben, C. Kirchberger, O. J. Haidn, Characterization of a GOx-GCH4 Single Element Combustion Chamber, Space Propulsion Conference 2014, Cologne, Germany;

[5] J. Hulka, Scaling of performance in liquid propellant rocket engine combustion devices, AIAA 2008-5113, 2003;

[6] M. P. Celano, S. Silvestri, G. Schlieben, C. Kirchberger, H. J. Haidn, T. Dawson, R. Ranjan and S. Menon, Numerical and Experimental Investigation for a GOX-GCH4 Shear-Coaxial Injector Element, Space Propulsion Conference 2014, Cologne, Germany;

[7] S.S Penner, On the development of rational scaling procedures for liquid-fuel rocket engines, Journal of jet Propulsion, 1957.

[8] D. K. Huzel, Modern Engineering for Design of Liquid-Propellant Rocket Engines, AIAA, 1992

[9] M. P. Celano, S. Silvestri, J. Pauw, N. Perakis, F. Schily, D. Suslov and O J. Haidn, Heat Flux Evaluation Methods for a Single Element Heat-Sink Chamber, Eucass;

[10] D. Calhoon, J. Ito and D. Kors, Investigation of Gaseous Propellant Combustion and Associated Injector/Chamber Design Guidelines, NASA, 1973.

[11] S. Gordon and B.J. McBride, Computer Program for Calculation of Complex Chemical Equilibrium, NASA, 1994.

[12] T. L. Bergman, F. P. Incropera, and A. S. Lavine, Fundamentals of heat and mass transfer, John Wiley & Sons, 2011.